



TECHNISCHE
UNIVERSITÄT
WIEN

Vienna University of Technology

Unterschrift des Betreuers

DIPLOMARBEIT

Biocompatible Composite Photopolymers for 3D Printing

ausgeführt am Institut für
Angewandte Synthesechemie
Bereich Makromolekulare Chemie
der Technischen Universität Wien

unter der Anleitung von
Ao.Univ.Prof. Dipl.-Ing. Dr.techn. Robert Liska
Projektass. Branislav Husar, PhD

durch

Sandra Orman, BSc.
Heimgartengasse 2/2, 3002 Purkersdorf

Wien, 14. April 2015

Unterschrift des Studenten

“A straight line may be the shortest distance between two points, but it is by no means the most interesting”

— Robert Holmes

Abstract

The market for bio-implants is growing every year due to the increase of chronic bone and joint diseases such as osteoarthritis, osteonecrosis, vertebral fractures, old age-related trauma and other diseases. 2012 this market was worth \$94.1 billion worldwide and is expected to grow 7.3% until 2017. Expansion of this field is inseparably related to the fields of biomaterials and development/improvement in processing techniques. The current approach in Regenerative Medicine and Tissue Engineering is to create temporary scaffolds from biocompatible, biodegradable materials that on one hand provides suitable mechanical properties and structure to replace/support the damaged tissue and on the other hand mimic the extracellular matrix of the concerned tissue and therefore helps cells to attach and proliferate. The degradation of the scaffold should result in non-toxic products that can easily be transported out of the system and the rate should not be faster than the growth rate of the regenerating tissue.

The scope of this work was to investigate the application of Additive Manufacturing Technologies (AMT) using photopolymerizable Thiol-Ene systems for potential bone replacement materials.

Vinyl esters have proven recently to be ideal candidates to replace acrylates and methacrylates as Ene component due to the low cytotoxicity of the monomers and potential degradation products. Starting from the only commercially available difunctional vinyl ester divinyl adipate different monomers were synthesized. As Thiol components three different trithiols with low cytotoxicity were investigated: trimethylpropane tris(3-mercaptopropionate) (TMPMP), ethoxylated trimethylpropane tris(3-mercaptopropionate) of molecular weight 700 (ETTMP700) and 1300 (ETTMP1300). This variety of materials covers a wide range of both mechanical properties and degradation behavior. To enhance the properties even further, inorganic particles were incorporated to form composite materials. The chosen manufacturing technique was Lithography-based Ceramic Manufacturing (LCM).

Zusammenfassung

Der Markt für Bio-Implantate wächst jedes Jahr auf Grund der zunehmenden Anzahl chronischer Knochen- und Gelenkserkrankungen wie Osteoarthritis, Osteonekrose, Wirbelbrüchen, altersbedingten Verletzungen und andere Erkrankungen. Im Jahr 2012 betrug der Marktwert \$94,1 Milliarden weltweit und bis 2017 wird ein Wachstum von 7,3% erwartet. Eine Expansion auf diesem Gebiet ist untrennbar mit der Entwicklung und Weiterentwicklung von Biomaterialien und Fertigungstechniken verbunden. Die aktuelle Herangehensweise in der Regenerativen Medizin und Gewebsrekonstruktion (*Tissue Engineering*) ist die Konstruktion eines strukturellen Gerüsts (*Scaffold*) aus biokompatiblen, biologisch abbaubarem Material, dass zum einen mechanische Stabilität und Form gewährleistet und zum anderen die extrazelluläre Matrix des betroffenen Gewebes imitiert und damit das Wachstum neuen Gewebes ermöglicht. Die Abbauprodukte des Scaffolds sollten keine Zelltoxizität aufweisen und sollten leicht vom Körper abtransportiert werden können, außerdem sollte die Abbaurate in etwa der Wachstumsrate des nachwachsenden Gewebes entsprechen.

Ziel dieser Arbeit war es, Additive Manufacturing Technologien (AMT) unter Verwendung photopolymerisierbarer Thiol-En Systeme im Hinblick auf die Fertigung potentieller Knochenersatzmaterialien zu untersuchen. Vinylester haben sich kürzlich als ideale Kandidaten erwiesen um die zur Zeit gebräuchlich Acrylate und Methacrylate als En-Komponenten zu ersetzen, da sowohl die Monomere selbst als auch potentielle Abbauprodukte geringere Toxizität aufweisen. Ausgehend von Divinyladipat, dem einzigen kommerziell erhältlichen difunktionellen Vinylester, wurden verschiedene Monomere synthetisiert. Als Thiol-Komponente wurden drei verschiedene trifunktionelle Thiole untersucht: Trimethylpropane tris(3-mercapropionat) (TMPMP), ethoxyliertes Trimethylpropane tris(3-mercapropionat) mit einem Molekulargewicht von 700 (ETTMP700) und 1300 (ETTMP1300). Diese Auswahl an Substanzen deckt einen breiten Bereich sowohl mechanischer Eigenschaften als auch Abbauverhaltens ab. Um die Eigenschaften

weiter zu verbessern wurde anorganische Partikel eingearbeitet und so einen Kompositwerkstoff zu erhalten. Die Fertigungsmethode der Wahl war Lithography-based Ceramic Manufacturing (LCM).

Danksagung

Ich möchte mich ganz herzlich bei allen bedanken, die mich während der letzten Monaten begleitet habend und deren Unterstützung direkt oder indirekt in diese Arbeit eingeflossen ist.

Allen voran gilt mein Dank Prof. Robert Liska für die Möglichkeit an diesem interessanten Thema zu arbeiten sowie für die kompetente Betreuung während des vergangenen Jahres. Auch Branislav soll hier keinesfalls unbedankt bleiben, dessen Unterstützung und Motivation mich bis zuletzt begleitet haben.

Weiters möchte ich mich bei der Firma Lithoz bedanken, allen voran Johannes Homa für die Möglichkeit der Kooperation und die Nutzung der LCM-Technologie, sowie Martin Schwentenwein für die Betreuung vor Ort. Natürlich gilt mein Dank auch allen anderen Lithoz Mitarbeitern, die mich herzlich aufgenommen und unterstützt haben, besonders Altan der ebenfalls als Diplomand bei Lithoz tätig war. Natürlich möchte ich mich auch bei allen anderen Mitgliedern der Forschungsgruppe Makromolekulare Chemie bedanken. Nicht nur für das angenehme Arbeitsklima und die ständige Bereitschaft mich fachlich zu beraten und zu unterstützen, sondern auch für das freundschaftliche Klima außerhalb des Labors. Besonderer Dank gilt Christan Gorsche und Daniel Bomze die zu jeder Zeit für Fragen und Probleme zur Verfügung standen.

Meinen Eltern Karin und Agah gilt mein Dank für ihre Motivation und Beistand während meiner gesamten Studienzeit.

Zu guter Letzt will ich meinem Verlobten Josef danken, ohne dessen Geduld und Unterstützung ich es nicht bis hierher geschafft hätte. Mit dir an meiner Seite kann ich alles erreichen.

Im Gedenken an Branislav Hùsar

Table of Content

Abstract.....	3	
Zusammenfassung.....	4	
Danksagung.....	6	
Introduction.....	9	
1 Bone Replacement.....	9	
2 Tissue Engineering.....	13	
3 Additive Manufacturing Technologies.....	22	
4 Photopolymers.....	30	
5 Thiol-Ene Chemistry.....	34	
Objective.....	37	
General.....	39	
1 State of the Art.....	39	
2 Selection of Formulations.....	48	
3 Synthesis of Monomers.....	54	Exp.
3.1 Synthesis of O,O'-(hexahydrofuro[3,2-b]furan-3,6-diyl) divinyldipate (GDVA).....	54	90
3.1.1 Optimizing GDVA synthesis.....		91
3.1.2 Upscaling GDVA synthesis.....		92
3.2 Synthesis of O,O',O''-((propane-1,2,3-triyltris(oxy))tris(ethane-2,1-diyl)) trivinyl triadipate (EGDVA)...	55	94
3.2.1 Upscaling EGDVA synthesis.....		
3.3 Synthesis of dipentaerythritol divinyl adipate (DPDVA).....	56	96
3.3.1 Upscaling DPDVA synthesis.....		
4 Photoreactivity.....	59	
4.1 Photo-DSC.....	59	99
4.2 FTIR-ATR Measurements.....	64	101

4.3 Photorheology.....	67	102
5 Nanoindentation.....	77	104
6 Degradation Studies.....	83	104
7 Lithography-based Ceramic Manufacturing.....	87	105
Conclusion.....	109	
Materials & Characterization Methods.....	114	
Abbreviations.....	123	
Literature.....	127	

Introduction

1 Bone Replacement

Natural human bone, even though it comes in all kind of shapes like flat plates to tiny irregular structures, has the same overall structure. It is a natural composite consisting in lags parts of collagen nanofibers (with diameters from 50-500 nm) reinforced with nanocrystallin hydroxylapatite (nano-HA, 4 nm diameter).¹ Generally bones can be divided into two types according to their architecture: cortical (or compact) bone and cancellous (or spongy) bone. The mechanical properties of those two types are shown in Table 1.^{2,3}

Table 1: Mechanical properties of cortical and cancellous bone

	Young's modulus [GPa]	Tensile strength [MPa]	Compressive strength [MPa]	Bending strength [MPa]
Cortical bone	15-20	50-150	100-200	250
Cancellous bone	0.1-2	-	2-20	-

A healthy human body consists of 206 bones of various shapes and sizes. About 80% of an adult skeleton is made up of cortical bone with about 10-30% porous inner structure. Its function is to maintain stability and support the body weight as well as protecting the inner organs. The remaining 20% of the human skeleton is formed of cancellous bone with a porosity varying from 30-90%. Inside this spongy structure lies the bone marrow which is constantly reproducing our blood cells. To achieve cell proliferation and nutrition flow, spongy bone has distinct porosity in a size range between 50 and 100 μm of interconnected pores.⁴ When it comes to manufacturing bone grafts there is always a balance between smaller pores, providing a bigger surface for cell proliferation and bigger pores that enable vascularization, flow of nutrients, oxygen and degradation products of the scaffold.⁵ For the matters of bone tissue engineering an optimal pore size of 325 μm was recommended.⁶ This of course has a massive impact on mechanical properties,

therefore materials have to be found that show sufficient mechanical stability and still have the desired degradation behavior and porosity. Depending on the application degradation time can vary from 9 months or more for spinal fusion and 3-6 months for cranio-maxillofacial applications.⁴

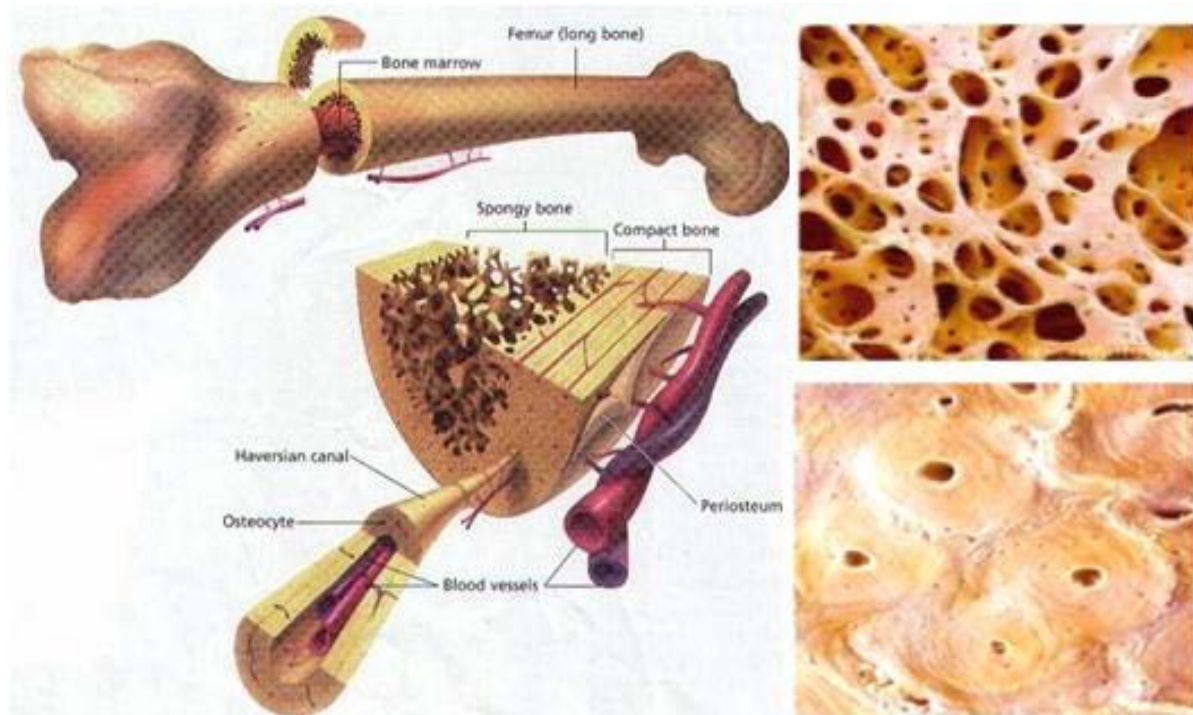
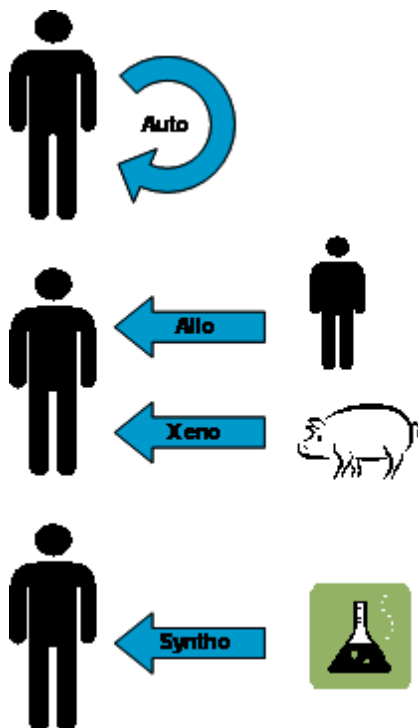


Figure 1: left: structure of human bone; right-top: SEM image of cancellous bone; right-bottom: SEM image of cortical bone

There are basically two processes present in natural bone tissue, namely bone remodeling and fracture healing. Bone has a very high regeneration capacity and is capable of repairing itself without the forming of scar tissue. This can be very impressively observed in embryonal and infant development. The skeleton of an embryo is mainly made up of cartilage and at birth the body consists of about 270 bones which further grew together during adulthood. The transformation or replacement of cartilage with bone is carried out by osteoblasts.⁷ When they are activated they start to form the organic bone component, called osteoid, mainly consisting of collagen, while present calcium phosphate starts to crystallize and form hydroxyl apatite. Most of those osteoblasts die along this process and some of them

get embedded into the bone tissue and transform into osteocyte. While the formation of new bone tissue mainly takes place during early adolescence and after injuries, bone remodeling is a constant process of optimization also taking place in adults. Bone tissue undergoing this process is broken down by osteoclasts and rebuilt. This mechanism is triggered by hormones controlling the blood's calcium levels. The osteoclasts create acidic conditions after attaching to the bone tissue and therefore degrade it whilst releasing minerals and other molecules stored in the bone matrix into the blood. Afterwards osteoblasts start to form new bone tissue.⁸

Thanks to these two mechanisms a healthy human skeleton is capable of repairing quite well but after major injuries bone replacements have to be used to substitute damaged natural bone in both structure and function. Depending on their origin replacements are divided into auto-, allo- and xenografts.



Autografts are considered the golden standard originating from the patient's own body and therefore bearing no risks of immune response. The main disadvantage is

that is requires another surgical site and many patients suffering from bone-related diseases lack sufficient material to be taken. Also risks like blood loss, infections and nervily damage have to be concerned.

Replacements taken from other human donors are called allografts. There is no second surgical site needed but the graft will cause an immune reaction forcing the patient to take suppressing medication.

Xenografts are taken from animals like pigs obviously also carrying the problem of immune reaction.⁹

If none of those are available or suitable synthetic grafts are used. Such artificial bone replacements can either be non-degradable, like many ceramics and metals/alloys or they can degrade during the regeneration of the natural bone. Non-degradable parts like plates, pins and screws often remain in the patient after bone healing which can later on cause problems and further surgeries.¹⁰ Therefore degradable implants are desirable that can be tailored considering structure and properties.

2 Tissue Engineering

The interdisciplinary field of tissue engineering (TE) combines medicine, biology, material science, chemistry and others to gain artificial grafts that can be used to replace or repair damaged tissue like bone, skin, blood vessels or cartilage.¹¹ Starting in the 1950s with inert materials that are basically not repelled by the body, nowadays so called third-generation biomaterials are supposed to induce tissue regeneration.¹² A more precise term that is often used in literature is Tissue Engineering and Regenerative Medicine (TERM)¹³.

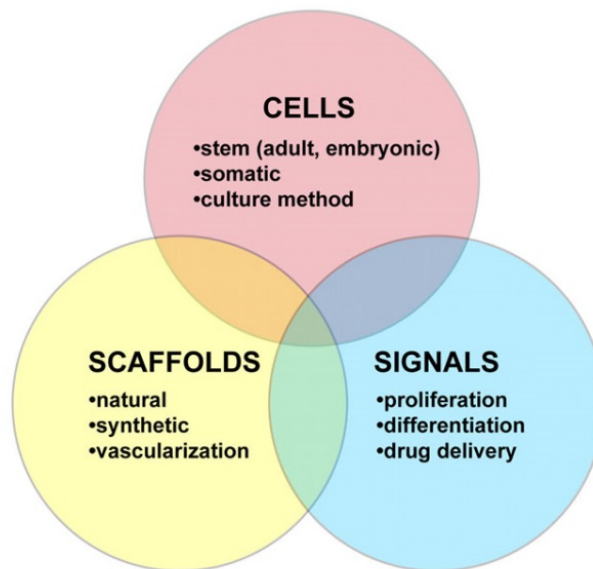


Figure 2: Main “pillars” of tissue engineering

There are generally two possible ways to achieve these ambitions.

One could either grow the needed tissue outside a biological environment prior to implantation, which is called the *in vitro* approach, or else directly implant a degradable scaffold into the damaged tissue of the patient following the *in vivo* approach. The *in vitro* pathway has the disadvantage of rather low “off-the-shelf” availability, which is critical for patients in emergency situations. To use this *in vivo* approach a biocompatible and biodegradable scaffold material is needed which is structured via suitable manufacturing techniques. A customized scaffold is

generated which is afterwards infused with nutrients and growth factors, seeded with cells and finally implanted into the patient.

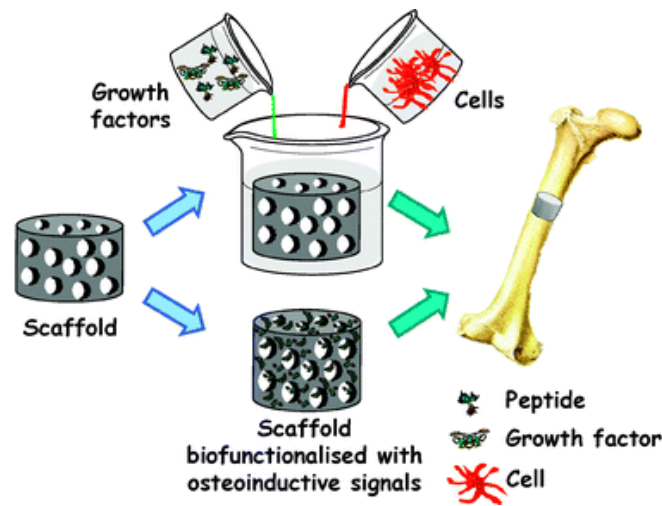


Figure 3: Schematic ways to create a synthetic bone graft (upper path: in vitro, lower path: in vivo)¹²

This implant should temporary take over the function of the damaged tissue and lead to tissue regeneration / formation of new tissue. It also should degrade over time in a about the same amount of time the new tissue is formed.

These scaffolds are quite challenging to produce because they not only are directly in contact with living cells and bio-factors but must also provide suitable mechanical properties and degradation behavior.⁴ Here the right manufacturing technique plays a critical role. As mentioned earlier porosity has a huge influence on cell-ingrowth and nutrition transport, therefore the fabrication method must be able to generate such structures with sufficient resolution.

2.1 Bone replacements

Still autologous bone transplants count as golden standard when it comes to bone replacements being the second most transplanted tissue of all.¹⁴ Recent developments though are promising alternatives to natural bone without its disadvantages like additional surgical sites, availability and rejection reactions.

Metals and Alloys

Implants made out of metals and alloys have been used since the beginning of the 20th century. They show high compressive strengths and very good fatigue resistance. Tantalum (Ta) based implants for example has been proven corrosion resistant and bioactive in vivo and porous scaffolds have been produced using Laser Engineered Net Shaping (LENS).¹⁵ Also Ta coated titanium (Ti) surfaces show enhanced cellular adherence and growth compared to the pure Ti surface.¹⁶ One drawback is that these kinds of implants are not biodegradable and there are concerns due to the release of metal ions.

Ceramics

Among different calcium phosphates (CaPs), Hydroxyl apatite (HA) and tricalcium phosphate (TCP) are widely used in restorative dentistry, orthopedics and maxillofacial surgery. These basic materials are amorphous or crystalline and are very similar to natural apatite which makes up about 60-70% of natural bone.¹⁴ Ceramics derived from HA are usually non-degradable and can be manufactured out of natural sources like corals (*Pro Osteon*TM) or synthetic ones (Synatite®, Cerabone®, Cerapatite®).¹⁴ Both HA and TCP ceramics can be manufactured via sintering processes or LCM. TCP scaffolds are able to degrade whereas the α -modification shows faster degradation than the β -modification and is therefore not very suitable for long-term implants. Due to the fact that β -TCP is completely reabsorbed by the body it improves the properties of pure HA implants regarding bone regeneration. Therefore combinations of those two materials are currently in the focus of research.¹³

Biopolymers

Commonly used polymers for bone tissue engineering occurring in nature are mainly collagen, alginate, silk, fibrin, chitosan and hyaluronic acid.¹⁷ These materials show several interesting properties such as strong bioactivity, ability to provoke cell adhesion, low immunogenic potential and chemical versatility.¹⁰ Disadvantages are a

high batch to batch variability as well as problems regarding quality and purification of the natural compounds.⁹

Bioglass

Bioglasses are amorphous, inorganic materials derived from acidic oxides such as aluminum oxide and silicon dioxide. Starting from resorbable 45S5 Bioglass® several bioactive glasses have been developed since (Novabone®, PerloGlas®).¹⁸ Such bioactive glasses are conditioned in a way that, upon contact with body fluids, they deposit carbonate-rich apatite layers.⁹ Through the chemical structure degradability, bioactivity and mechanical properties can be adjusted.¹⁹ A big drawback is the rather poor mechanical stability and low fracture toughness of most bioglasses. Also the flexural strength between 40-60 MPa is too low for many applications.²⁰

Synthetic Polymers

They combine properties like degradation and bioactivity with advantages of highly tunable mechanical and chemical properties. Also they are accessible through a variety of processing techniques. Synthetic polymers can roughly be divided into degradable/bioactive and non-degradable/bioinert polymers. Most widely used degradable and bioactive synthetic polymers in the biomedical application are poly(ϵ -caprolactone), poly(α -hydroxy acids), poly(carbonates), poly(propylene fumarates) and poly(anhydrides).¹⁰ Also resorbable polymers like poly(lactic acid), poly(vinyl alcohol) and poly(glycolic acid) are frequently used, especially in drug-delivery systems. A problem with degradable polymers is bulk erosion. This is caused by the release of acidic degradation products into the surroundings of the scaffold which leads to a locally decreasing pH-value which catalyzes further degradation and can also lead to tissue irritation and necrosis^{21, 22}.

Common non-degradable and inert polymers that are used for bone replacements are poly(ethylene) in all its modification (LDPE, HDPE, UHMWPE), poly(ethylene terephthalate), poly(tetrafluoroethylene), poly(urethane) and poly(methyl-)methacrylates. The latter is often used as autopolymerizing bone cement for fixation

of implants and suffers major drawbacks due to heat release during polymerization and shrinkage.²³

Composites

Often the desired properties for an implant can't be achieved by a single material. Composites consist of two or more distinctly different materials such as polymers and ceramics. By for example creating an interconnected CaP-polymer scaffold, advantages from both materials can help to reach mechanical and physiological requirements.⁴ Often improvements regarding mechanical properties like rigidity, stiffness and toughness are of interest.⁹ Usually such composites developed for biomedical application are composed of a continuous matrix (often a synthetic- or bio-polymer) and a reinforcement phase (mainly inorganic; particles, fibers, whiskers or lamellas). The term *nanocomposite* applies to mixtures with one of the phases having dimensioning below 100 nm.¹ There are three possible combinations of matrix and reinforcement materials:

organic/organic (for example synthetic polymers like PVA reinforced with collagen fibers)

inorganic/inorganic (CaPs and silicates, though not a composite in strict sense)

organic/inorganic (polymer matrix reinforced with inorganic particles, fibers etc.)

The latter are also topic of this work and show promising developments during the last years as shown by the work of Dorozhkin et al.²⁴, Rezwan et al.²⁵ and Murugan u. Ramakrishna²⁶. They resembles the natural bone structure best, which itself is a composite of organic matrix material (collagen) and inorganic reinforcement (CaP and HA).² The most prominent CaPs used are hydroxyl apatite (HA) and tricalcium phosphate (TCP as α and β polymorphs). Using these filling materials result in the ability to form bonds with the host tissue resulting in a strong interface.²⁷

Currently used for surgical purpose are composites of poly(lactide) or poly(glycolide) with CaP-fibers.¹⁴ Also selfhardening composites consisting of methacrylates like

bis-GMA with inorganic fillers are used as bone cements. They are applied in regions with high mechanical stress but are non-degradable and suffer rather low bioactivity.¹⁴

2.2 Shaping Methods

There are a number of methods used to shape suitable scaffolds, all with their advantages and disadvantages. Roughly they can be divided into non-Additive Manufacturing Techniques and Additive Manufacturing Techniques. Since this work is interested in composite materials the methods listed below are those also capable of producing porous nanocomposites.

Foam replica method uses polymeric foams (usually polyurethane) that are impregnated with an aqueous suspension until all the pores are filled. After the excessive suspension is removed via centrifugation the structure is dried then slowly heated up to 300-800°C resulting in decomposition of the polymeric template. Finally the scaffold is sintered to densify the structure.²⁸

Solvent Casting and Particulate-Leaching is a combination of two methods resulting in 3D porous scaffolds. During this process a salt is dissolved in an organic solvent together with a polymer. The solvent is removed resulting in a solid polymer with embedded salt crystals. Those salts are then leached away using water leaving pores in the polymer that can be controlled over the polymer/salt ratio.²⁹

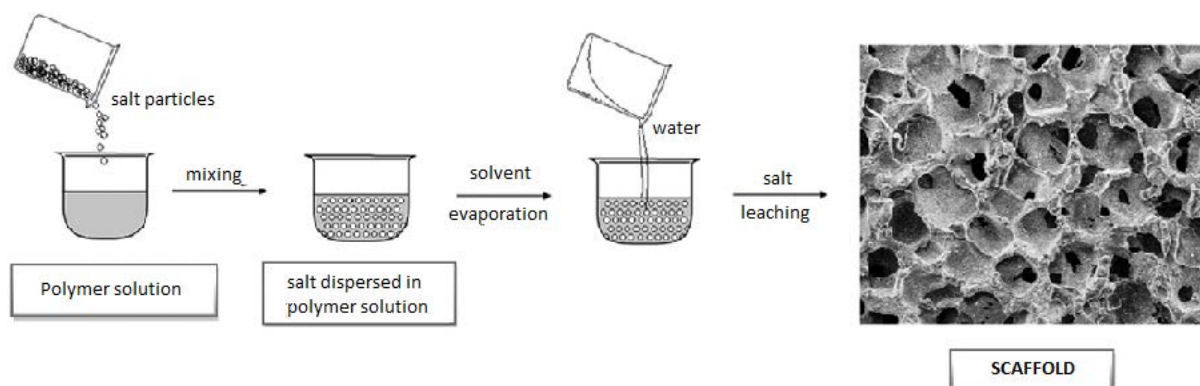


Figure 4: Scaffold preparation using solvent casting combined with salt leaching technique³⁰

Freeze Drying or lyophilization creates pores by dehydration under vacuum. To control the resulting porosity, the polymer is dissolved in a solvent with added water and frozen at different temperatures, allowing the formation of ice crystals with different size. The frozen material is dried under reduced pressure to remove water and solvent, leaving pores in the polymer.³¹

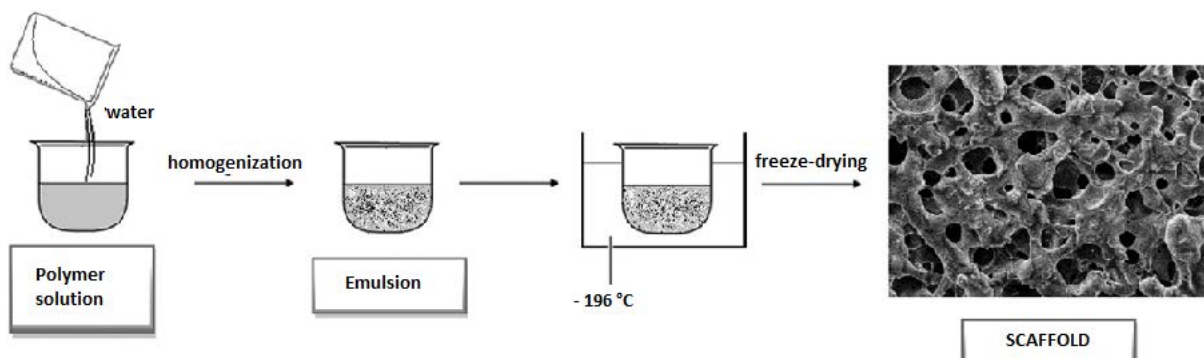


Figure 5: Scaffold preparation using emulsion freeze-drying technique³⁰

Gas Foaming uses high pressure CO_2 gas that is dispersed into a polymer mixed with a porogen like sodium chloride until saturated. When the pressure is reduced to atmospheric level the solubility of CO_2 rapidly decreases resulting in nucleation and gas bubble formation.³²

Phase separation is based on a system wanting to lower its free energy by separating into more than one phase. In case of polymers there are usually two phases, a polymer-rich, which solidifies when the solvent is removed, and a polymer-lean phase. To achieve uniform pore distribution the separation conditions have to be controlled precisely.³³

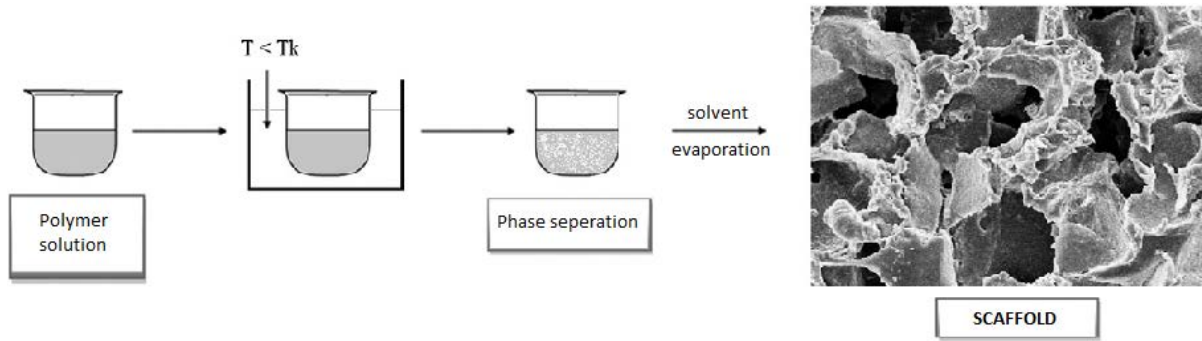


Figure 6: Scaffold preparation using thermally induced phase separation technique³⁰

Electrospinning creates non-woven polymer nanofibers through a high electric field. Between two electrodes the polymer solution is injected via a needle initiating a jet due to the electrostatic forces. The fibers deposit on a grounded collector forming a scaffold with interconnected pores. Adjusting the field strength influences the resulting polymer structure.³⁴

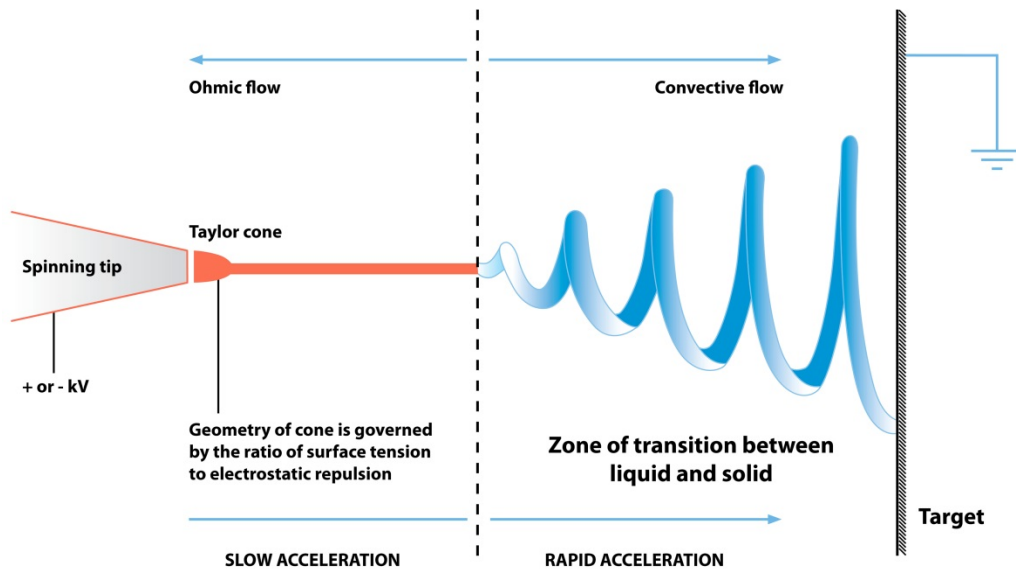


Figure 7: Fiber formation by electrospinning³⁵

Rapid Prototyping or Additive Manufacturing Technology uses computer generated data like Computer Tomography (CT), Magnetic Resonance Imaging (MRI) or Computer Aided Design (CAD) data to create objects with arbitrary structure.³⁶ The scaffold is usually produced in a layer-by-layer manner which allows precise control of geometry, pore size and interconnectivity. The next paragraph will go more deeply into the topic of AMT considering it a promising method to create the desired scaffolds.

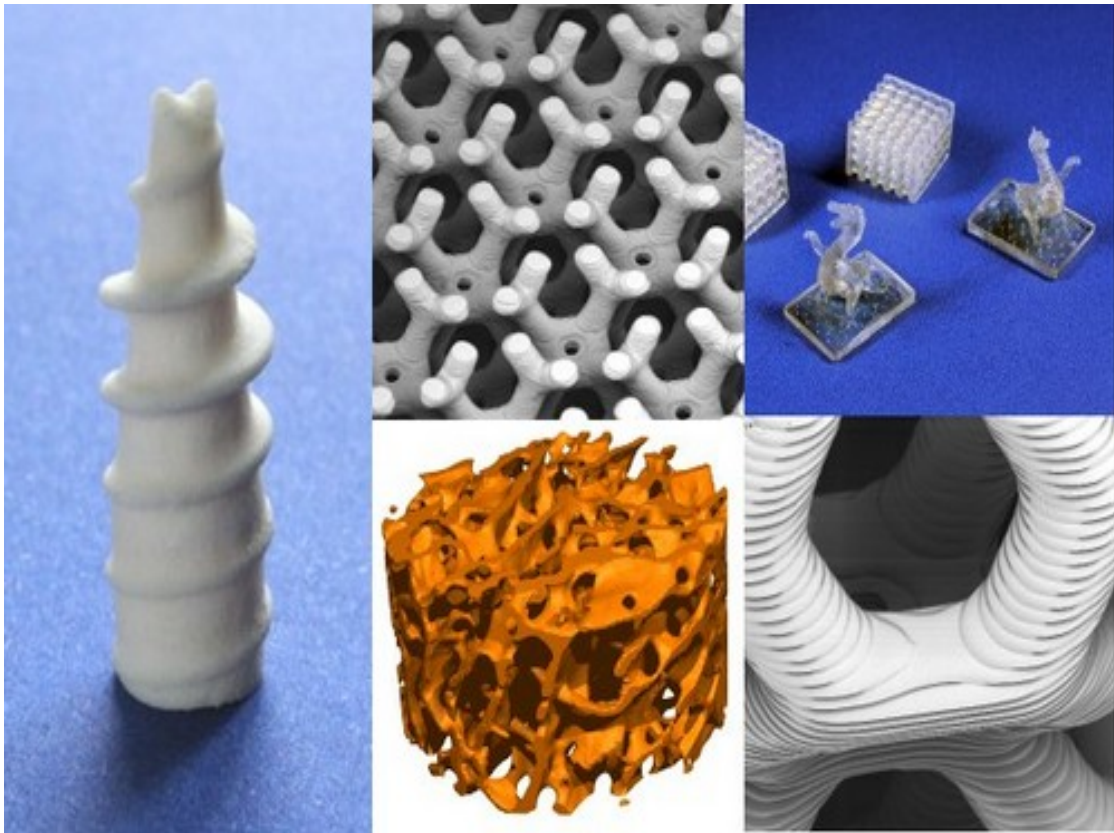


Figure 8: Parts created by AMT³⁷

3 Additive Manufacturing Technologies (AMTs)

This term along with Solid Freeform Fabrication (SFF) and Rapid Prototyping (RP) synonymously describes methods to create 3-dimensional objects without molds or casts. The big advantage of those techniques is that complex 3-dimensional structures can be fabricated with very high feature resolution without needing an expensive mold, which makes it the ideal way of generating single-lot production lines. Also does neither cost nor production time grow significantly with the part's complexity. Most AMTs work with a layer-by-layer concept which makes them not really 3D rather than 2½D-processes with a fixed height in the z-axis. The overall concept is shown in Figure 9.

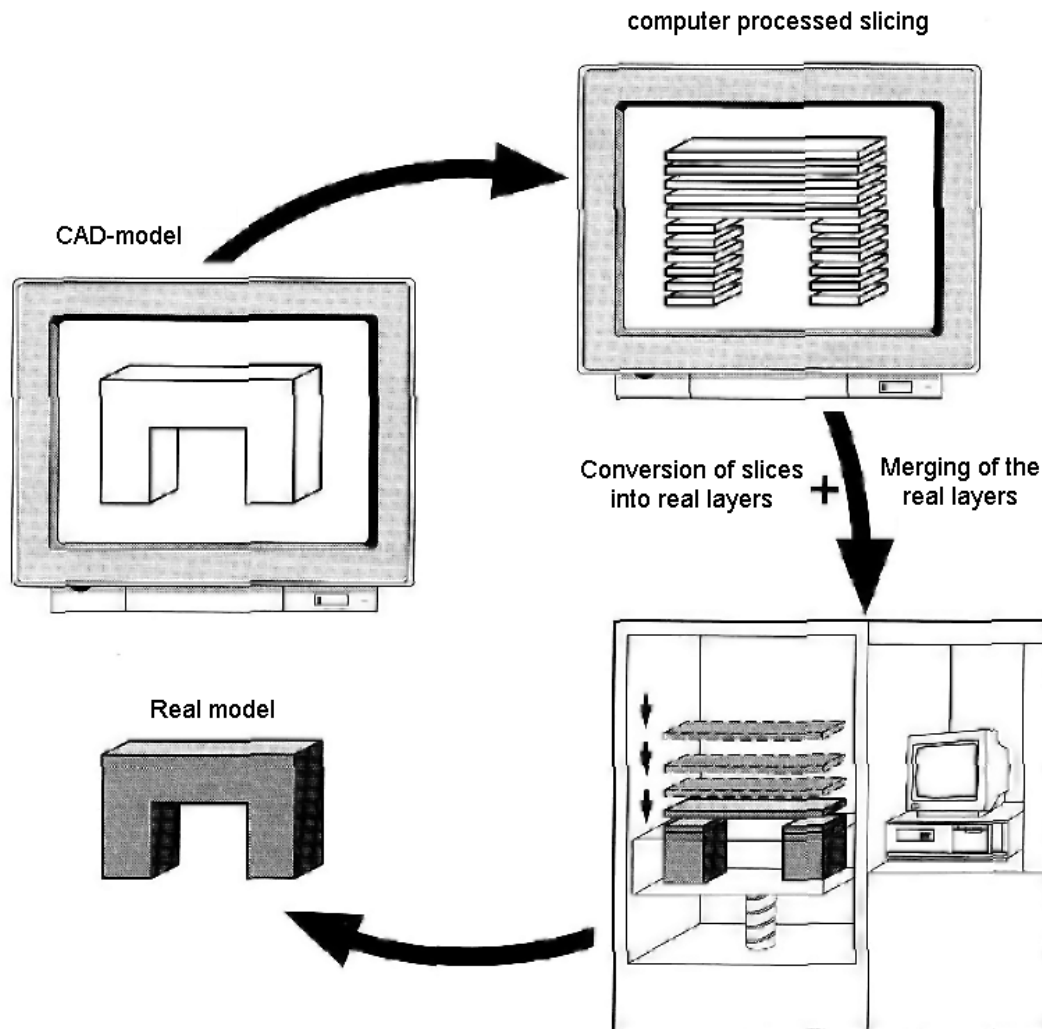


Figure 9: Principle of AMT layer-by-layer technology³⁸

Further information on this topic is provided by Hutmacher et al.³⁹, Leong, et al.⁴⁰, Gibson et al.⁴¹ and Gebhardt³⁸.

Usually AMTs are categorized regarding the underlying mechanism of the solid material formation:

- Solid sheets techniques
- Melt techniques
- Processing of particles and powders
- (Photo)polymerization-based methods

All of these techniques have in common that they work without tools or molds and the parts are built in a layer-by-layer manner and furthermore the complexity is virtually unlimited which are the main advantages compared to traditional manufacturing methods.

Solid sheet techniques

This method produces parts by stacking layers of foil or paper with individual cross-section on top of each other and then binds them together

Laminated Object Manufacturing (LOM)

With this method 3D-models can be obtained rather simply. The individual layers are cut out of typically paper but also other materials like metal or polymer foils. Every sheet is coated with a thermally activated adhesive that is activated by a heated roller to bond the layers together. Usually the layers are cut out using a laser. Advantages are low cost, a simple procedure and the ability to create larger objects. Main disadvantages are inferior and anisotropical mechanical properties as well as poor resolution.

Solid Foil Polymerization (SFP)

Here, unlike in LOM, sheets of partially polymerized materials are used a feedstock. Usually the layers solidify and connect via exposure to UV-light and the uncured parts act as support structures if necessary. After finishing the building process uncured material is removed by a suitable solvent.

Melt techniques

Here the processed materials are heated above their melting temperature and solidification occurs upon cooling of the material.

Fused-Deposition Modeling (FDM)

This technique is based on extrusion, where the layers are produced by melting and extruding the respective polymer locally. Due to heat conductivity of the polymer upon deposition the individual layers are connected to form the final part. To build overhanging parts supporting structures are needed but nonetheless it's a very efficient method when it comes to material consumption. Basically any thermoplastic polymer can be processed such as ABS or poly(lactic acid) which is a big advantage. The rather poor resolution and high surface roughness compared to SLA for example are a drawback of this method.

Ballistic Particle Manufacturing (BPM)

This method basically shoots small droplets of molten feed material onto a movable substrate and those droplets solidify when hitting the substrate. Temperature is here a critical parameter because too hot droplets will cause the structure to loose shape when they hit and droplets that are too cold will not bond sufficiently with the previous layers. This method is used for the processing of metals, profiting from a very fine grain structure due to the immediate solidification which keeps the amorphous structure of the metal.

Shape Deposition Manufacturing (SDM)

SMD is rather noteworthy upon RP methods because it combines AMT principles with conventional machining. The material is first deposited in near-net shape for the first layer and afterwards machined to the desired geometry. If needed, supportive material is added for the next layers. After this the layers get shot-peened resulting in lower residual stresses and a smooth surface. The main advantages are high accuracy and a good surface finish but the involving machining steps making this procedure time consuming and raise the production costs.

Processing of particles and powders

As the title intends these AMTs use grains of different sizes and shapes as feed material. Either by the input of energy to sinter or melt the granules or by the application of a liquid binder those particles are bond together. Usually the binder is removed after structuring by high temperature or solvents to obtain better mechanical properties.

Spatial Forming (SF)

Here photopolymerization is combined with the usage of inks containing (metal or ceramic) particles. In the first step a negative shape is printed using a ceramic pigmented ink that is curable by UV-light exposure. After the mold has reaches a certain height is it filled with the virtual ink which contains the metal particles. The structure is cured and milled flat afterwards and thereafter the whole sequence is repeated several times to give the desired 3D object. Resolutions of about 8µm have been reported for this AMT.⁴²

Selective Laser Sintering (SLS)

This technique is based on lithography with a laser beam scanning the surface of the feed material, similar to SLA which is explained later on. The feed consists of a powder bed of small granules between about 20-50 µm diameter. The laser beam starts so sinter the particles together upon hitting them, forming the desired structure. Because the remaining powder supports the structure during the building process no additional supportive structures are needed. Another advantage of this method is the ability to process advanced thermoplastic materials like ABS or polyamides (PAs) and even metals. This makes SLS a very capable AMT-methodology able to produce the toughest components. The limitations and drawbacks of this technology are high acquisition costs, rather low accuracy compared to stereolithography and high shrinkage that results from the high processing temperature.

Laser Engineered Net Shaping (LENS)

This method is quite similar to SLS. The solid material is obtained by deposition of a powder that is simultaneously melted by a laser beam and solidifies under cooling. The mechanical properties of the resulting material are nearly identical to the intrinsic compounds but the surface is very rough and usually requires machining operation as a finishing step.

3D-Printing (3DP)

Basically 3D-Printing can be seen as a hybrid of FDM and SLS. A print head is used to jet a binder onto a powder bed. Wherever this binder comes in contact with the particles they bind together and form a solid material. This method gives access to a broad range of composites by the variation of powder and binder; still this cheap method is mainly used to create prototypes for visual aid rather than functional parts.

(Photo)polymerization-based methods

The following techniques have in common that they are based on the concept of in-situ converting a liquid to paste-like resin into a solid. This can occur either via thermal excitation or upon irradiation with light.

Stereolithography (SLA)

Though the oldest technique in this section, SLA is still benchmark for resolution and precision among AMTs. This photopolymerization-based method uses a laser beam that scans the surface of a vat containing the liquid resin. Polymerization takes place only where the light directly hits the photosensitive resin resulting in a layer of desired shape. After curing one layer like this the whole structure is moved downwards and the top of the previously cured layer is coated with fresh resin. By repeating this procedure over and over finally a 3D-part is obtained. The main disadvantage of this method is that the resulting polymers have rather poor mechanical properties compared to thermoplastics. Also the presence of air on the surface during the polymerization can cause problems due to oxygen inhibition.

Digital Light Processing (DLP)

Also based on photopolymerization, this method simultaneously cures a whole layer using a digital light processor. Also the irradiation takes place at the bottom of the resin-filled vat, excluding ambient oxygen. Compared to SLA it is faster and also more economic regarding cost of the equipment and material consumption. Unfortunately it doesn't reach comparable resolution and surface quality. Also, like all AMTs on the base of photopolymerization, the achievable mechanical properties are limited. In this work a further development of this technique was investigated; working around these limitations by using Lithography-based Ceramic Manufacturing (LCM) to create composites of organic photopolymers and inorganic particles.

Solid Ground Curing (SGC)

SGC is another method using photopolymerization also irradiating a whole layer simultaneously but unlike DLP a previously prepared mask is used. This mask is printed on a glass plate and has to be changed for every individual layer. Also for each layer the resin has to be sprayed onto the building platform and uncured resin has to be removed after polymerization and replaced with wax before a new sequence can be started. The wax works as supportive structure and is removed after the whole process is finished. High equipment costs and considerable consumption of polymer are the main disadvantages of this technique and also oxygen inhibition can be an issue.

Polyjet™-Technology

This technology is basically a hybrid between a conventional UV-based AMT and an inkjet printer as known from office application. In contrast to SLA or DLP no selective photopolymerization of a homogeneous monomer layers takes place but it selectively deposits the resin for the whole layer similar to a flatbed UV-printer. To fabricate 3D parts multiple layers are deposited on top of each other in the same manner. The main advantage is the possibility to deposit different materials at the same time. For example a wax-like supportive structure can be printed alongside

with the respective resin allowing the fabrication of complex geometries not feasible by other AMTs.

Liquid Thermal Polymerization (LTP)

Based on thermally induced polymerization this method uses laser in the infrared region of the electromagnetic spectrum. Apart from that it is akin to SLA. The polymerization is induced where the laser hits the resin. Main problems with this approach are thermal shrinkage, heat dissipation and distortion of the cured parts.

Two-Photon Induced Polymerization (2PP)

This is one of the most recent developed methods on the base of photopolymerization. It can be called a true 3D-process because, unlike other techniques which assemble 2D layers to create an object, the focal point of the laser “writes” in a volume of polymerizable resin using ultrashort laser pulses. After the whole object is printed in this manner unpolymerized resin is removed and the final part is obtained. The non-linear principle of 2PP allows resolution beyond the diffraction limit offering great potential for the production of structures with exceptional feature resolution on the smallest length scales.

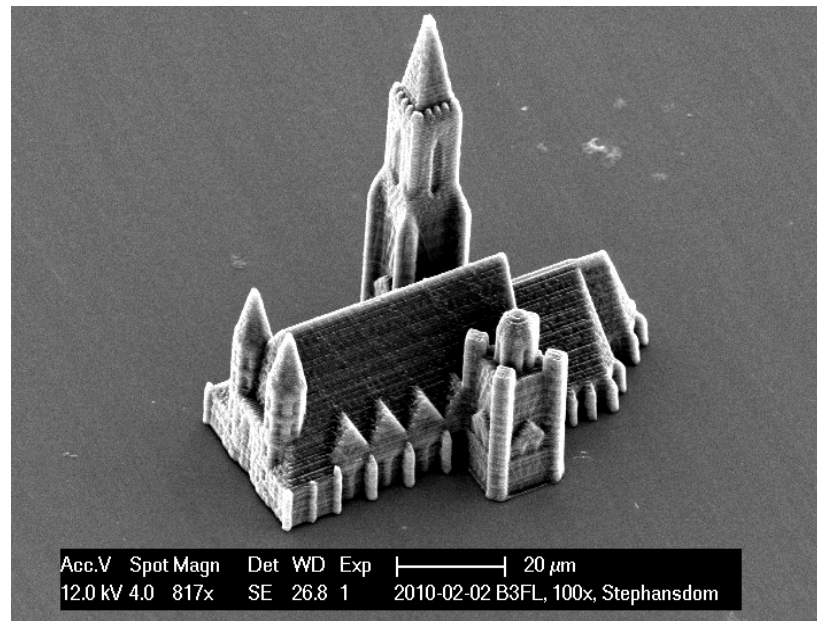


Figure 10: St. Stephens cathedral, Vienna⁴³ made by 2PP

Lithography-based Ceramic Manufacturing (LCM)

This technology enables the production of precise and dense ceramic parts by using a photolithographic process. A slurry containing a photocurable resin and ceramic particles is cured with methods similar to DLP providing high accuracy combined with economic material consumption. Afterwards the green part is sintered to remove the photopolymer and obtain a dense ceramic object with density of over 99.4% and 4-point bending strength of almost 430 MPa.⁴⁴ Although such properties can be achieved through conventional methods LCM is especially interesting for prototype manufacturing and high precision application. Within this work a new application was investigated by using this technique to obtain biodegradable ceramic parts. This can be done by not removing the used photopolymer after the process. Remaining in the final part the cleavable bonds in the polymer can undergo hydrolytical degradation releasing the inorganic particles into the surroundings. This method combines the advantages of DLP regarding economic means and speed with the possibility of grafting high precision porous structures of degradable organic/inorganic composites.

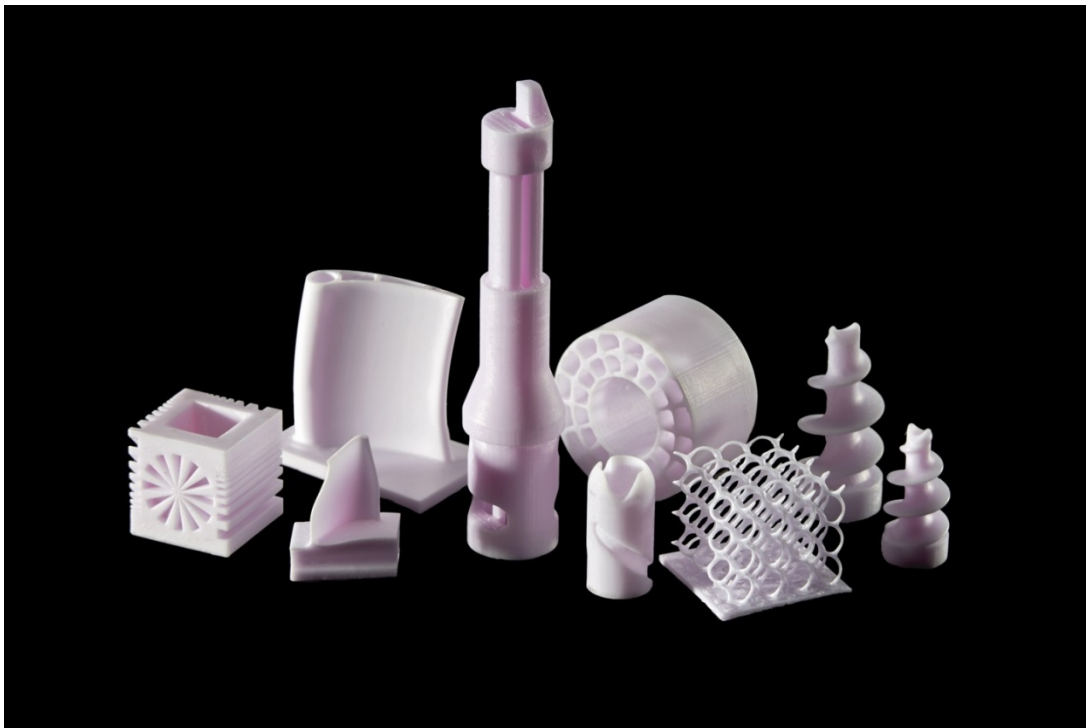
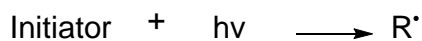
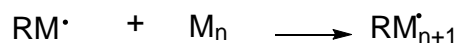


Figure 11: Several parts manufactures by using LCM

4 Photopolymers

Per strict definition a photopolymer is a polymeric material that is sensitive to light and changes its properties upon irradiation with light of a certain wavelength. An extended definition, used in many scientific publications, describes a polymeric material, which has been fabricated by means of photopolymerization starting from a liquid or past-like monomer formulation or resin. Photopolymerization is based on chemical reactions that involve light excitation by photons from UV-, visible (VIS)- or near-infrared (NIR)- range. There are a number of economic and ecological advantages compared to conventional thermal polymerization. Usually the used formulations are solvent-free and non-polluting and the polymerization can be done at room temperature (RT) which means low energy requirements and low costs. The main problems are oxygen inhibition and rather costly monomers. Another disadvantage was that due to the absorption of light by additives of the formulation, photoinitiator by-products or the resin itself, photopolymerization was limited to the fabrication of thin layers. Fortunately, new technologies and developments in chemistry solved this problem and lead to an expansion into the fields of Additive Manufacturing Technologies (AMT), allowing to produce three dimensional structures.

During photopolymerization the respective resin formulation is cured by using a photoinitiator (PI) that undergoes photolysis – it cleaves upon irradiation and produces free radicals. These radicals add to a reactive, polymerizable monomer starting a chain reaction. Next step, the propagation, is a continuously repeated addition of monomer to the growing polymer chain. Via recombination or disproportionation the polymerization process is terminated.

Initiation**Propagation****Termination**

combination



disproportionation

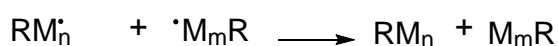


Figure 12: Mechanism of photopolymerization

Photoinitiators

Beside the chosen monomer or monomer mixture the used photoinitiator is a key substance for the formulation. It converts radiation energy from UV or visible light to start the radical reaction and also influences both the curing speed and the properties of the resulting polymer. Therefore several variables have to be considered when choosing a photoinitiator such as monomer chemistry (functionality, reactivity), light source (UV, LED) and in case of 3D printing especially curing speed⁴⁵. Since the desired application lies in the medical field, substances remaining in the polymer matrix have to be considered because they might diffuse to the polymer surface over time or leach into the body during degradation. So also for the photoinitiators biocompatibility and cytotoxicity is very important⁴⁶. Bryant et al. investigated cytotoxicity of 4 common UV photoinitiators, Irgacure-907, Irgacure-651, Irgacure-184, Irgacure-2959 and 2 visible light systems consisting of Camphorquinone (CQ) / 4-N,N-dimethylaminobenzoate (DMAB) and

CQ/Triethylamine (TEA)⁴⁷. It has shown that the major influences on cytotoxic behavior are hydrophobicity and concentration of the photoinitiating system.

Radical photoinitiators can be categorized in two types according to their photofragmentation. This could either occur as a result of α -cleavage (Type I) or through hydrogen abstraction or electron/proton transfer from a donor molecule (Type II).

Usually the Type I α -cleavage takes place next to the carbonyl group. Typical Type I initiators are benzoin ethers, dialkoxy acetophenones, hydroxyalkyl phenones and morpholine ketones. Figure 13 shows the principle mechanism of an α -cleavage process where two reactive species are generated to initiate the polymerization.

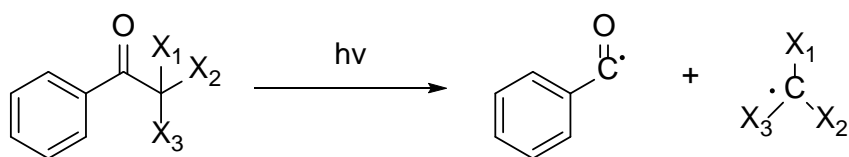


Figure 13: Mechanism of Type I Photoinitiator

Type II initiators are bimolecular and form radicals through hydrogen abstraction from a co-initiator by electron-proton transfer. Examples for such initiators are benzophenones, thioxanthenes, ketocoumarines and camphor quinones. Amines are often suitable donors. They transfer an electron to the excited ketone and form a radical ion pair intermediately. In a second step the reactive radicals are generated by proton transfer. Figure 14 shows the mechanism on the example of CQ/DMAB which is used for biomaterial applications.⁴⁸

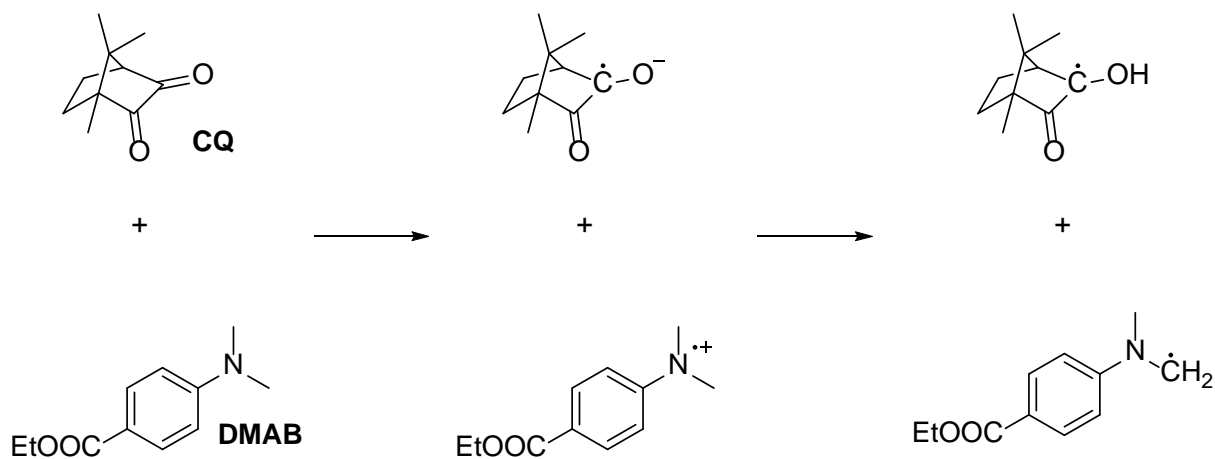


Figure 14: Mechanism of Type II photoinitiator

Due to its biradical character oxygen can cause inhibition of the photopolymerization. It attaches to the reactive ends or induces hydrogen abstraction which terminates the propagation as shown in Figure 15.

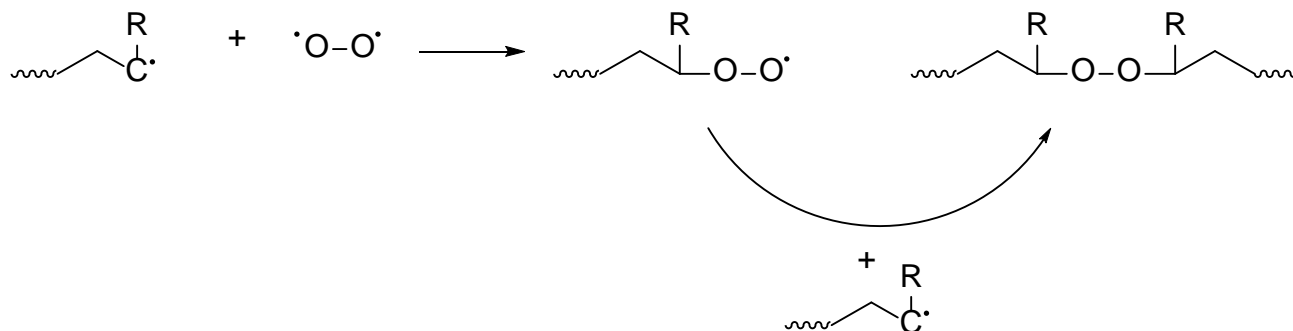


Figure 15: Inhibition due to oxygen

The problem with oxygen inhibition is that lower double bond conversion can result in highly unwanted migratables in biomedical application due to danger of side reactions in vivo as well as poor mechanical properties. Adding multifunctional thiols to the system is one way to overcome this problem which was also investigated in this work.

5 Thiol-Ene Chemistry

Thiol-ene reactions fulfill most of the criteria for a so called “click” reaction, which is described as simple, high yielding, easily cleaned by non-chromatographic methods, regioselective and stereospecific, insensitive towards water and oxygen, done under mild, solventless or aqueous conditions.⁴⁹

The thiol-ene mechanism involves 2 steps, first the addition of a thiyl radical, formed by the cleaved photoinitiator, to an unsaturated carbon-carbon bond (the ene component) in an anti-Markivnikov way forming a carbon-centered radical, second the abstraction of hydrogen of a thiol by this radical.⁵⁰ In an ideal system in the absence of ene-homopolymerization these two steps strictly alternate. The mechanism is shown in Figure 16

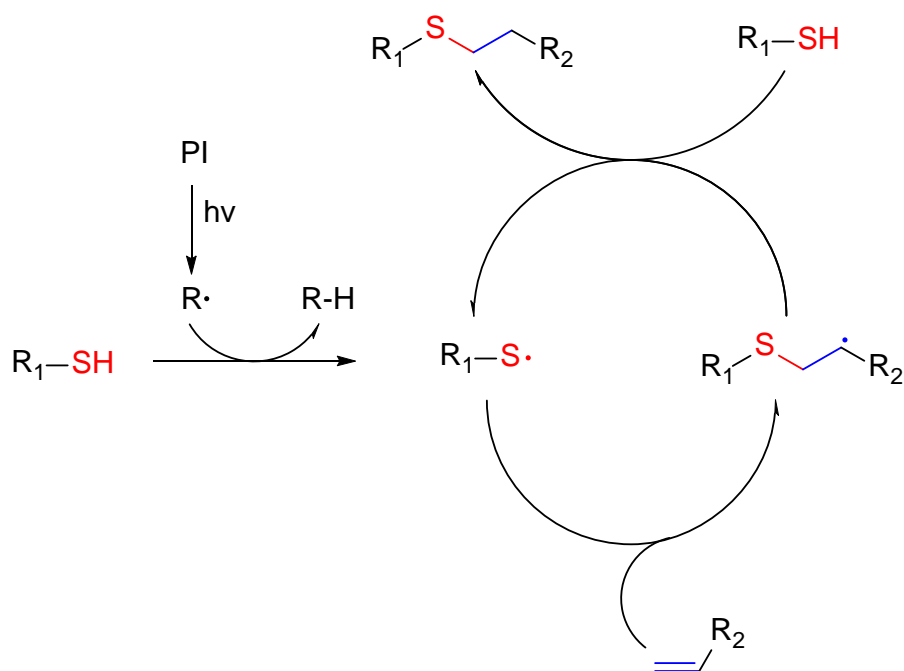


Figure 16: Idealized thiol-ene photopolymerization cycle

As previously mentioned, oxygen inhibition is quite a big problem in photopolymerization. But in the case of the thiol-ene reaction, peroxy radicals are able to abstract hydrogen from the thiols, creating a highly reactive thiyl radical that can propagate further chain transfer reactions, as shown in Figure 17.⁵¹ Only 1-10% of thiol is sufficient to reduce oxygen inhibition significantly.⁵²

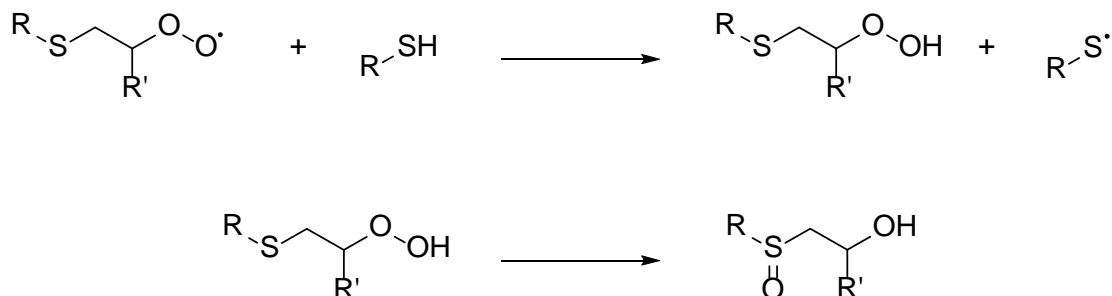


Figure 17: Formation of hydroperoxides in presence of thiols and rearrangement to β -hydroxy sulfoxide

Compared to conventional homopolymers thiol-ene polymers have other important differences regarding physical and mechanical properties. These significantly altered behavior results from the different polymerization mechanism leading to a step-growth like mechanism by alternating propagation and chain-transfer. When monomers like (meth)acrylates are used, that are capable of undergoing radical homopolymerization, the step-growth like polymerization is in concurrence with the acrylate chain growth of the homopolymer. Those systems are in literature sometimes referred to as thiol-acrylate systems and are depicted in Figure 18.

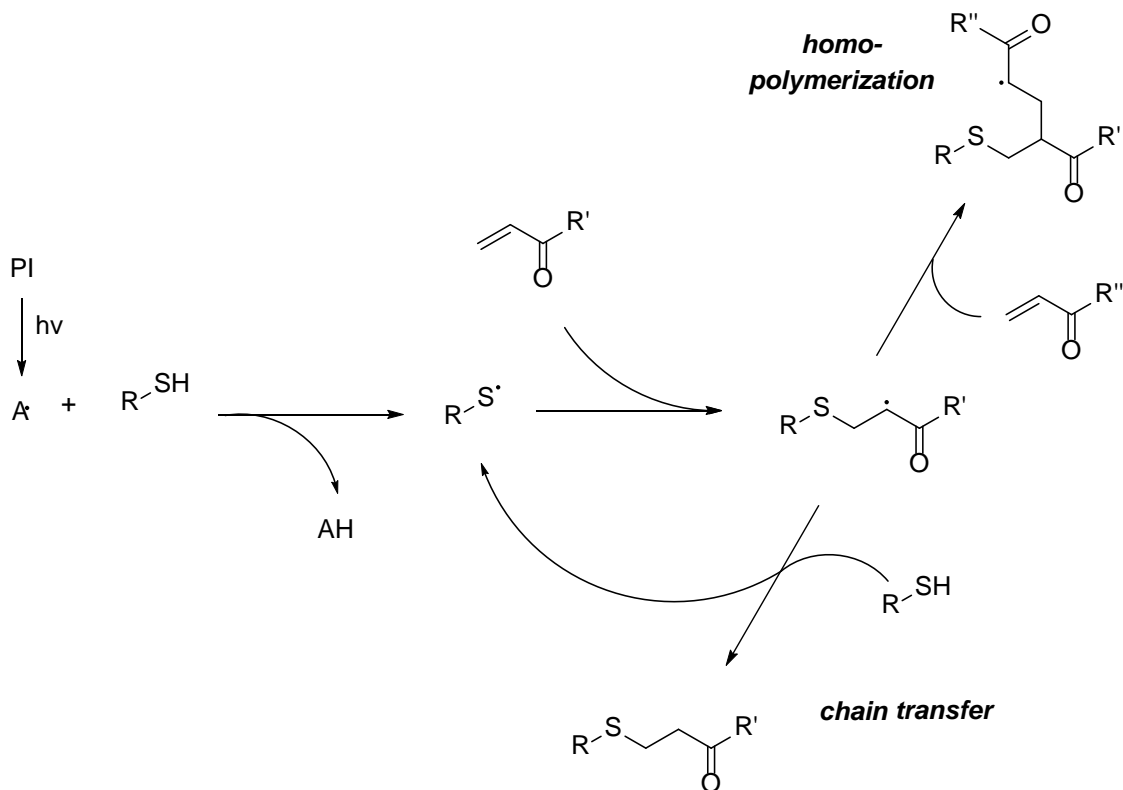


Figure 18: Thiol-acrylate mechanism

As Result of this step-growth like mechanism a delay of the gel point during polymerization can be observed and the resulting polymers show highly homogeneous polymer architecture as well as reduced shrinkage by approximately 40% compared to conventional polymers.⁴⁹ This results in reduced shrinkage stress in the final material leads to a better mechanical performance. The limitations of this concept lie in the change of the network architecture to a point where negative effects on hardness, stiffness or heat resistance occur due to a loose network.

Other drawbacks of thiol-ene polymerization are quite low shelf stability of the formulations as well as bad smell of most thiols.

In theory any ene can be used in thiol-ene polymerization; nonetheless there are quite huge differences regarding reactivity. Because electron density has a main influence on reactivity, monomers with high ene electron density such as vinyl esters are the most reactive species towards a thiol-ene reaction.⁵³

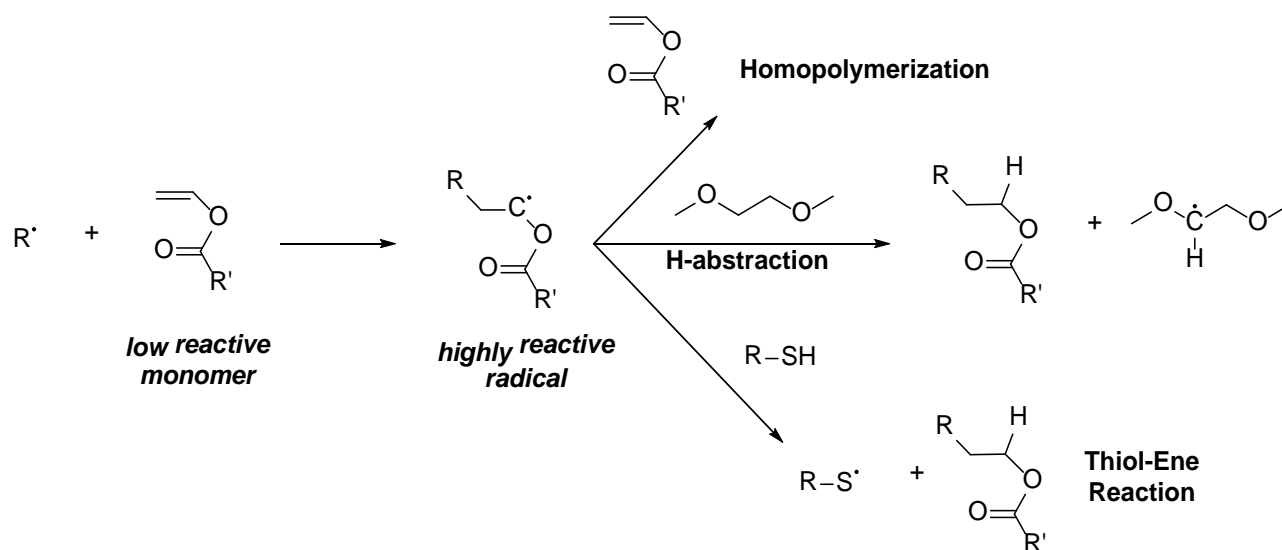


Figure 19: Thiol-vinyl mechanism

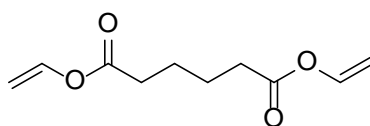
Objective

Regenerative Medicine and Tissue Engineering (TERM) are promising ways of sustaining a healthy body up to high ages. The ability to repair tissue defects by creating objects like scaffolds and bio-implants is highly desirable. Additive Manufacturing Techniques (AMT) are one approach to create 3D objects with high resolution (pore structure, geometry, wall thickness) that are suitable, custom made scaffolds. To use AMT methods based on photopolymerization, photosensitive resins are necessary which are irradiated with UV light to build complex structures in a usually layer-by-layer manner. Frequently used monomers for photopolymerization are acrylates and methacrylates. Unfortunately, when it comes to biomedical application, they show major drawbacks like poor biocompatibility and cytotoxic effects and, in the case of methacrylates, rather low photoreactivity.

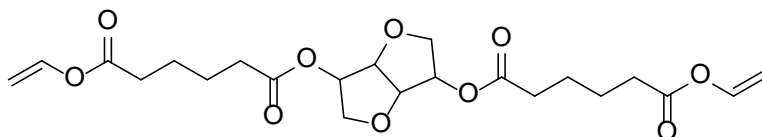
As an alternative, vinyl esters are suitable monomers that have proven to be 2-3 orders of magnitude less cytotoxic than acrylates. Their disadvantage lies in a rather poor photoreactivity, but in combination with thiol-ene chemistry this property can be significantly improved.

The Lithography-based Ceramic Manufacturing (LCM) technique provides another way of improvement. By incorporation of inorganic particles photopolymer composites with enhanced mechanical properties can be built.

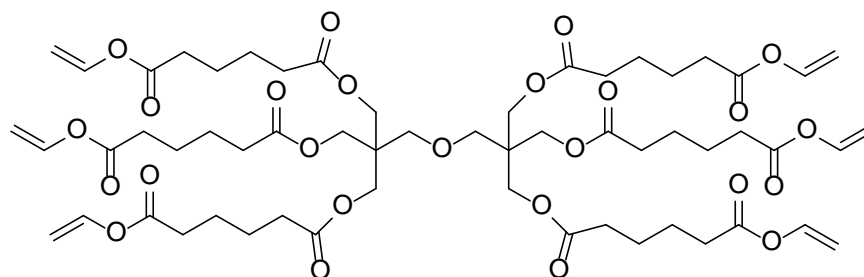
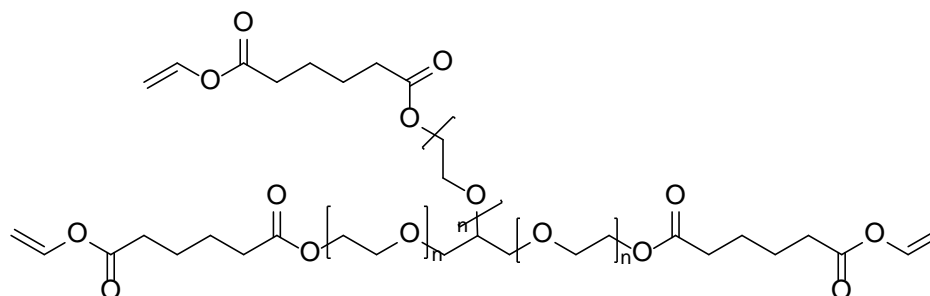
The aim of this work is to verify the application of both the thiol-ene chemistry and the LCM technology for potential bone replacements using commercially available thiols in combination with different multifunctional vinyl esters.



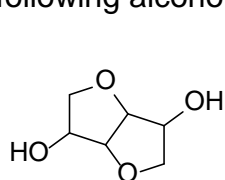
divinyl adipate (**DVA**)



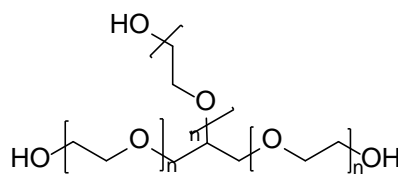
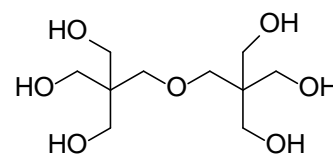
O'-O'-(hexahydrofuro[3,2-*b*]furan-3,6-diyl) divinyl diadipate (**GDVA**)

dipentaerythritol divinyl adipate (**DPDVA**)O'-O', Oⁿ-((propane-1,2,3-triyltris(oxy))tris(ethane-2,1-diyl)) trivinyl triadipate (**EGDVA**)

To achieve these targets, investigations should be done on two pathways. The first part is to synthesize new multifunctional vinyl esters, because only divinyl adipate (DVA) is commercially available. Therefore a transesterification reaction with the lipase CAL-B (*Candida Antarctica*) has to be optimized towards yield and purification. Three different vinyl esters should be synthesized based on the following alcohols:



dianhydro-D-glucitol

ethoxylated glycerol
n=6-7

dipentaerythritol

Afterwards photoreactivity of the monomers should be determined via photo-DSC, photorheology and FTIR-ATR measurements.

The second part should concentrate on additive manufacturing. This includes manufacturing parts with LCM technology, rheology studies, mechanical analysis such as nanoindentation and investigation of the degradation behavior.

General

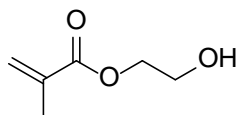
1 State of the Art

1.1 Photopolymers for Bone Tissue Engineering

Various photocurable polymers are used in tissue engineering both of natural and synthetic origin. Both bring along several advantages and disadvantages and selections have to be made depending on the desired application. The following section should give an overview of currently used in Tissue Engineering and Regenerative Medicine to obtain porous scaffolds.

Proteins

A prominent representative of this type of photopolymer is modified gelatin. Gelatin is the irrepressible hydrolyzed form of collagen, usually gained from bone and/or tendons of cows or pigs, in which reactive groups can be introduced via free amino groups of lysine units and free carboxylic groups of glutamic and aspartic acid. Modified with methacrylic anhydride (MAA) gelatin as reported by Chen et al. and Schuster et al. is only soluble in water and forms brittle hydrogels due to a high amount of hydrogen bridges along the amide backbone.^{54, 55} Reactive diluents have been used to add flexibility to these systems and disrupt the hydrogen bridges leading to improved mechanical properties.⁵⁶ Via DLP a 3D scaffold has successfully been produced made from waterborne resin consisting of modified gelatin, poly(ethylene glycol) dimethacrylate and hydroxyethyl methacrylate.⁵⁵ Furthermore soft hydrogels were processed by 2PP from methacrylated gelatin with high resolution of 1.5 μm . Stem cells seeded onto these scaffolds differentiated as expected upon osteogenic stimulation.^{57, 58}



hydroxyethyl methacrylate (**HEMA**)

Polysaccharides

Based on glycosaminoglycan, hyaluronic acid is present widely throughout connective tissues. It is usually modified with MAA⁵⁹, 2-isocyanatoethyl methacrylate (ICEMA), 2-aminoethyl methacrylate (AEMA)⁶⁰ or GMA.⁶¹ It can also be modified with a primary hydroxyl group of the photoinitiator I2959 by reaction of a carboxylic group.⁶² Mechanical Properties of scaffolds based on hyaluronic acid can be adjusted over a broad range from 10^2 to 10^5 Pa via the concentration of crosslinker and the degree of substitution.⁶¹

Also part of current research is chitosan, a linear polysaccharide composed of randomly distributed β -(1-4)-linked D-glucosamine and N-acetyl-D-glucosamine. Thanks to the reactive free amino group in the polymer backbone photoreactive groups, such as GMA⁶³, ethylene glycol acrylate methacrylate (EGAMA)⁶⁴ or azidobenzoic acid (AZBA)⁶⁵ can be attached. Qiu et al. modified chitosan with a methacrylic group for photoreactivity and a benzoyl group for improved solubility and were able to produce scaffolds via salt leaching.⁶⁶ Those scaffolds were seeded with fetal bovine osteoblasts and showed good biocompatibility and osteoconductivity after being implanted subcutaneously in rats.

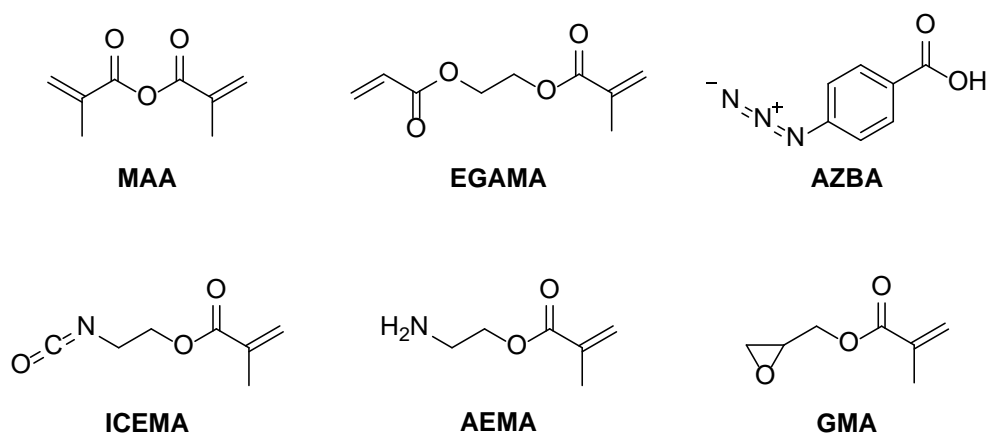
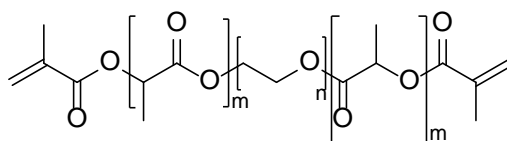


Figure 20: Typical reagents used to introduce photoreactive groups

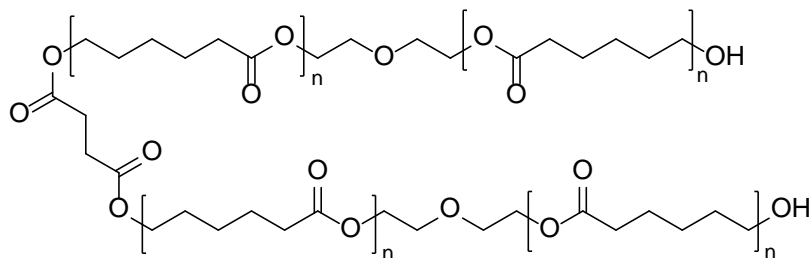
Polyesters

Polyesters derived from naturally occurring hydroxyl acids like lactic, glycolic and caproic acid, are state-of-the-art materials for biomedical application. For example BioScrew[®] and Bio-Anchor[®] are commercial products used for orthopedic fixations made of L-PLA and RapidSorb[®] is made of poly(L-lactide-co-glycolide). Photopolymerizable PLA for bone tissue engineering has mainly been studied in Anseth's group. Already 3D scaffolds with 80% porosity were prepared by salt leaching.⁶⁷⁻⁶⁹ Davis et al. stated that 3D shaping by AMT of PLA should be done at elevated temperature because the melting point of macromers with a molecular weight of about 2000 Da is slightly above room temperature.⁷⁰ The main degradation products of such polyester networks upon hydrolysis are poly(meth)acrylic acid, lactic acid and oligo(ethylene glycol).⁶⁸ Unfortunately degradation takes place in a bulk erosion mechanism leading to massive decrease of mechanical properties in rather short time.⁷¹ Another problem with those polymers is cytotoxicity. Mild inflammation was observed for subcutaneously implanted films⁶⁸ as well as scaffolds implanted in the craniums of rats.⁶⁷



dimethacrylated PLA-*block*-PEG-*block*-PLA

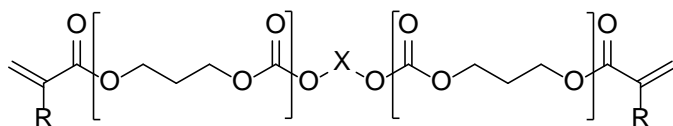
As alternative to acrylated PLA Wang et al. investigated a block copolymer of PLA and poly(norbornene) (PNB) with cinnamate pendant groups synthesized by ring-opening polymerization of lactides.⁷² The PNB block enhances the mechanical properties while PLA bestows biocompatibility. Another rather rarely used alternative is poly(ϵ -caprolactone) (PCL), because of its slow degradation rate. Blending of poly(ϵ -caprolactone fumarate) (PCLF) with diethyl fumarate (DEF)⁷³ or N-vinyl pyrrolidone (NVP)⁷⁴ not only enables photocuring at room temperature but NVP also increases double bond conversion and degradation rate due to increased hydrophilicity.



poly(ϵ -caprolactone fumarate) (**PCLF**)

Polycarbonates

A biocompatible and mechanically tough elastomer which is already used in tissue engineering is poly(trimethylene carbonate) (PTMC). It is used for biodegradable orthopedic tacks and screws (Acufex[®]) and flexible suture material (Maxon[®]). PTMC is usually prepared via ring-opening polymerization of trimethylene carbonate in the presence of catalyst followed by end-capping with photoreactive groups like (meth)acrylate⁷⁵, coumarin⁷⁶ or phenylazid.⁷⁷ The molecular weight of the initial macromere has big influence on the mechanical properties of PTMC resulting in elastic modulus up to 8 MPa.⁷⁵ It is notable that PTMC as well as PTMC-co-PCL undergo surface erosion mechanisms, resulting in almost constant mechanical properties during degradation⁷⁶⁻⁷⁸. Cell culture experiments with endothelial cells show no apparent cytotoxicity for PTMC networks.⁷⁹

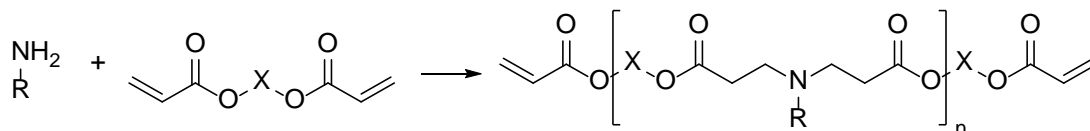


acrylated **PTMC** (R=H)
methacrylated **PTMC** (R=Me)

Poly(β -amino ester)

Synthesized via poly-Michael addition reaction of diacrylates with primary or secondary amines, poly(β -amino ester)s (PBAE) are biodegradable linear polymers. They have an excellent cytotoxicity profile and are already used in polymeric gene delivery.⁸⁰ Anderson et al. synthesized a large combinatorial library of liquid PBAEs

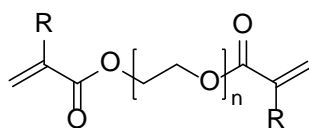
with various degradation profiles and elastic moduli (4-350 MPa).⁸¹ When implanted subcutaneously, mild inflammatory reactions were observed.⁸²



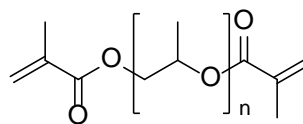
Diacrylated poly(β -amino ester) from a primary amine

Poly(ethylene glycol)

This water-soluble polymer is already used in a wide range of biomedical applications. Due to its hydrophilic nature it is highly hydrates and effectively repels proteins.⁸³ Though when modified with specific signaling molecules targeted cells can attach while others at the same time can't do so. Reactive groups – usually acrylic (PEGDA) or methacrylic (PEGDMA) - can easily be incorporated via the reactive end groups of PEG. Because it is not hydrolysable only the ester bonds are cleavable. Mechanical properties and degradation behavior can be tuned via the oligomer chemistry. More flexible materials are obtained by using longer PEG chains whereas the rate of mass loss decreases with increasing hydrophobicity. Hydrogels with improved compression strength have been prepared by Killion et al. by adding PEGDMA to poly(propylene glycol) dimethacrylate (PPGDMA).⁸⁴ A PEGDMA-based composite with HA nanoparticles surface grafted with PEG monomethylacrylate has been proposed as bone substitute by Li et al.⁸⁵ Also PEG-based hydrogels were already shaped into scaffolds using SLA⁸⁶ or 2PP.⁸⁷



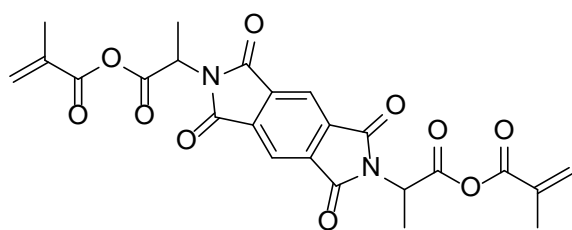
PEGDA (R = H)
PEGDMA (R = Me)



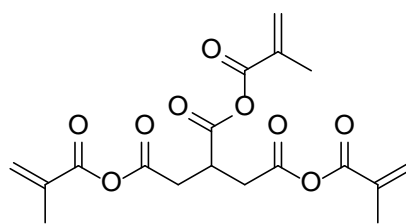
PPGDMA

Methacrylated anhydrides

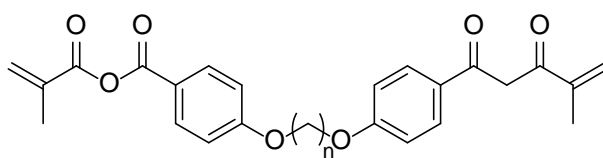
Polyanhydrides are already used in orthopedics and as drug-delivery systems and are FDA approved biocompatible and biodegradable polymers.^{88, 89} A large set of various dicarboxylic acids of natural or synthetic origin with hydrophobic spacers have been methacrylated by Muggli et al.⁹⁰ Anseth et al. developed a set of polymerizable anhydrides for injectable bone-cement application.⁹¹ By using monomers with a rigid spacer such as pyromellityl imidoalanine (MPMA-ala) or branched monomers such as tricarballic acid (MTCA), high elastic moduli of the resulting polymers were observed.⁹² Crosslinked networks release the original di- or triacid along with rather low molecular polymethacrylic acid upon degradation, resulting in a decrease of pH value in the tissue after implantation.⁹³ Still the degradation follows the surface erosion mechanism and can be adjusted from 2 days for polymerized methacrylated sebacic acid (poly(MSA)) to 1 year by using solely hydrophobic 1,3-bis(4-carboxyphenoxy)hexans (MCPH).⁹⁴ To prevent a drop of tensile modulus over degradation incorporation of CaCO_3 as filler has proven useful, also reducing acidity.⁹³ Li et al. added nanoneedle-like HA to improve mechanical properties by a factor of 3.⁹⁵



MPMA-ala



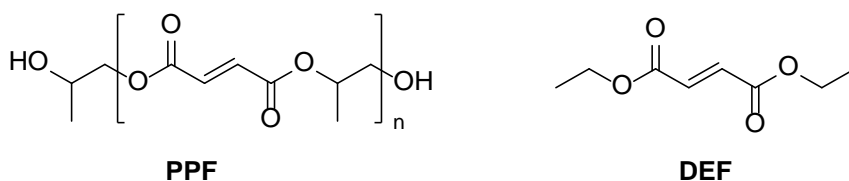
MTCA



MCPH n=4

Poly(propylene fumarate)

This biodegradable polyester is prepared by polycondensation of fumaric acid and propylene glycol. The polymer network forms upon radical crosslinking of double bonds along the polymer backbone. To be utilized in SLA the highly viscous PPF has to be diluted with diethyl fumarate (DEF) to reduce viscosity.⁹⁶ The resulting mechanical properties for photo-crosslinked PPF/DEF are comparable to natural bone (elastic modulus of 20-200 MPa and fracture strength of 20-70 MPa).⁹⁶ By reducing the DEF content even stronger materials can be obtained but with the drawback of decreased building speed.⁹⁷ Other ways to influence mechanical properties are PI concentration and the molecular weight of initial PPF.⁹⁸ Hydrolytical degradation results in propylene glycol, fumaric acid, and poly(fumaric acid), which can be excreted from the body. The main problem is autocatalytic degradation, caused by high concentration of acidic species, leading to rapid loss of mechanical properties.²⁵

*New polymers based on vinyl carbonates, vinyl carbamates and vinyl esters*

There is a great interest in replacing state-of-the-art monomers for photopolymerization like acrylates and methacrylates due to several disadvantages. Some (meth)acrylates are already used for dental application and bone cements but they show irritancy and cytotoxicity caused by Michael addition reaction with amino or thiol groups of proteins and amino acids.^{99, 100} Another problem is that upon degradation poly(meth)acrylates result in poly(meth)acrylic acid that can't be transported out of the body, leading to local decrease of pH value effecting the surrounding tissue and the further degradation behavior. To deal with these problems several alternatives have been investigated by Liska's group, namely vinyl carbonates, vinyl carbamates and vinyl esters.^{53, 101-106} Until now the radical crosslinking polymerization of these monomers has rarely been described and the

only biomedical applications are contact lenses and drug carrier systems. Regarding in vitro cytotoxicity with osteoblast-like cells these monomers have proven to be less cytotoxic than methacrylates by an order of magnitude and even 2-3 orders less than acrylates.¹⁰⁴ When it comes to photoreactivity, curing speed and final double bond conversion the vinyl monomers lie between acrylates and methacrylates meaning that they are sufficiently photoreactive to be employed in lithography-based AMTs. Although when abstractable hydrogens are present in the spacer the photoreactivity drops significantly. To overcome this low reactivity multifunctional thiols can be added.^{53, 106} A positive side effect of the lower reactivity is enhanced storage stability¹⁰² and with recent improvements in stabilization concepts also the thiol-ene formulations show great storage stability.¹⁰⁷ The mechanical properties are comparable to those of polyacrylates with the same spacers and all obtained polymers were significantly stiffer than PCL, reaching almost the same values as PLA. Another advantage shows upon degradation where poly(vinyl ester)s and poly(vinyl carbonate)s form low molecular weight neutral poly(vinyl alcohol) as degradation product, which is FDA approved.¹⁰² All this makes these new monomers suitable candidates for tissue engineering scaffolds.

1.2 AMT in Bone Tissue Engineering

Additive manufacturing techniques are a powerful tool for the application in tissue engineering. The ability to generate geometries of high complexity along multiple axes from different materials is nearly unmatched. Also the possibility to utilize medical imaging as basis for design and construction of scaffolds is a very big advantage.¹⁰⁸ A further gain of AMT is the combination of automation and flexibility in design. Also vascularization of tissue engineered bone is only possible in 3D proven by Hutmacher et al.¹⁰⁹ But though around for nearly half a century additive manufacturing for tissue engineering is still in its infancy.¹¹⁰

To create a tissue replacement via additive manufacturing several steps are followed. First the corresponding computer model is needed, generated either by 3D CAD software or a 3D scanner. The model is translated into an STL file, the current

standard file for faceted models.¹¹⁰ Then a suitable AMT is employed to create the scaffold for tissue engineering application.

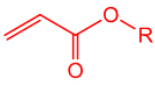
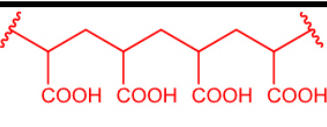
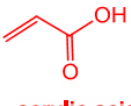

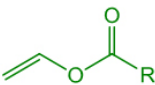
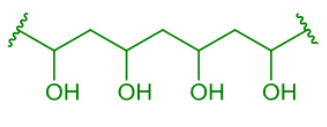
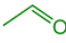
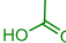
3D printing on the basis of inkjet technology for processing of powder materials was the first AMT employed for tissue engineering.¹¹¹ Because the process is done at room temperature the incorporation of growth factors is possible.¹¹² A problem of this technique especially towards bone tissue engineering is the fact that the pore size of the material is dependent on the powder size and often pores are closed by the stock material.⁴⁰ PCL and PCL-HA scaffolds with honeycomb-like structures have already been produced with different sizes of pores using the extrusion-based technique *FDM*.¹¹³ Shantz et al. showed that osteoid formation could be obtained with such scaffolds when they are previously seeded with periosteal cells under osteogenic conditions.¹¹⁴ With *SLS* Sudarmadji et al. were able to produce scaffolds with different structural configurations and porosity.¹¹⁵ Recently the application of *SLS* for nanocomposite scaffolds has been studied by Duan et al.¹¹⁶ showing the potential of composites through the combination of proper mechanical properties and good biocompatibility. *SL* has been utilized by several research groups; one in particular successfully investigated the capability of *SL* to fabricate multi material bioactive poly(ethylene glycol) scaffolds.¹¹⁷

Current problems are mainly limitations due to a lack of suitable polymers meeting the desired mechanical and chemical properties.

2 Selection of Formulations

Monomers

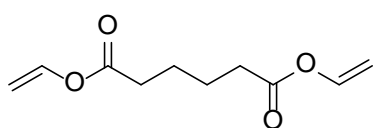
One part of this work was to replace state-of-the-art reactive groups for photopolymerization which are usually acrylates and methacrylates for the application in tissue engineering and regenerative medicine. They are highly reactive, show good storage stability and are processable without solvents which are good properties for AMT. But when it comes to biomedical application they lack suitable biocompatibility due to cytotoxic of the monomers and degradation products. Especially acrylates show rather high cytotoxicity (LC_{50} is 0.02 mM), and for methacrylates the values are still not very good (LC_{50} is 0.7 mM) (*in vitro* biocompatibility essay with osteoblasts and endothelial cells).¹⁰² The main problem are residual reactive double bonds which remain unprocessed after the preparation procedure of the scaffold, which can undergo Michael addition with free amino and thiol moieties in proteins and amino acids. Those unwanted reactions can cause irritation. Regarding degradation another problem comes up. Hydrolysis of (meth)acrylates results in poly(meth)acrylic acid with rather high molecular weight which cannot be transported within the body and therefore decreases the local pH-value causing inflammation reactions and bulk erosion.

Monomers	Main degradation products		Hydrolysed product of unpolymerized group
Acrylates		 high M_w poly(acrylic acid)	 acrylic acid 
Vinyl esters		 poly(vinyl alcohol)	 acetaldehyde $\xrightarrow[\text{in vivo pathway}]{\text{AcDH}} \text{NAD}^+ \rightarrow \text{NADH} + \text{H}^+$  acetic acid

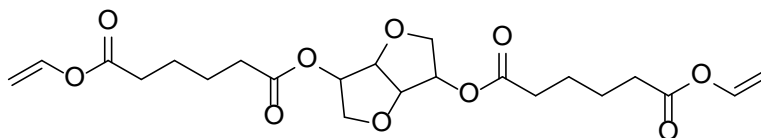
* AcDH=acetaldehyde dehydrogenase; NADH= nicotinamide adenine dinucleotide

Compared to (meth)acrylates unreacted double bond will have a significantly lower reactivity towards Michael addition reactions with amino groups of proteins and amino acids of the body resulting in lower cytotoxicity. The values of in vitro biocompatibility assays with osteoblasts and endothelial cells of DVA are $LC_{50} = 4.4 \text{ mM}^{102}$ which is 2 orders of magnitude lower than acrylate values.

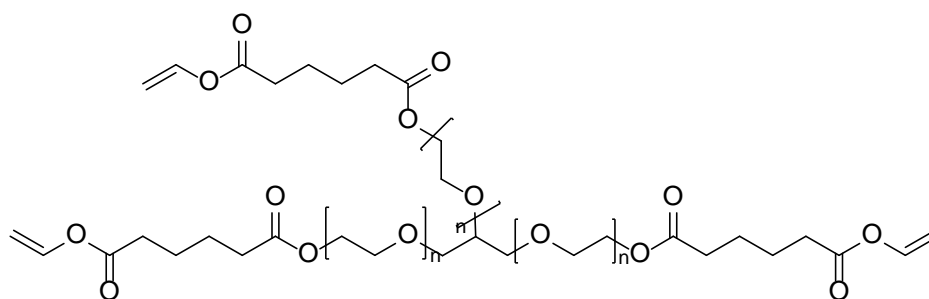
Whereas both degradation products of poly(vinyl esters), the poly(vinyl alcohol) and the acetic acid are FDA approved, also acetic acid is a very small molecule and can be easily transported out of the tissue. Because divinyl adipate (DVA) was the only commercially available multifunctional vinyl ester, three others were synthesized in addition via transesterification reaction. This gave access to a broader range of mechanical properties and degradation behavior. The synthesized vinyl esters were O,O'-(hexahydrofuro[3,2-b]furan-3,6-diyl) divinyl adipate (GDVA), O,O',O''-((propane-1,2,3-triyltris(oxy))tris(ethane-2,1-diyl)) trivinyl triadipate (EGDVA) and dipentaerythritol divinyl diadipate (DPDVA).



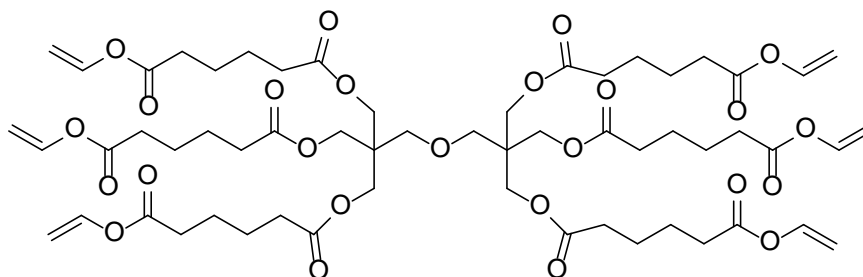
Divinyl adipate (**DVA**)



O,O'-(hexahydrofuro[3,2-b]furan-3,6-diyl) divinyl diadipate (**GDVA**)



O,O',O''-((propane-1,2,3-triyltris(oxy))tris(ethane-2,1-diyl)) trivinyl triadipate (**EGDVA**) $n=6-7$



Dipentaerythritol divinyl adipate (**DPDVA**)

GDVA was chosen because the synthesis is already established, providing a good starting point for optimization and up scaling. Also the bicyclic sugar molecule which was introduced as spacer is FDA approved. The monomer derived from ethoxylated glycerol (EGDVA) was chosen due to its rather flexible structure and the hydrophilic PEG-spacer, which are influencing mechanical properties as well as degradation behavior. Finally DPDVA with its star-shaped structure was synthesized to investigate the potential of dense crosslinking along with a large number of cleavable ester bonds. This again would influence mechanical properties and degradation behavior.

The reactivity of vinyl ester monomers is significantly lower compared to acrylates and can be further decreased in presence of abstractable hydrogens.¹⁰² The resulting propagating radical is not resonance stabilized and therefore highly reactive. Those radicals tend to abstract hydrogens from the formulation forming low reactive radicals in turn, rather than undergo homopolymerization. To prevent this, thiols can be added to the reaction formulation providing easily abstractable hydrogens and forming reactive thiyl radicals $RS\bullet$ after abstraction of these hydrogen by the propagating radical.

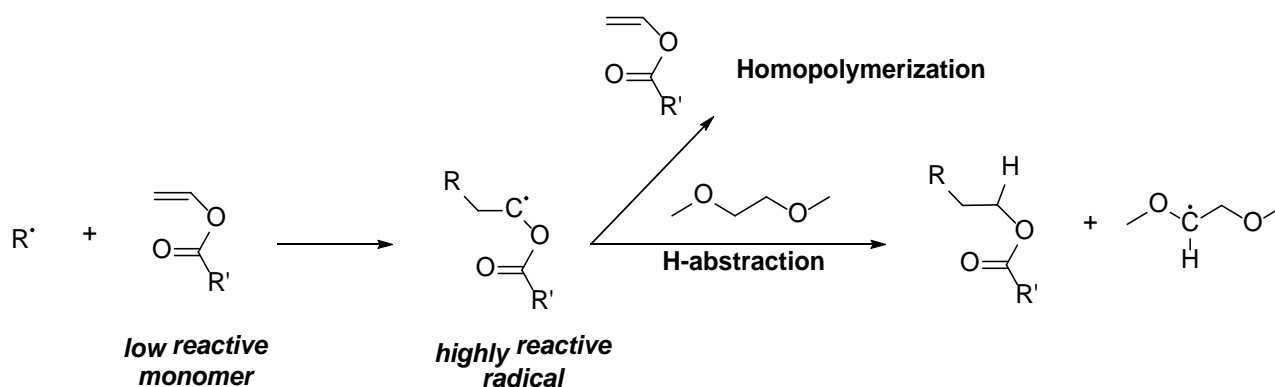
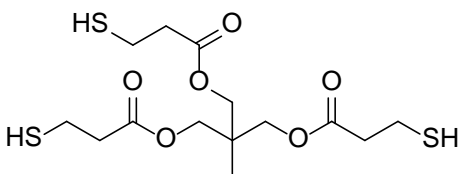


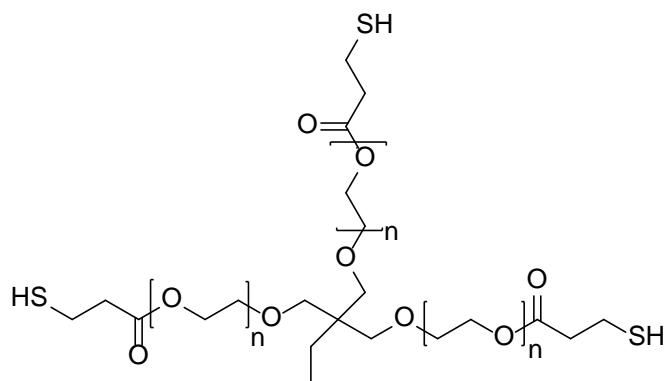
Figure 21: Reaction paths of vinyl esters in radical polymerization

For the applied thiol-ene mixtures a set of different thiols and vinyl esters were used. The thiols were used as received from Bruno Bock: Trimethylopropane tri(3-mercaptopropionate) (TMPMP) and two ethoxylated-trimethylopropane tri(3-

mercaptopropionates) with different molecular weights, one $700 \text{ g}\cdot\text{mol}^{-1}$ (ETTMP700) and one $1300 \text{ g}\cdot\text{mol}^{-1}$ (ETTMP1300)



Trimethylopropane tri(3-mercaptopropionate)
(**TMPMP**)



$n=2$ Ethoxylated trimethylopropane tri(3-mercaptopropionate) 700 (**ETTMP700**)
 $n=7$ Ethoxylated trimethylopropane tri(3-mercaptopropionate) 1300 (**ETTMP1300**)

They provided a variety in hydrophilicity, degradability and chain lengths, which influence degradation behavior and mechanical properties as well as network density.

Utilization of thiol-ene chemistry results in another positive outcome, producing homogeneous networks with enhanced mechanical properties. Therefore the introduction of thiols results in reduced crosslinking density, increased flexibility as well as higher toughness and an overall less brittle polymer.¹¹⁸

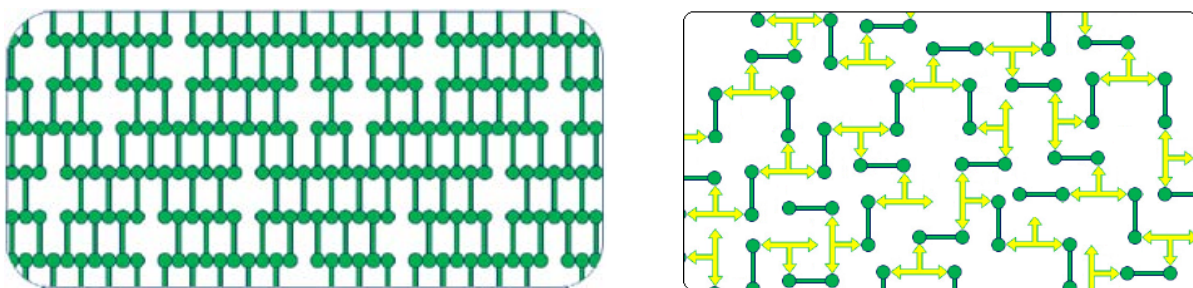
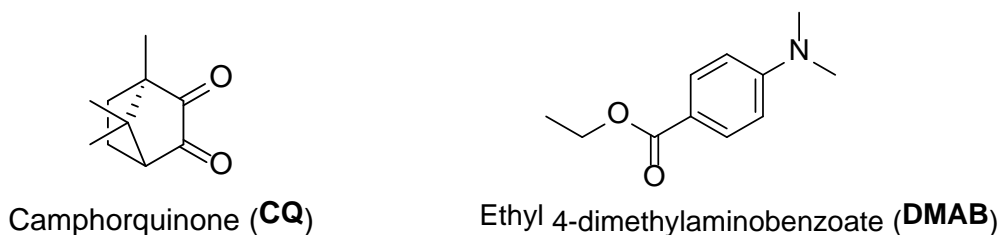


Figure 22: left: idealized vinyl ester polymer network; right: idealized triThiol-Ene polymer network

To cover a broad spectrum of properties in this work, three different ratios of every triThiol were tested with each monomer: 5%, 15% and 30% of thiol-functionality per double bond of the corresponding vinyl ester.

Photoinitiator

For the application in AMT photoinitiators with absorption maxima and tail-out at high wavelengths are desired. State of the art photoinitiator for dental applications is a bimolecular camphorquinone (CQ) / dimethylaminobenzoate (DMAB) system with a $n \rightarrow \pi^*$ transition at 468 nm.



These Type II photoinitiators have a tendency for discoloration, could be considered non cytotoxic but show rather low reactivity due to their bimolecular mechanism. A widely used cleavable Type I photoinitiator for UV curing of white and thick clear coatings is the highly reactive bisacylphosphine oxide based PI Irgacure 819 from the company BASF. It has its $n \rightarrow \pi^*$ transition at about 390 nm and tail-out up to 440 nm. In this case not only the benzoyl radical but also the phosphorus radicals produced are capable of initiating the polymerization (Figure 23).

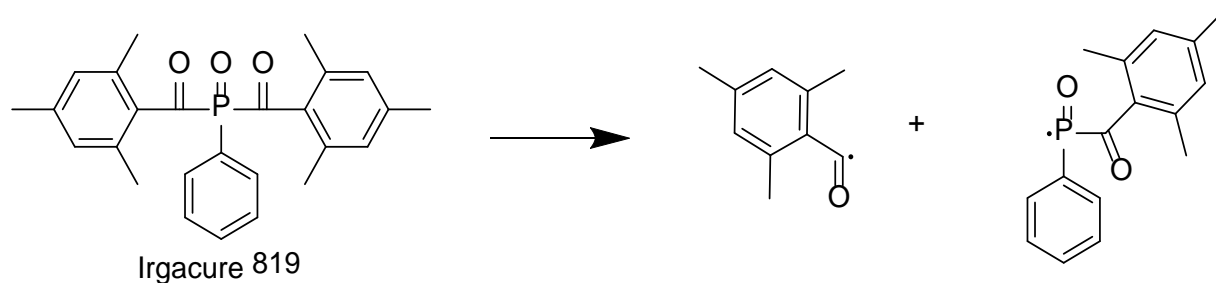


Figure 23: Cleavage of Type I PI (Irgacure 819)

Unfortunately, according to previous investigation, it was not possible to utilize Irgacure 819 for lithography-based Ceramic Manufacturing.

Therefore for this work the diacylgermane-based photoinitiator Ivocerin has been chosen.

Ivocerin is a visible light photoinitiator with an absorption maximum at $\lambda_{\text{max}} = 408 \text{ nm}$ and tail-out up to 460 nm.¹¹⁹ The cleavage mechanism of this Type I photoinitiator is shown in Figure 24. It shows significantly improved bleaching behavior compared to CQ/DMAB systems and has already been approved for dental usage.¹¹⁹

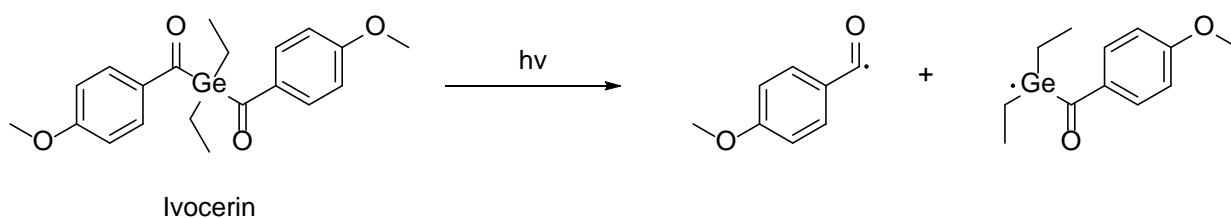
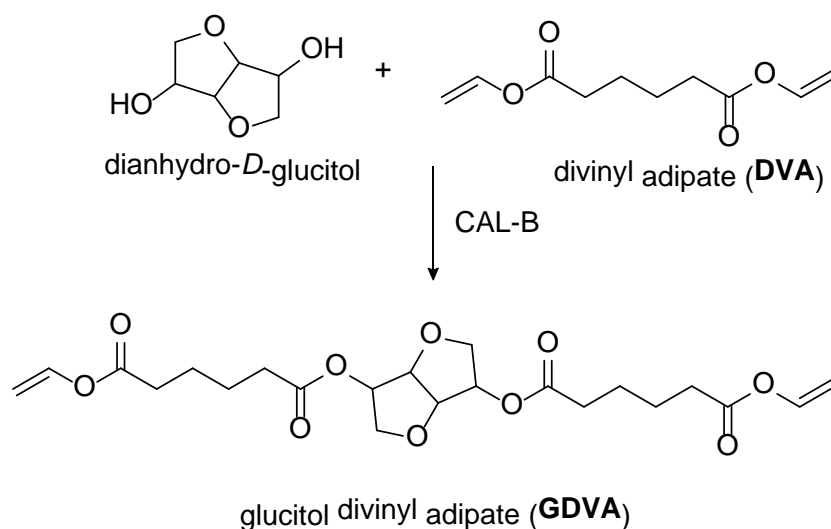


Figure 24: Cleavage of Ivocerin

3 Synthesis of Monomers

Within this work new monomers should be synthesized to be utilized in thiol-ene chemistry. Starting from commercially available divinyl adipate (DVA) three other multifunctional vinyl esters were synthesized. The first reaction was also investigated as a model reaction for optimization and upscaling.

3.1 Synthesis of O,O'-(hexahydrofuro[3,2-b]furan-3,6-diyl) divinyladipate (GDVA)



Dianhydro-*D*-glucitol was converted in a transesterification reaction with 6 equivalents divinyl adipate (DVA) using the lipase *candida antarctica* (CAL-B) and pyrogallol as stabilizer. The reaction was carried out without a solvent. After a reaction time of 44 hours the reaction mixture was filtered to remove the lipase and excessive DVA was removed under vacuum. Purification was done by column chromatography. 1.5 g (48% yield) GDVA were obtained as yellowish oil. Characterization was done via $^1\text{H-NMR}$ which showed that no divinyl adipate was left after workup and no monosubstituted product was present.

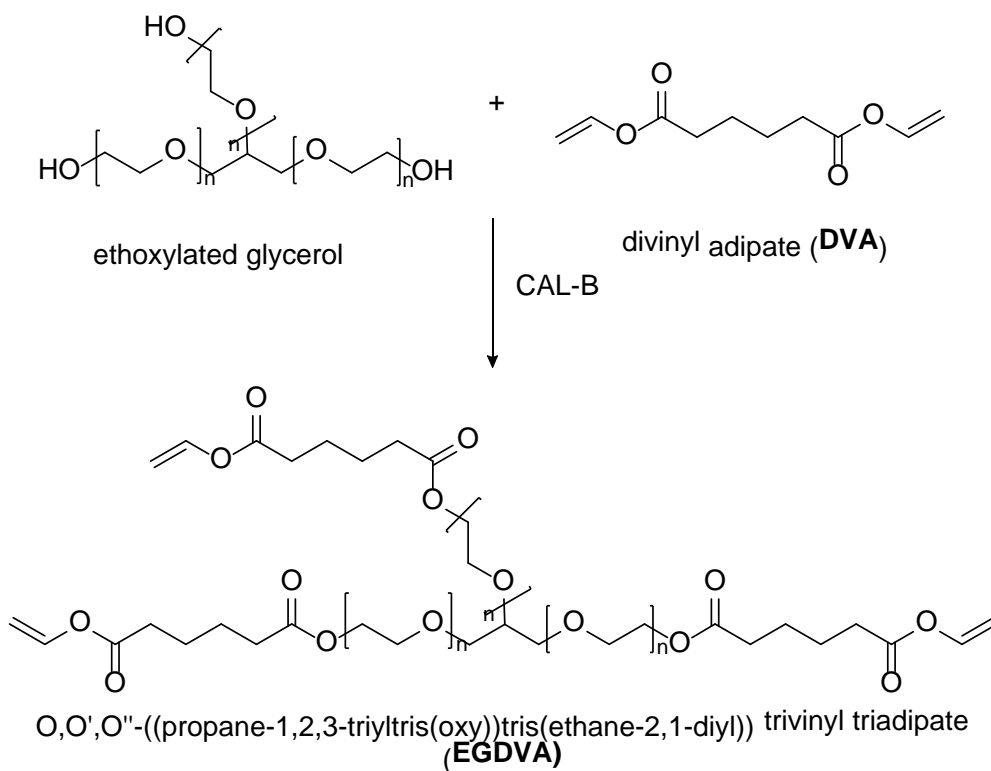
To optimize yield and workup the reaction was repeated with elongated reaction time and the lipase was added in 4 equal portions. Furthermore the column chromatography was replaced with aqueous extraction, keeping in mind that it was not necessary to remove DVA completely. The amount of remaining DVA was

measured via the refractive index, knowing that up to 10 wt% DVA were acceptable for LCM. With these alterations yields could be increased up to 67% and the workup was significantly simplified. It is notable that it was possible to recover most of the unreacted DVA (~80%) through distillation for further usage. Also the lipase could be reused (in a 1:1 ration with fresh lipase) after washing with distilled acetone and drying in vacuum.

All following reactions were done accordingly to the previous optimization experiments with GDVA regarding reaction time and the portion wise adding of lipase.

After the optimization step the reaction was investigated towards upscaling. Considering that further application of the synthesized monomers should be on a more or less industrial scale the transesterification reaction was carried out using a fivefold amount of educts and following the beforehand optimized reaction and workup. Surprisingly even higher yields could be obtained (up to 84% yield).

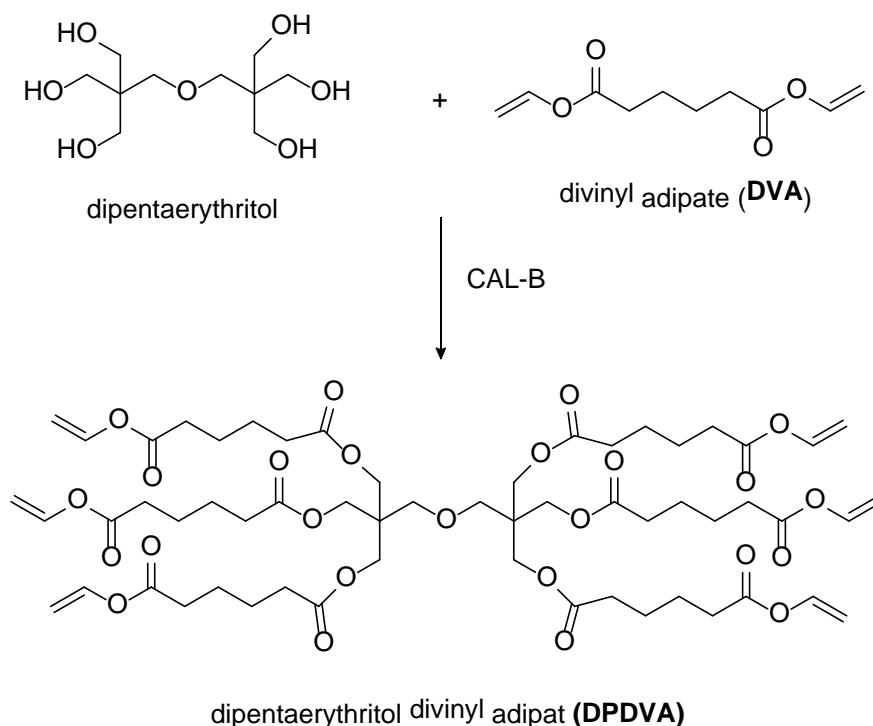
3.2 Synthesis of O,O',O''-((propane-1,2,3-triyltris(oxy))tris(ethane-2,1-diyl)) trivinyl triadipate (EGDVA)



Analogical to the previous synthesis, ethoxylated glycerol was converted in a solvent-free transesterification reaction with 9 equivalents DVA using lipase CAL-B and pyrogallol. After 4 days reaction time the mixture was filtrated to remove the lipase. The used lipase was washed, dried and collected to be reused in a similar reaction. To remove pyrogallol the mixture was subsequently extracted with water and ~80% of the excessive DVA could be removed via distillation. EGDVA was obtained as yellow oil in 67% yield. According to $^1\text{H-NMR}$ all OH-groups are converted and the amount of remaining DVA was calculated via NMR. This showed that ~4% DVA still remain in the product.

Up-scaling experiments were also done with this synthesis. Following the previous experiments with GDVA, a fivefold amount of educts was used and yields between 44% and 56% were achieved.

3.3 Synthesis of dipentaerythritol divinyl adipate (DPDVA)



In the first attempt, this reaction was carried out similar to the previous two. Dipentaerythritol was mixed with 18 equivalents DVA and reacted for 4 days. Unfortunately, solid dipentaerythritol is not soluble in DVA under the reaction conditions therefore no product was received after the workup.

Therefore it was decided to carry out the reaction in solution. To find a suitable solvent several aspects had to be considered. On one hand it should of course be able to dissolve dipentaerythritol but on the other hand it had to stand the reaction temperature of 65°C and most important not be harmful for the lipase^{120, 121}. Furthermore it should react with neither educts nor product. After several experiments considering the solubility of dipentaerythritol in a number of solvent that meet the other requirements only water-free DMSO was left. Therefore the reaction then was carried out in abs. DMSO under argon to keep out ambient humidity. Dipentaerythritol was dissolved prior to adding DVA and lipase and then again reacted for 4 days at 65°C. After the reaction time the lipase was filtered off and washed with distilled acetone for further usage. The problem now was to get rid of the DMSO without decomposing the product. Again several experiments were done investigating the solubility of the product in different solvent. It was not possible to dissolve DPDVA in water, acetonitrile, petrol ether, acetone, dichloromethane, methanol or ethanol. Only DMSO and pyridine were suitable solvents. It turned out that the best way was to extract the reaction solution in a mixture of 1:1 water/PE with the DMSO from the reaction solution mixable with the aqueous phase. Through this procedure the product is dissolved into the aqueous/DMSO phase and remaining DVA and unreacted product goes into the PE phase. After removing the solvents under vacuum a yellowish solid was obtained. NMR analysis showed unreacted OH-groups indicating that the conversion was only partial (which was expected due to steric hindrance) although DVA was used in large excess. To separate unreacted dipentaerythritol further solubility experiments were performed. They showed that dipentaerythritol was very good soluble in water whereas DPDVA was only soluble in DMSO. This information was used and the crude product was first grinded under liquid nitrogen and afterwards extracted with water/CH₂Cl₂. The remaining solid was collected via centrifugation obtaining a white solid (13% yield).

The final solid product is very unlikely to still contain significant amounts of DVA, which has a melting point of 28°C and no evaporation was observed in this range during melting point analysis of DPDVA. The degree of substitution was determined via $^1\text{H-NMR}$. Two different approaches were used. On one hand the ratio of integrals between the central hydrogens ($-\text{O-CH}_2\text{-C-CH}_2-$) and the vinyl ester signals was calculated and on the other hand the ration of the hydrogen peaks next to the central ester respective OH-functionalities was calculated and compared. Both methods show comparable results and a degree of substitution (DS) of ~2.2.

4 Photoreactivity

To get an idea of the impact of thiol-ene chemistry on the reactivity of vinyl esters and to compare the newly synthesized monomers with an existing systems the photoreactivity was investigated via Photo-DSC, photorheology and FTIR-ATR. The received data were also used as guide to choose a suitable mixture for the structuring experiments to follow. Alongside with the commercially available DVA, the two liquid vinyl ester monomers GDVA and EGDVA were mixed with three different thiols in three different ratios to cover a broad spectrum.

4.1 Photo-DSC

Photo-DSC measurements can be utilized to calculate a number of useful values. In case of this work two were especially of interest namely the time to reach the maximum heat of polymerization (t_{\max}) and the time after which 95% of the polymerization reaction is completed (t_{95}). The latter is very significant towards the decision which mixture is suitable for Lithography-based Ceramic Manufacturing (LCM) because it gives direct indication of the expected time a layer will need to cure and therefore the possible production speed. The photoinitiator concentration was 0.5 wt% and for storage stability 0.05 wt% of pyrogallol were added to all formulations. Thiols were added in 5, 15 and 30% ration of thiol per double bond. All photo-DSC measurements were done in triplicate. The mixtures names are built up according to their composition:

[name of vinyl ester]_[% thiol][abbreviation of thiol]

eg. *DVA_15E7* is composed of divinyl adipate with 15% ETTMP700

DVA ... divinyl adipate

GDVA ... O,O'-(hexahydrofuro[3,2-b]furan-3,6-diyl) divinyladipat (glucitol divinyl adipate)

EGDVA ... O,O',O''-((propane-1,2,3-triyltris(oxy))tris(ethane-2,1-diyl)) trivinyl triadipate (ethoxylated glycerol divinyl adipate)

T ... TMPMP ... trimethylolpropane tri(3-mercaptopropionate)

E7 ... ETTMP700 ... ethoxylated-trimethylolpropan tri-3-mercaptopropionate

MW = 700 g*mol⁻¹

E13 ... ETTMP1300 ... ethoxylated-trimethylolpropan tri-3-mercaptopropionate

MW = 1300 g*mol⁻¹

The influence of thiol-ene chemistry is clearly visible in all of the resin formulations when compared to the corresponding pure vinyl ester. The presence of thiol providing easily abstractable hydrogen and the additional chain transfer results in increased reactivity and lower t_{\max} values due to the reactive thiyl radical. The higher the amount of thiol present in the system, the faster the maximum heat of polymerization is reached. It is also the case that thiols with higher molecular weight accelerate the systems more than those with lesser molecular weight which can be seen in Figure 25.

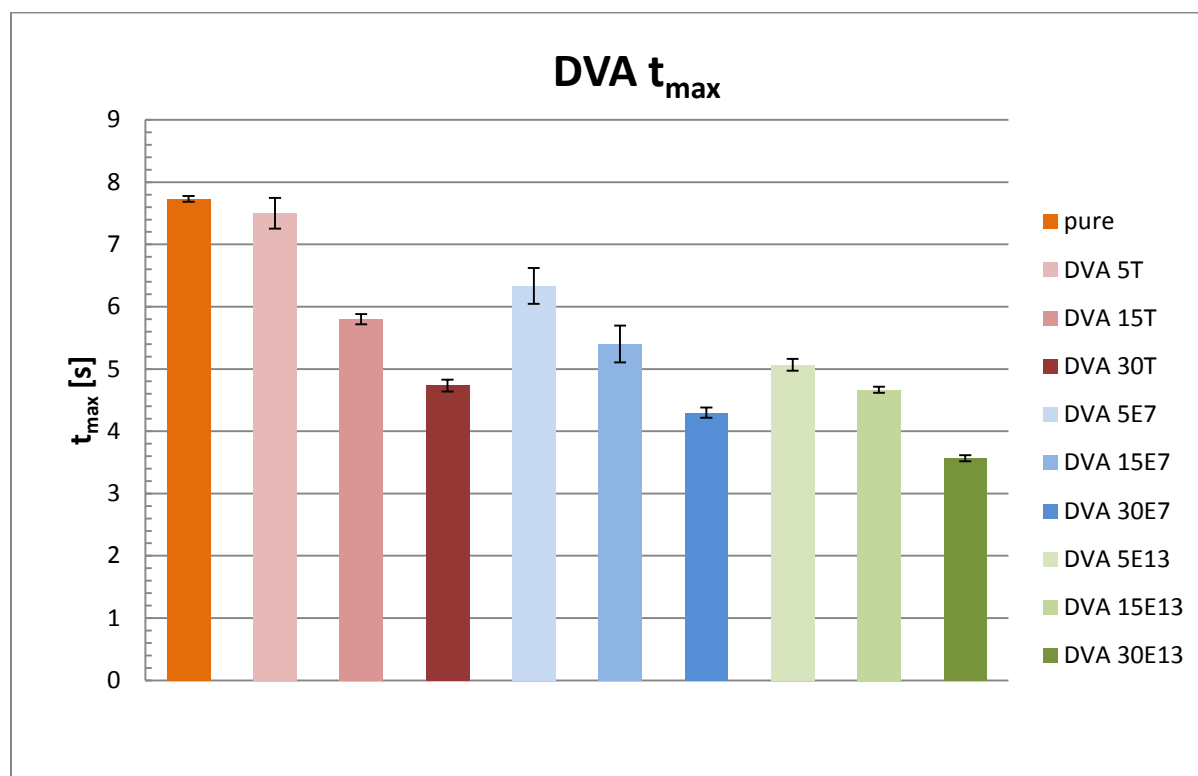


Figure 25: t_{\max} values for DVA mixtures from Photo-DSC measurements

When it comes to t_{95} values the influence of the thiols is not as easily explained. For DVA the statement that higher amounts of thiol and higher molecular weights also result in lower t_{95} values is true as seen in Figure 26.

Compared with DVA, GDVA shows lower t_{\max} values for the pure vinyl ester formulation as well as for the mixtures with the thiols except for the largest one (ETTMP1300). This can be explained by the higher amounts of abstractable hydrogens available in GDVA.

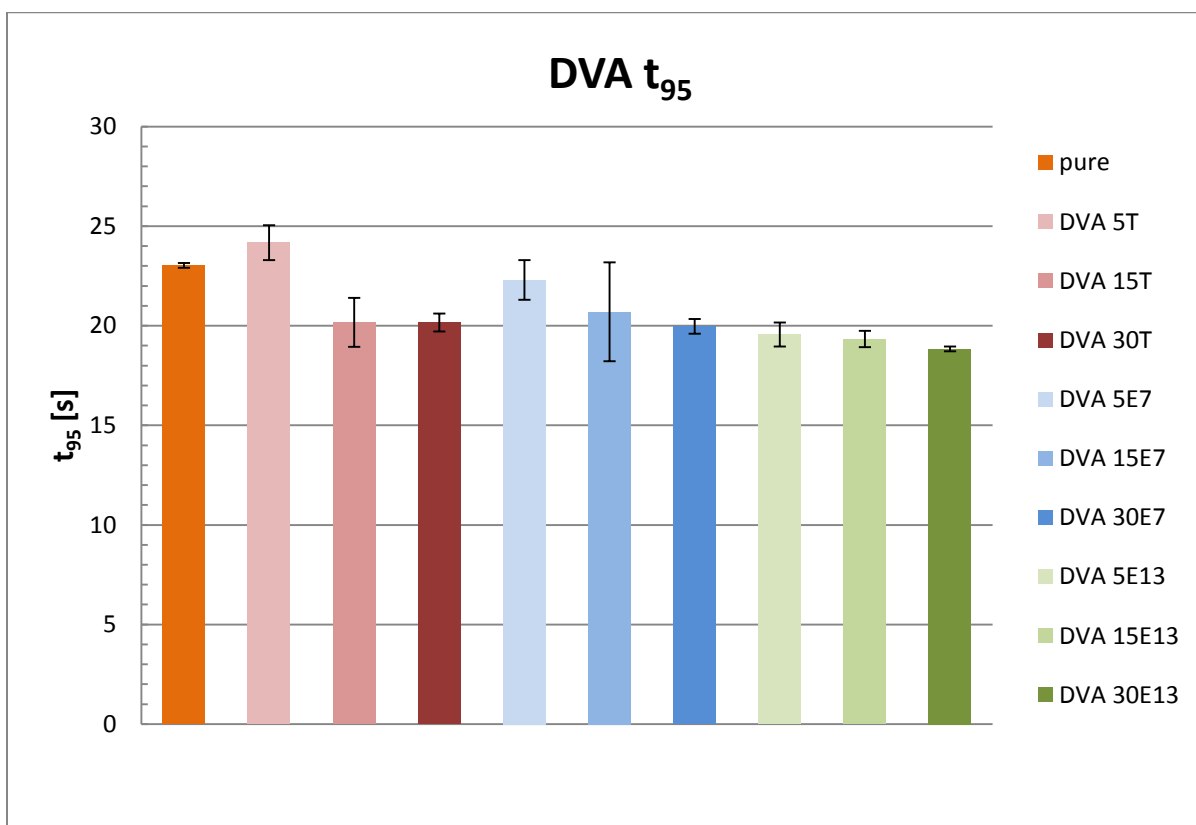


Figure 26: t_{95} values for DVA mixtures from Photo-DSC measurements

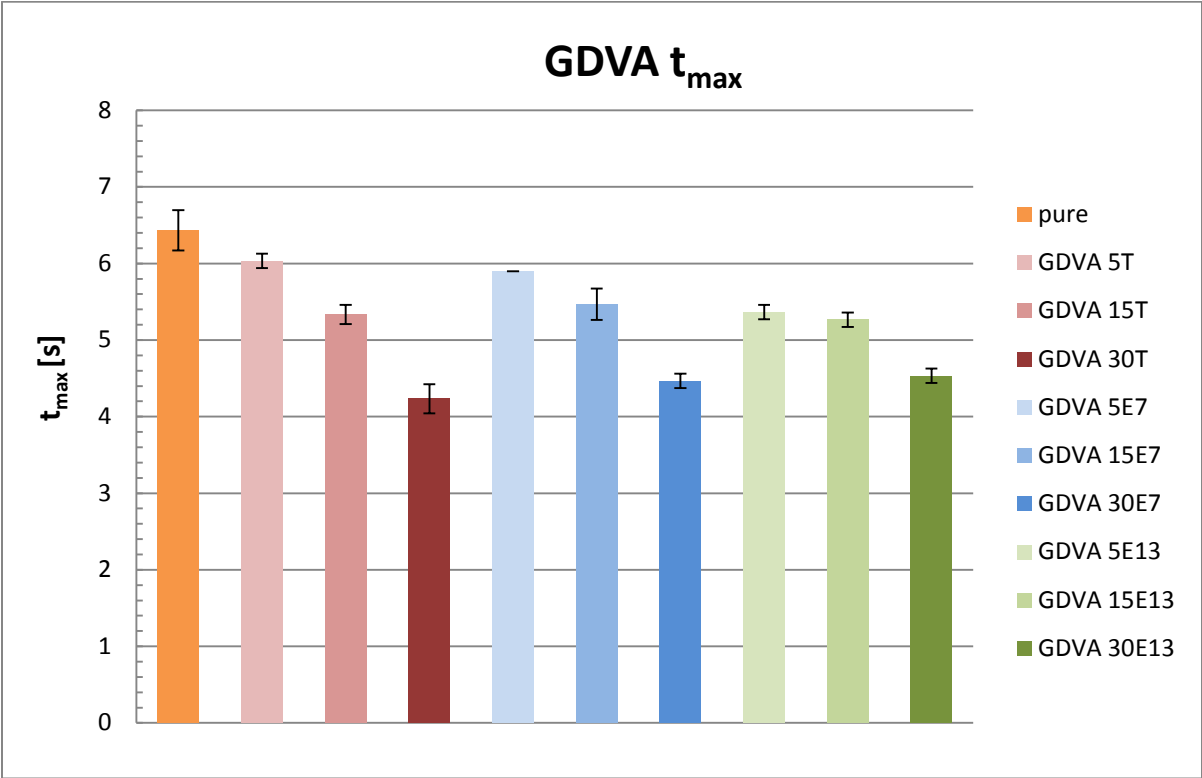


Figure 27: t_{\max} values for GDVA mixtures from Photo-DSC measurements

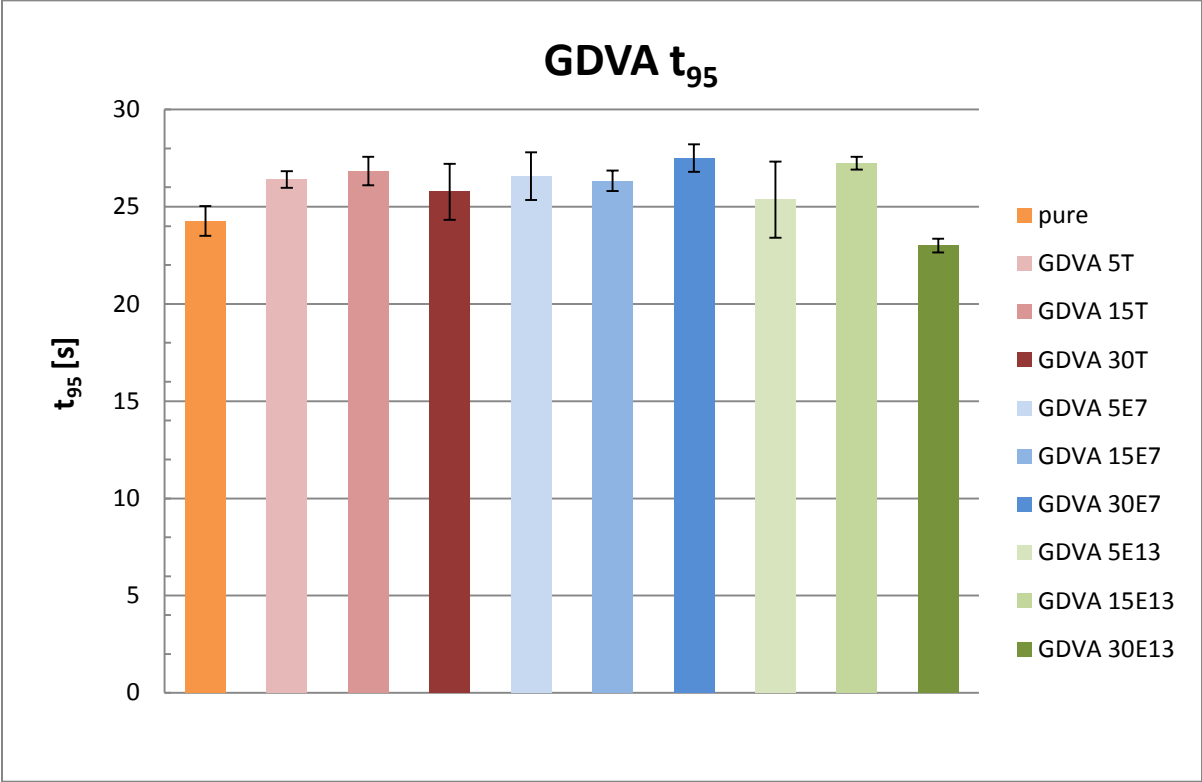


Figure 28: t_{95} values for GDVA mixtures from Photo-DSC measurements

The statement that addition of thiols accelerates the vinyl ester system is also true for GDVA as seen in Figure 27, but it seems that the t_{95} values of GDVA seen in Figure 28 are not significantly influenced by the addition of thiols irrespective of amount and molecular weight. Only the highest amount of the biggest thiol was able to lower the t_{95} value, all other formulation even show a slightly increased value.

Interestingly the impact on EGDVA was more prominent. The t_{max} values seen in Figure 29 follow the expected trend nicely but the t_{95} values were rather unexpected. Whereas the thiol with the lowest molecular weight significantly increased t_{95} even in the lowest concentration, the thiol with the highest molecular weight decreased the value at least until a concentration of 15% thiol per double bond. In this case it seems likely that steric effects play an important role of how accessible the formed thiyl radicals and the corresponding double bonds are.

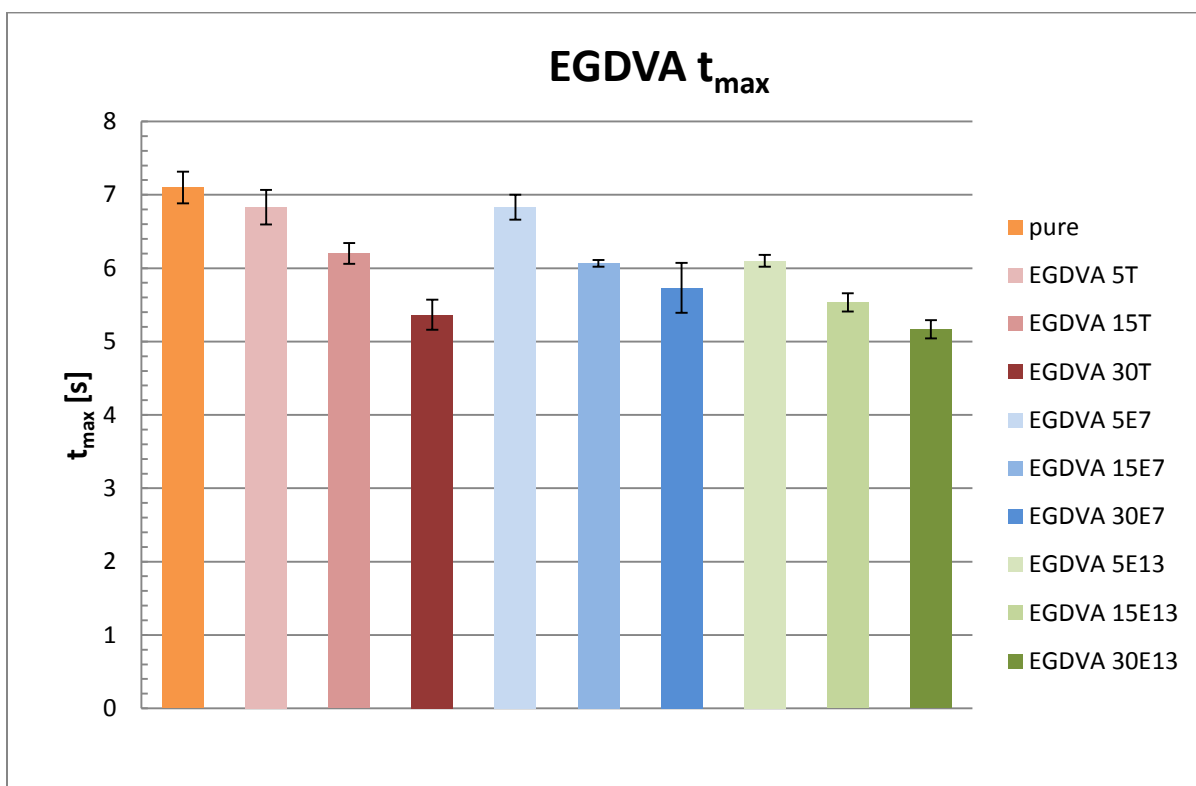


Figure 29: t_{max} values for EGDVA mixtures from Photo-DSC measurements

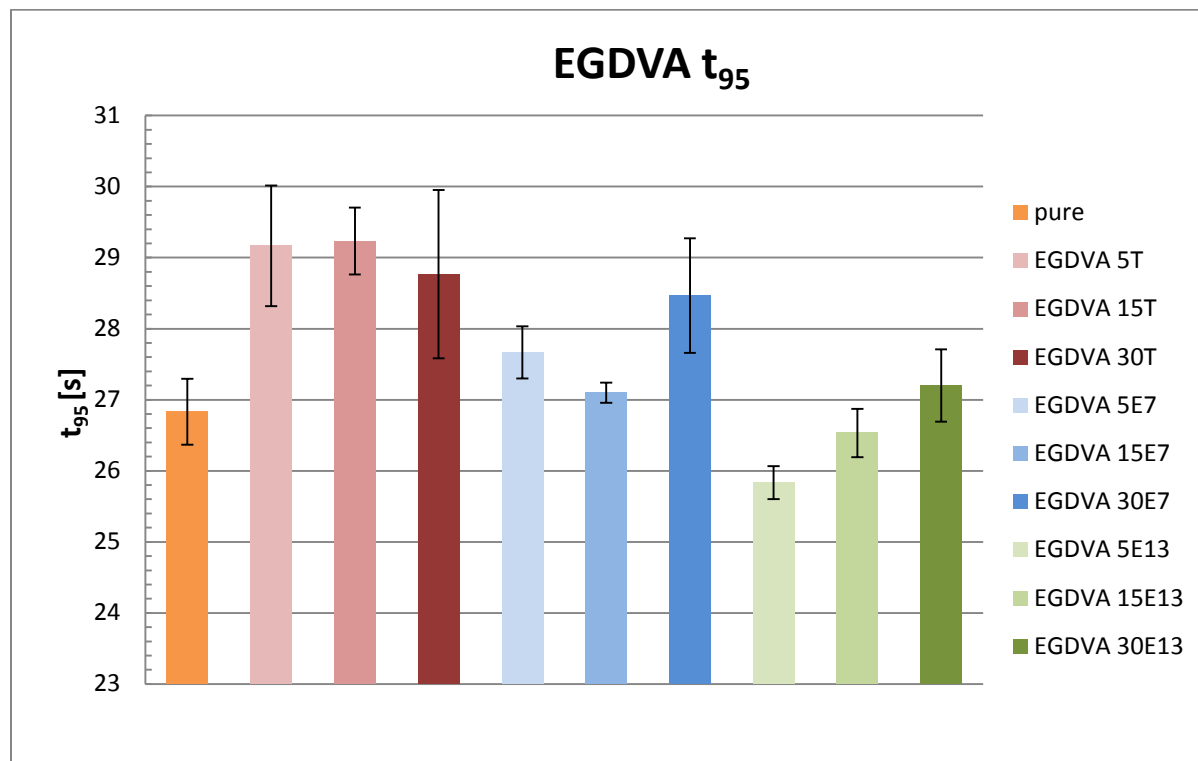


Figure 30: t_{95} values for EGDVA mixtures from Photo-DSC measurements

Overall it can be said that the smallest triThiol TMPMP shows the biggest influence correlated to the used concentration and that the addition of thiol accelerates the photopolymerization of vinyl ester systems by the means of reaching the maximum heat of polymerization.

Unfortunately it was not possible to calculate DBC and polymerization rate from photo-DSC measurements due to the lack of data of the real ratio of homopolymerization and step-growth in thiol-ene polymerization which have a different heat of polymerization.

4.2 FTIR-ATR Measurements

To evaluate the influence of thiol-ene chemistry on double bond conversion FTIR-ATR measurements were performed. Therefore the same mixtures as used in the photo-DSC were used. For each mixture both the unreacted monomer and the

corresponding polymer were measured. The cured samples were prepared in a silicone mold using the INTELLI-RAY 600 light oven from Uvitron.

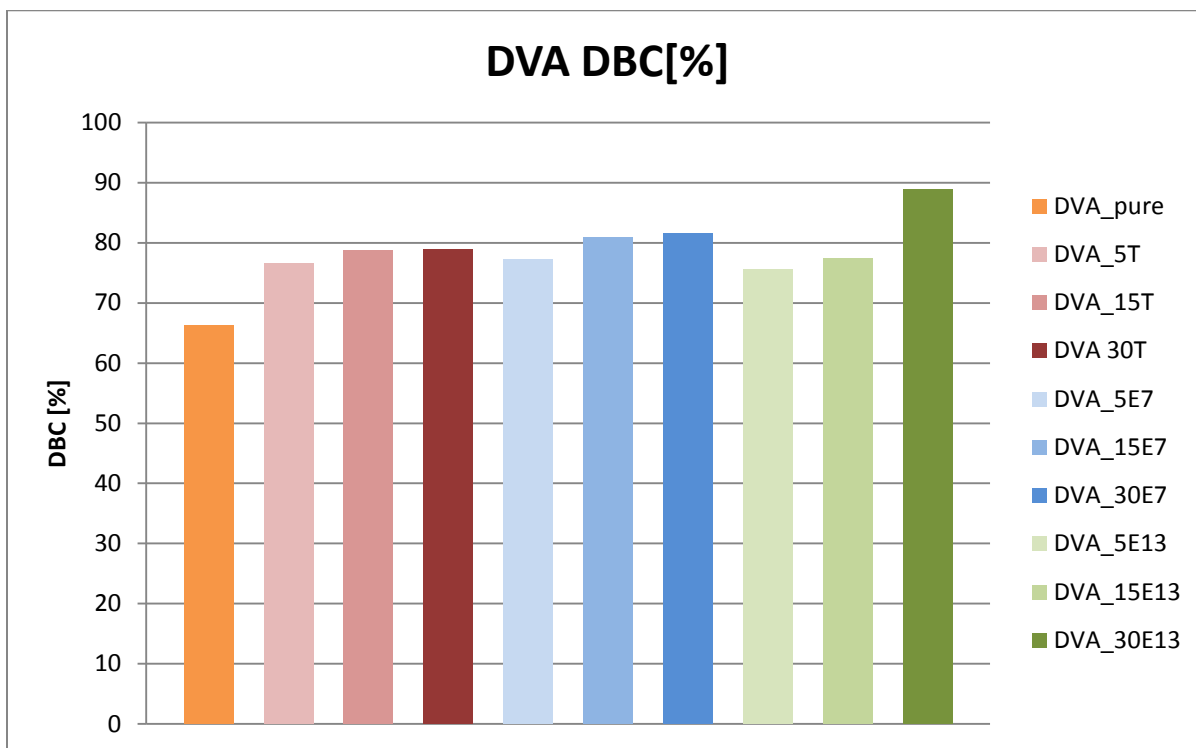


Figure 31: Double bond conversion for DVA mixtures calculated by FTIR-ATR

Here again a clear trend is visible. With increasing amount of thiol it was possible to increase the overall conversion of vinyl groups. This is true for all three monomers though it is pronounced differently in the various mixtures. DVA on its own already reaches a double bond conversion of approx. 67% that can reach up to nearly 90% with 30% of the triThiol ETTMP1300 as seen in Figure 31. This can be explained by sterical deliberation. As the photopolymerization proceeds the mobility of unreacted monomer molecules decreases resulting in lower conversions. The added thiol reduces the density of the resulting network - which is also results in delayed reaching of the gel point – and the improved monomer mobility causes higher conversion.

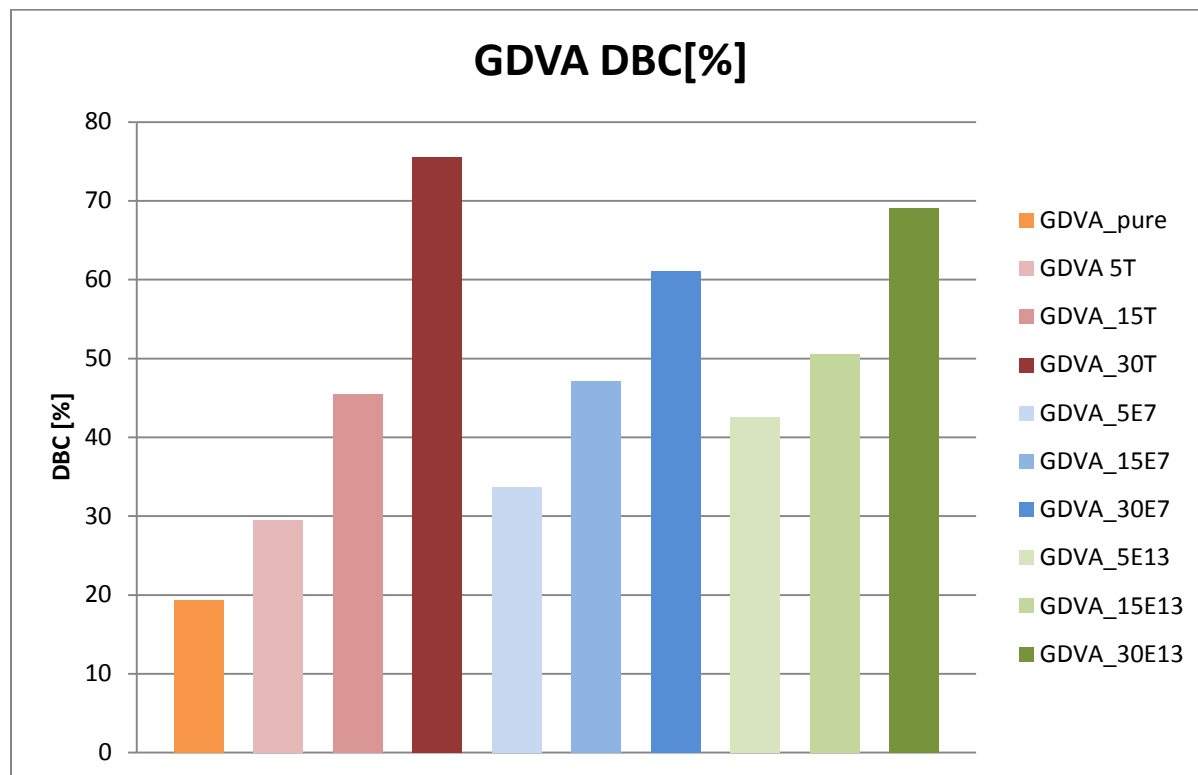


Figure 32: Double bond conversion for GDVA calculated by FTIR-ATR

Investigating the results for the synthesized vinyl esters another interesting effect can be seen. It should be noticed that conversion for both GDVA (approx. 20%) and EGDVA (approx. 47%) is significantly lower compared to DVA as seen in Figure 32 & Figure 33. This could be the case because GDVA is a rather small and rigid molecule and has a lot of abstractable hydrogens whereas EGDVA also has a high number of abstractable hydrogens but is a lot more flexible. Comparing the conversions of GDVA and EGDVA it seems that size and molecular weight of the vinyl ester determine which thiol has the biggest influence on the double bond conversion. In case of GDVA the highest conversion of 75% was reached with 30% TMPMP – the smallest thiol, whereas in case of EGDVA best results (68%) were obtained with 30% of the triThiol ETTMP700. It seems that the thiol needs to match the vinyl ester in terms of size although this does not seem to be the case for DVA.

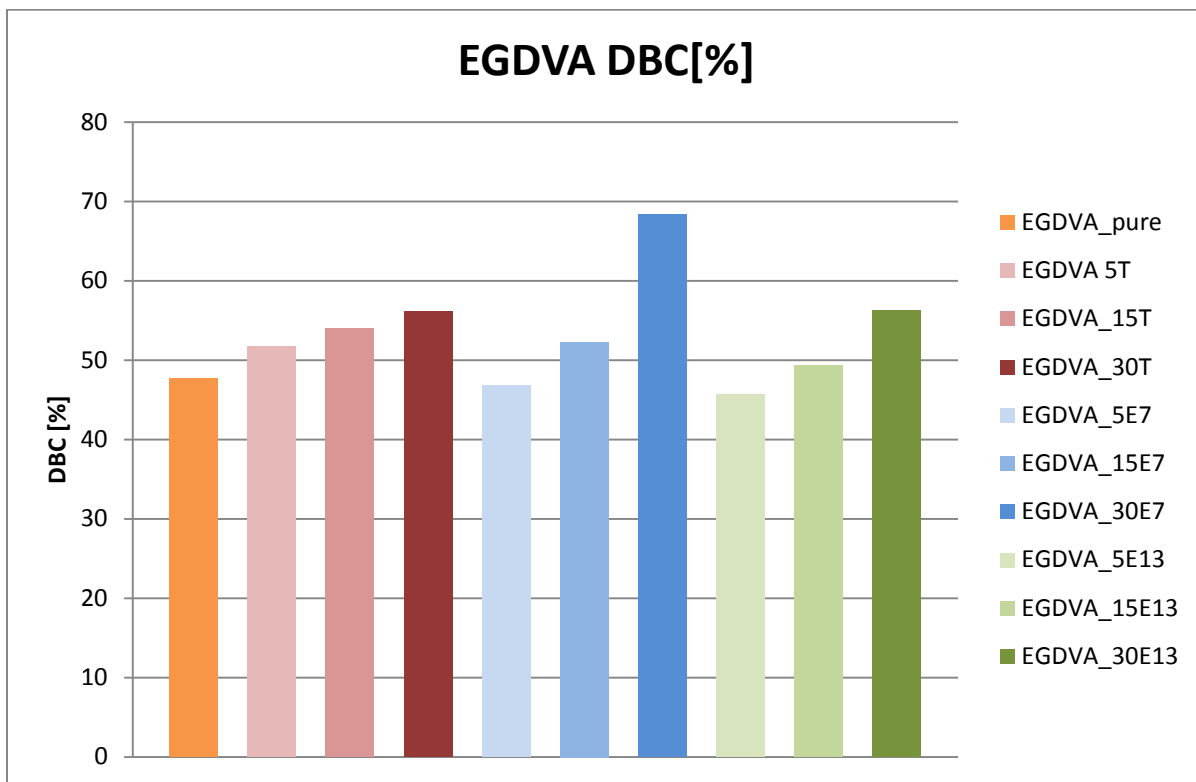


Figure 33: Double bond conversion for EGDVA calculated by FTIR-ATR

4.3 Photorheology

To further investigate the real-time behavior of the photopolymerization and also studying properties like gel point, storage and loss modulus, photorheology experiments were performed. With this method it was possible to track the progress of the polymerization simultaneously with IR and rheology measurements. Figure 34 shows two spectra of a formulation recorded at the beginning and the end of polymerization reaction with the peaks of interest circled (S-H stretching at 2580 cm^{-1} , C=C bending at 6120 cm^{-1}). The double bond and thiol conversion was calculated by integration of the peak area.

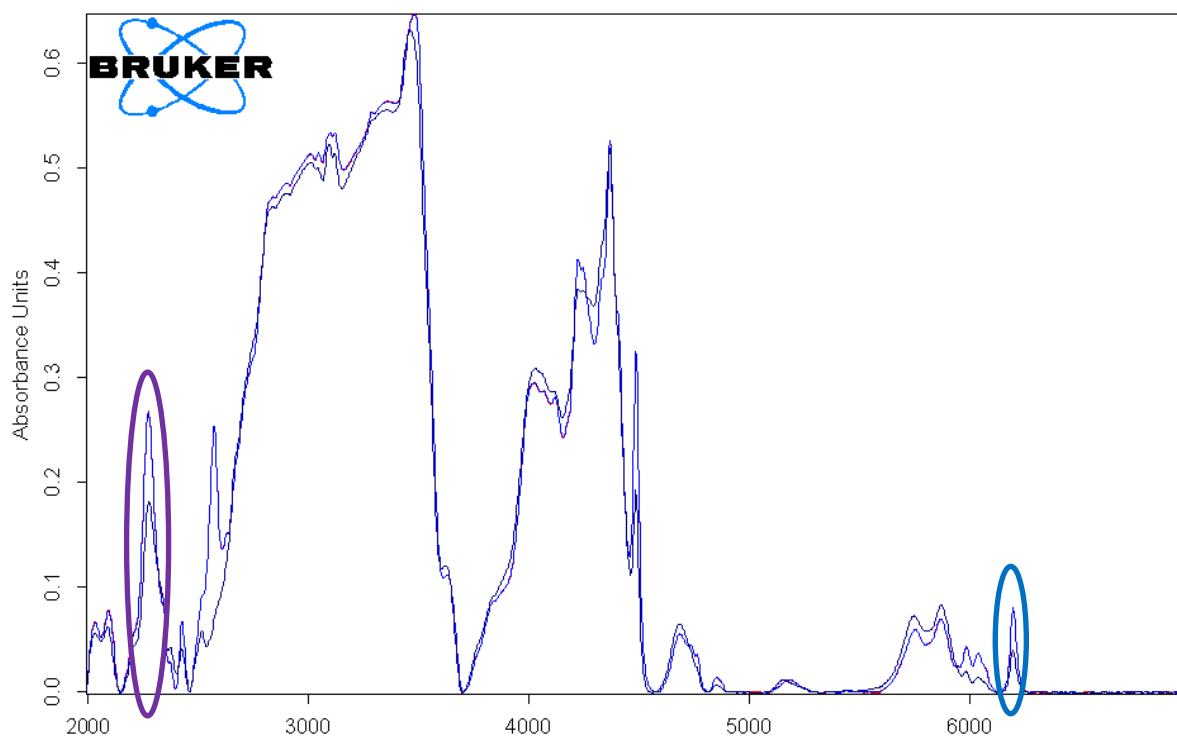


Figure 34: Combined MIR and NIR spectrum at start and end of the photopolymerization

In Figure 35 the typical curves recorded from the rheology measurements can be seen. The irradiation starts at 60 seconds. The point of intersection of those two curves is known as the gel point and is very useful to characterize polymers by marking the liquid-to-solid transition.

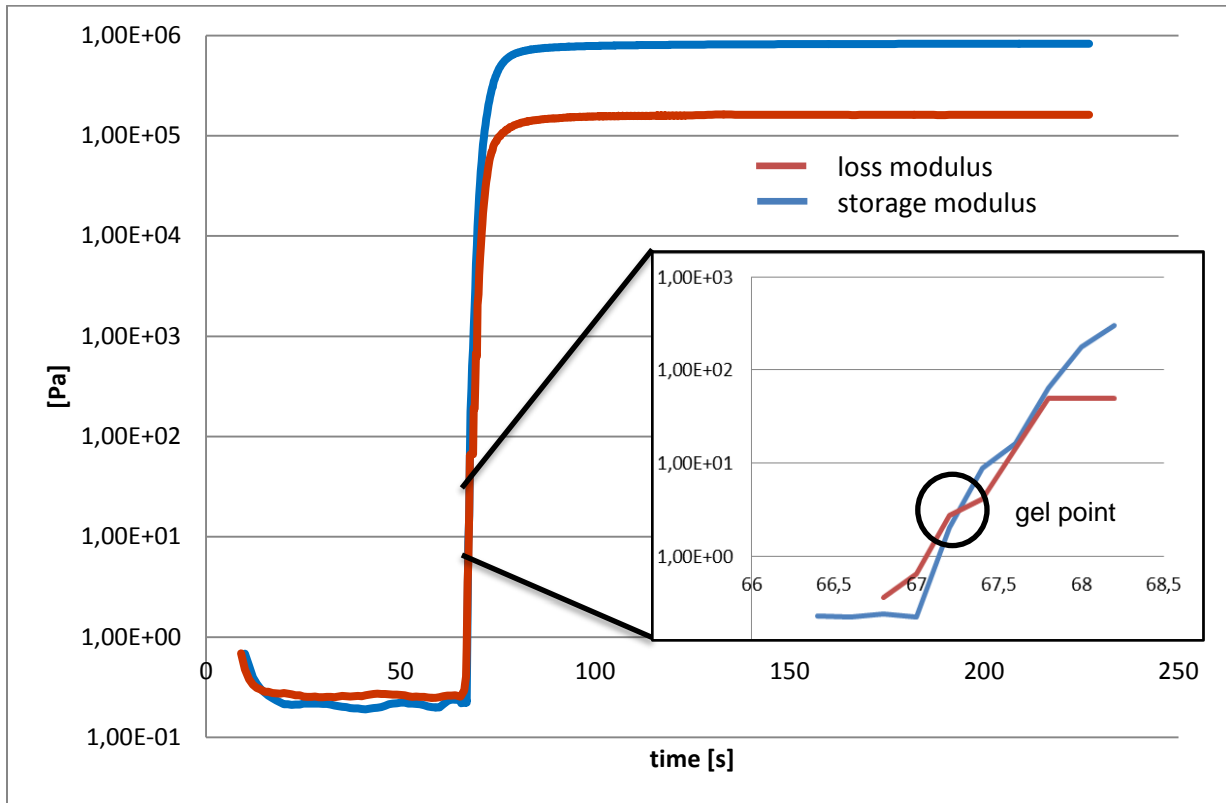


Figure 35: Rheology curves received during photorheology experiments

By keeping a constant measurement gap and measuring the required force to do so, information on the shrinkage of the polymer can be gathered as seen in Figure 36.

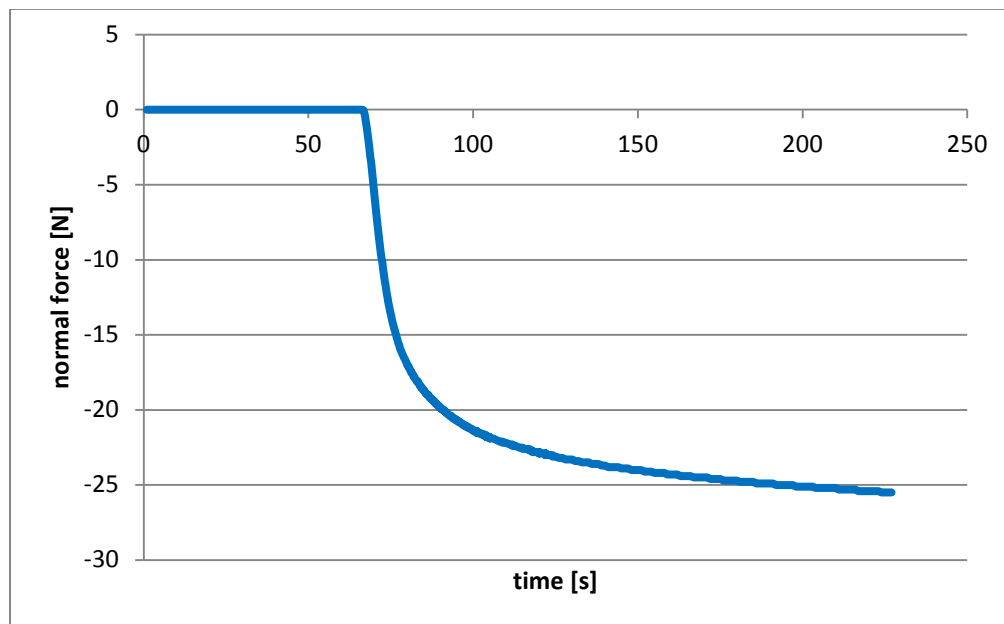


Figure 36: Shrinkage behavior during photorheology measurement

In principle this method provides a large amount of very useful data to characterize both the photopolymerization and the resulting polymer. Unfortunately the used NaCl windows are mechanically weak and tend to break after nearly every measurement. To still prove that the full possibilities of this measurement configuration can be utilized, systems with reduced reactivity and therefor conversion, by adding unusually high amounts of pyrogallol as inhibitor. For those entire mixtures 0.5 wt% of photoinitiator and 0.5 wt% pyrogallol were used. Thiols were added in 5, 15 and 30% ration of thiol per double bond. All measurements were done in triplicate. The mixtures names are built up according to their composition:

[name of vinyl ester]_[% thiol][abbreviation of thiol]

eg. *DVA_15E7* is composed of divinyl adipate with 15% ETTMP700

DVA ... divinyl adipate

GDVA ... O,O'-(hexahydrofuro[3,2-b]furan-3,6-diyl) divinyladipat (glucitol divinyl adipate)

EGDVA ... O,O',O''-((propane-1,2,3-triyltris(oxy))tris(ethane-2,1-diyl)) trivinyl triadipate (ethoxylated glycerol divinyl adipate)

T ... TMPMP ... trimethylolpropane tri(3-mercaptopropionate)

E7 ... ETTMP700 ... ethoxylated-trimethylolpropan tri-3-mercaptopropionate

MW = 700 g*mol⁻¹

E13 ... ETTMP1300 ... ethoxylated-trimethylolpropan tri-3-mercaptopropionate

MW = 1300 g*mol⁻¹

It is important to keep in mind that the results of those measurements can only give trends but no absolute values. To still be able to characterize all formulations regarding their truly achievable double bond conversion, FTIR-ATR measurements were already done in the previous section. Table 2-4 contain the calculated data from the photorheology measurements including the double bond conversion at the gel point (DBC_g), the double bond conversion (DBC) and the time needed to reach 95 % of the final DBC (t₉₅).

Table 2: Results for DVA-mixtures from photorheology measurements

Formulation	Gel point [s]	DBC _g [%]	DBC [%]	t _{95%} [s]	Thiol Conversion [%]
DVA_pure	7.6 ± 0.1	8.5 ± 0.5	15.5 ± 0.2	40.5 ± 3.5	-
DVA_5T	6.4 ± 0	14.4 ± 1.2	27.0 ± 0.3	44.2 ± 5.9	18.0 ± 0.1
DVA_15T	6.4 ± 0.1	24.0 ± 1.2	36.6 ± 0.1	36.6 ± 9.8	26.8 ± 0.2
DVA_30T	6.3 ± 0	36.6 ± 0.9	49.6 ± 0.2	33.4 ± 1.8	40.4 ± 0.1
DVA_5E7	5.5 ± 0.1	13.1 ± 0.4	29.9 ± 0.2	44.7 ± 2.1	19.6 ± 0.1
DVA_15E7	5.6 ± 0.1	24.8 ± 0.7	43.6 ± 0.3	39.7 ± 1.4	31.8 ± 0.3
DVA_30E7	5.8 ± 0	37.1 ± 0.7	53.1 ± 0.1	32.7 ± 2.3	44.4 ± 1.0
DVA_5E13	2.4 ± 0.2	13.1 ± 0.8	67.1 ± 0	38.7 ± 1.8	49.7 ± 1.7
DVA_15E13	3.3 ± 0.1	30.4 ± 0.6	58.0 ± 0.3	35.2 ± 2.6	37.8 ± 2.2
DVA_30E13	2.9 ± 0.1	44.1 ± 0.5	69.8 ± 0.5	25.3 ± 1.8	37.9 ± 1.1

The time to reach the gel point with DVA mixtures seems to not depend on the amount of added thiol but only on the molecular weight of it as seen in Table 2. The higher the molecular weight the faster the gel point is reached. This correlates with the increased reactivity caused by the thiol-ene chemistry. Also the time to reach 95% conversion is only influenced by the size of the used thiol. The other values namely DBC_g, DBC and thiol conversion are increasing along with increasing amount of thiol from every size investigated. Besides the increased reactivity of thiol-ene systems the effect of sterical deliberation plays a role in this outcome. The density of the formed networks decreases with rising amount of thiols enhancing the mobility of remaining monomers and therefore improving the achievable conversion. The increasing DBC_g with increasing amount of thiol has another positive effect by reducing shrinkage stress which is caused by the formation of polymer chains after the transition of the gel point.

The moduli displayed in Figure 37 and 38 represent average values at the end of each measurement. A straight line was fitted to the plateau of the rheology curve as seen in Figure 35. Results for DVA show significant increase of both storage and loss modulus with the addition of thiols. This is caused by increased conversion as result of thiol-ene chemistry. Another effect which can be seen is that with too high amounts of thiol the properties begin to decrease again. This is because the formed networks are getting too loose.

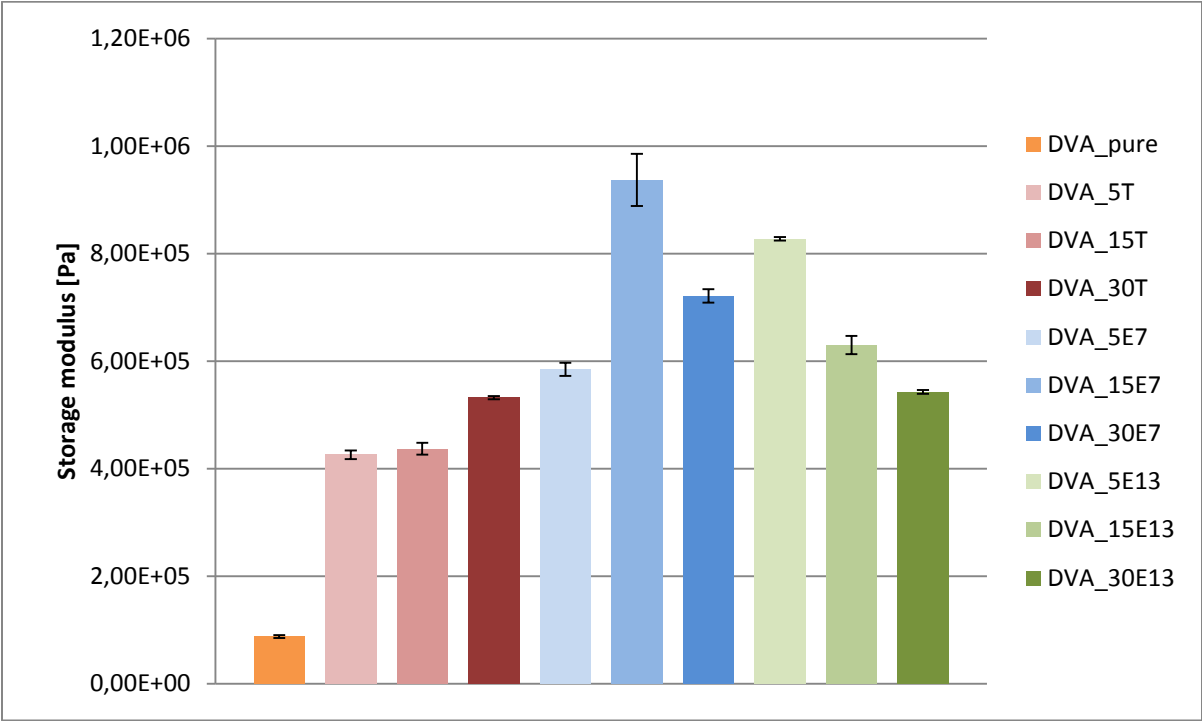


Figure 37: Storage modulus of DVA calculated from photorheology

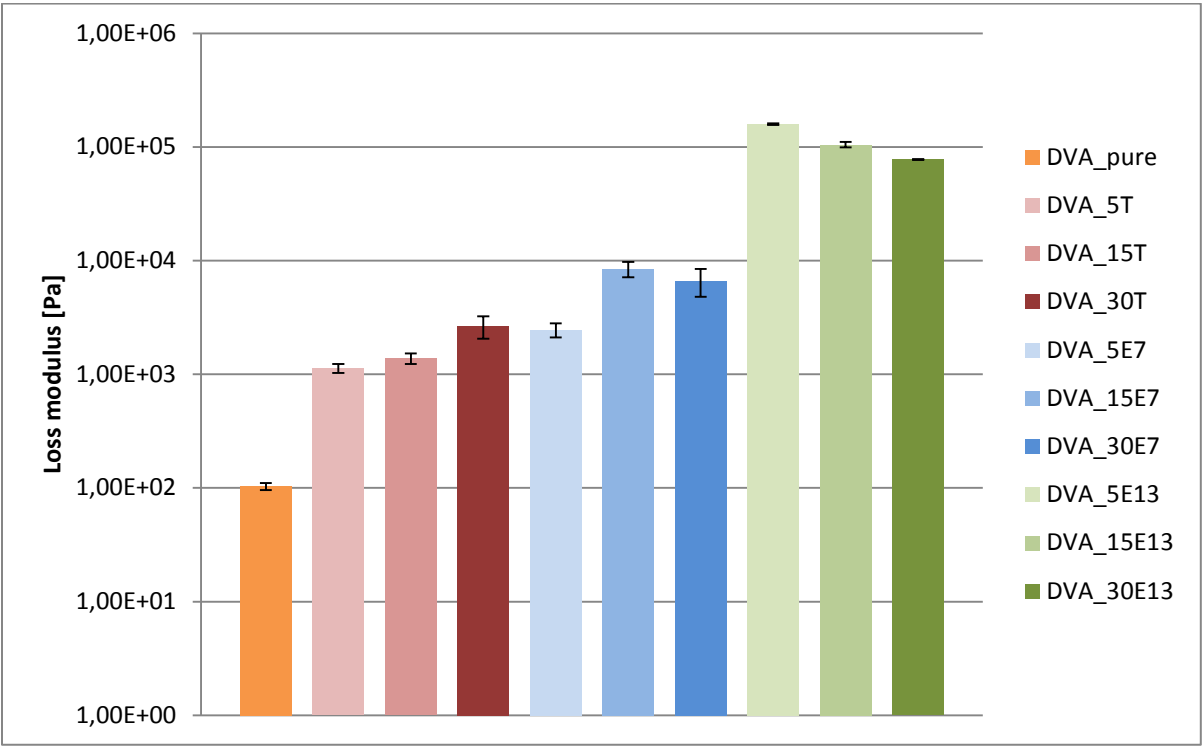


Figure 38: Loss modulus of DVA calculated from photorheology

Table 3: Results for GDVA-mixtures from photorheology measurements

Formulation	Gelpoint [s]	DBC _g [%]	DBC [%]	t _{95%} [s]	Thiol Conversion [%]
GDVA_pure	6.4 ± 0.1	11.1 ± 1.0	34.0 ± 0.5	64.8 ± 2.7	-
GDVA_5T	5.9 ± 0	16.1 ± 0.4	32.9 ± 0.6	53.7 ± 6.6	19.9 ± 0.7
GDVA_15T	8.9 ± 0.1	24.2 ± 1.4	40.6 ± 0	60.9 ± 4.3	24.9 ± 0.1
GDVA_30T	11.3 ± 0	39.6 ± 0.8	51.2 ± 0	58.4 ± 1.8	35.5 ± 0.3
GDVA_5E7	7.1 ± 0.2	18.1 ± 0.4	37.9 ± 0.3	60.3 ± 2.8	20.1 ± 0.4
GDVA_15E7	6.3 ± 0	25.5 ± 0.2	48.6 ± 0.1	70.2 ± 4.4	29.7 ± 0.1
GDVA_30E7	7.3 ± 0	37.8 ± 0.9	57.3 ± 0.2	54.7 ± 3.1	42.1 ± 0.5
GDVA_5E13	5.2 ± 0.1	18.8 ± 1.2	45.5 ± 0.6	60.6 ± 1.7	26.4 ± 1.4
GDVA_15E13	4.8 ± 0.1	28.0 ± 0.5	57.1 ± 0.1	54.2 ± 2.5	33.3 ± 0.4
GDVA_30E13	4.7 ± 0.3	37.3 ± 0.7	67.1 ± 1.6	54.0 ± 2.3	46.2 ± 0.6

As seen in Table 3 for mixtures containing GDVA and the smallest triThiol TMPMP (T) the effect of delay of the gel point can be observed. This effect, if achievable, is known to increase conversion by prolonging the time in which the monomers in the system are able to move around more freely finding possible reaction partners. Like before with DVA, the time to reach 95% conversion is not significantly influenced by the amount of added thiol and, in this case, also not very much by the size. All other effects explained before apply as well for mixtures containing GDVA. The conversion is increased both at the gel point and overall.

The moduli for GDVA mixtures are shown in Figure 39 and 40. Here the results differ within the concentration range of the used thiols. With the smallest triThiol TMPMP both storage and loss modulus decrease although double bond and thiol conversion are increased. This can be explained by the lowering network crosslinking density with higher amounts of TMPMP. For the second triThiol ETTMP700 (E7) the trend is in the opposite direction. Here the positive effects of thiol-ene chemistry on conversion and network uniformity increase with rising amounts of thiol. With the largest triThiol ETTMP1300 (E13) both effects compete with each other. At 15% thiol-ratio the effects combine in a positive way whereas at 30% thiol the values start to drop again because the network gets to loose.

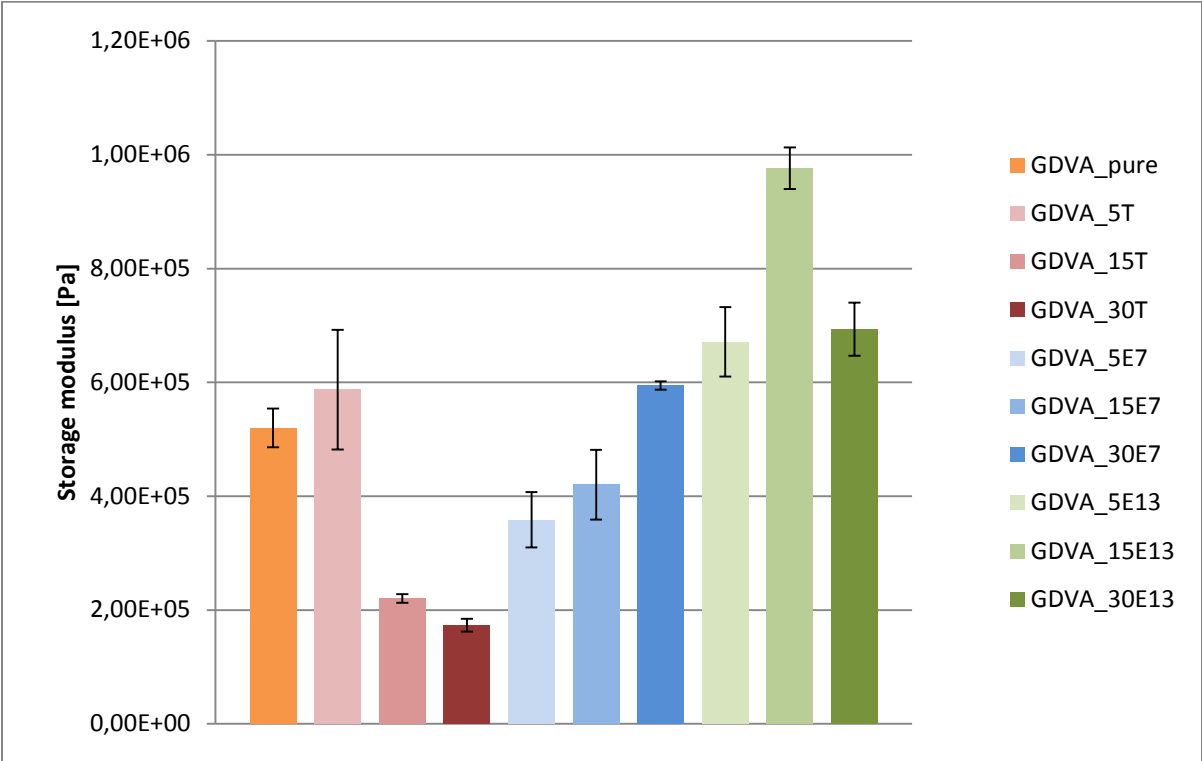


Figure 39: Storage modulus of GDVA calculated from photorheology

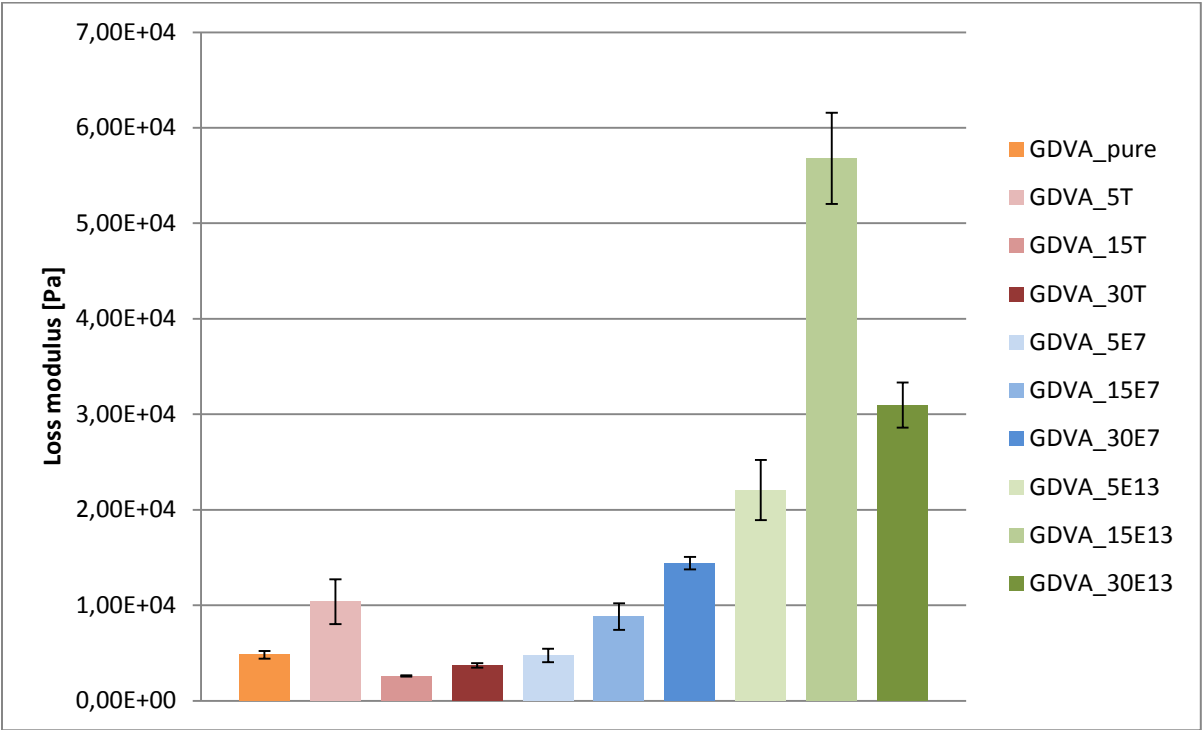


Figure 40: Loss modulus of GDVA calculated from photorheology

Table 4: Results for EGDVA-mixtures from photorheology measurements

Formulation	Gelpoint [s]	DBC _g [%]	DBC [%]	t _{95%} [s]	Thiol Conversion [%]
EGDVA_pure	4.3 ± 0	14.7 ± 0.7	57.1 ± 0.8	58.8 ± 4.8	-
EGDVA_5T	3.8 ± 0.1	18.9 ± 1.7	57.1 ± 0.7	54.7 ± 6.2	36.7 ± 4.5
EGDVA_15T	5.7 ± 0	24.1 ± 0.9	57.6 ± 0.2	65.9 ± 2.9	51.6 ± 0.2
EGDVA_30T	5.3 ± 0	31.0 ± 0.5	57.8 ± 0.1	53.1 ± 3.1	54.2 ± 0.4
EGDVA_5E7	7.3 ± 0	17.3 ± 2.1	45.1 ± 0.2	64.5 ± 5.9	32.3 ± 0.3
EGDVA_15E7	4.4 ± 0.2	24.0 ± 1.9	62.7 ± 0.2	53.1 ± 2.8	55.6 ± 1.9
EGDVA_30E7	3.3 ± 0	30.4 ± 0.9	62.9 ± 0.3	41.5 ± 6.6	54.2 ± 0.2
EGDVA_5E13	4.3 ± 0	17.7 ± 2.7	53.8 ± 0.8	46.8 ± 8.9	34.3 ± 1.1
EGDVA_15E13	4.3 ± 0	20.3 ± 1.2	56.8 ± 1.1	49.4 ± 4.6	41.2 ± 4.5
EGDVA_30E13	3.9 ± 0	27.3 ± 0.8	61.3 ± 0.1	51.6 ± 3.7	48.6 ± 0.3

Within this measurements EGDVA seems the least influenced in terms of DBC by the addition of thiols as seen in Table 4. Although the conversion at the gel point increases with rising amounts of thiol as is was the case with the other mixtures. EGDVA shows a surprisingly high DBC at the end of the reaction in spite of the high inhibitor concentration used.

The moduli of the EGDVA mixtures are depicted in Figure 41 and 42. The storage moduli show the same behavior as previously seen with mixtures of GDVA and the largest triThiol ETTMP1300. Here it is the case for all mixtures that at 15% thiol-content the moduli are the highest and drop again with higher amount of thiol. The effect on the decrease of network crosslinking density seems more pronounced with this specific vinyl ester. The loss modulus values for EGDVA with 5% of the smallest thiol TMPMP seems to be an outlier but the remaining values are only slightly influenced by the added thiols. Again a too high amount of the largest thiols lead to a drop of the loss modulus as seen in Figure 42.

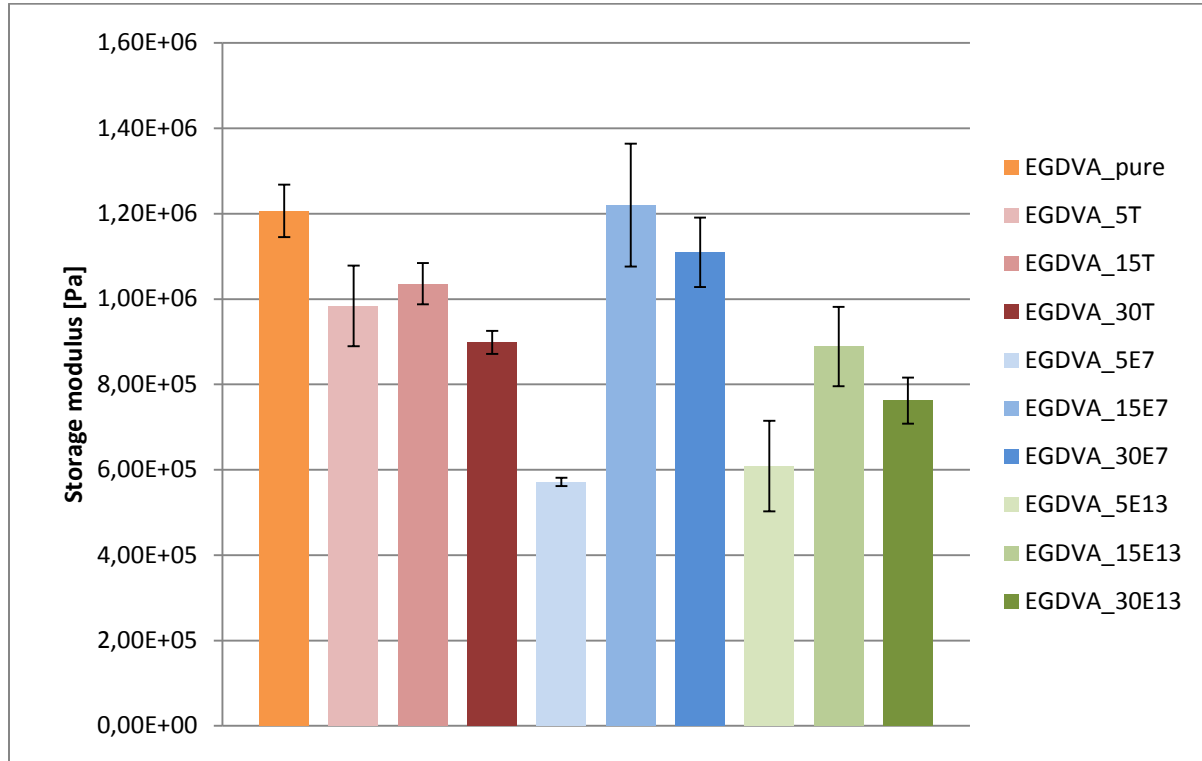


Figure 41: Storage modulus of EGDVA calculated from photorheology

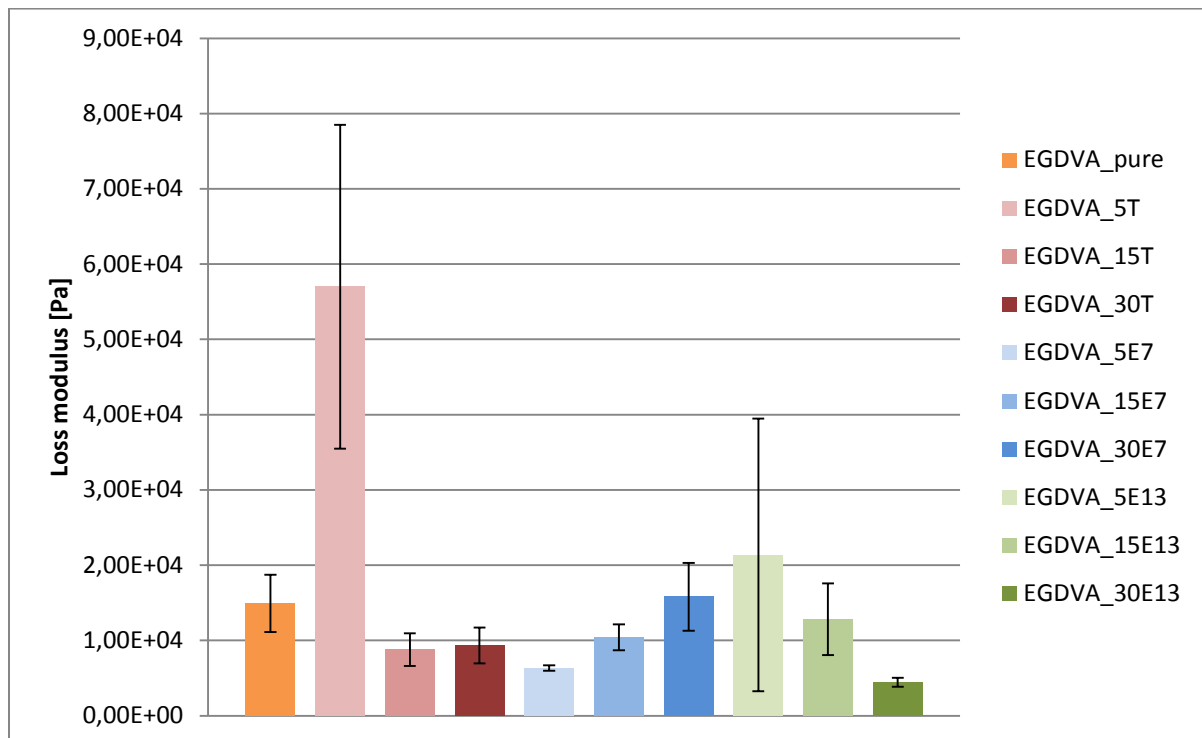


Figure 42: Loss modulus of EGDVA calculated from photorheology

5 Nanoindentation

In general it has to be expected that an addition of thiol leads to decreased network density and therefore also a decrease of Young's modulus and hardness. The received data indicates that it is not as simple as that and a number of parameters influence the resulting properties. To get results comparable to the photorheology measurements, the same formulations were used with 0.5 wt% photoinitiator and 0.5 wt% pyrogallol as storage stabilizer. For each mixture a sample was cured using a silicone mold and the INTELLI-RAY 600 light oven from Uvitron, each sample was measured five times and standard derivation was calculated.

Table 5: Nanoindenter results for DVA

mixture	Young's modulus E_r [kPa]	hardness H_{IT} [kPa]
pure	1070 ± 255	210 ± 9
5T	2050 ± 80	270 ± 10
15T	1890 ± 460	260 ± 5
30T	2200 ± 70	310 ± 20
5E7	2410 ± 190	320 ± 30
15E7	2680 ± 19	340 ± 30
30E7	2280 ± 180	400 ± 50
5E13	14700 ± 1160	1550 ± 230
15E13	9960 ± 360	1190 ± 70
30E13	2940 ± 40	470 ± 6

The mixture names contain [% thiol][symbol of thiol]

eg. 15E7 contains 15% ETTMP700

T ... TMPMP ... trimethylolpropane tri(3-mercaptopropionate)

E7 ... ETTMP700 ... ethoxylated-trimethylolpropan tri-3-mercaptopropionate

MW = $700 \text{ g} \cdot \text{mol}^{-1}$

E13 ... ETTMP1300 ... ethoxylated-trimethylolpropan tri-3-mercaptopropionate

MW = $1300 \text{ g} \cdot \text{mol}^{-1}$

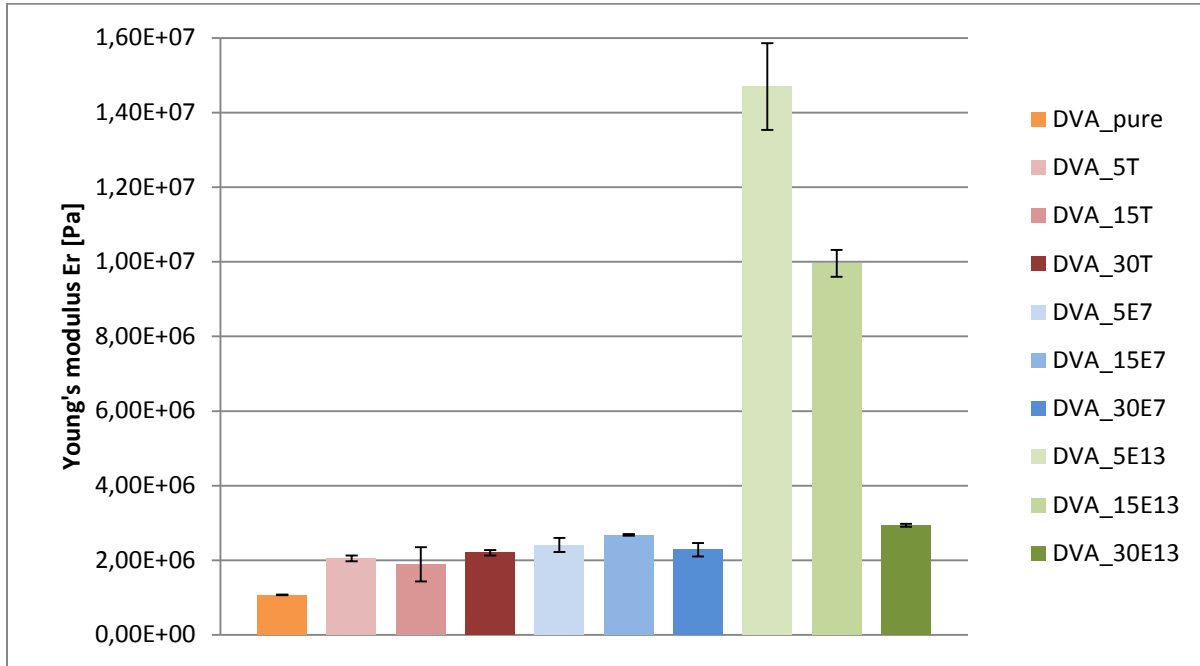


Figure 43: Young's modulus measured via nanoindentation for DVA

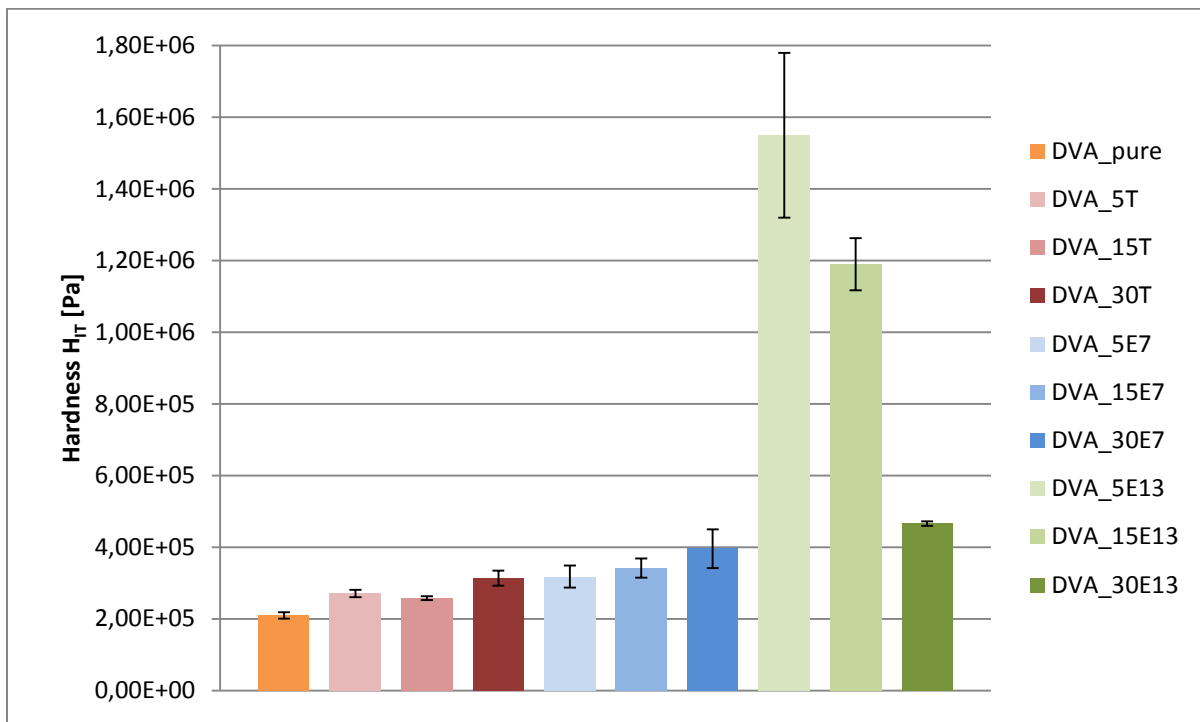


Figure 44: Hardness measured via nanoindentation for DVA

The results for DVA as seen in Table 5 show that for this vinyl ester the addition of thiols lead to increased Young's modulus and Hardness explained by the improved conversion through the thiol-ene reaction. Especially the largest triThiol ETTMP1300 seems to have a big impact on those values. ETTMP1300 also had the biggest positive influence on double bond conversion (DBC) as can be seen in Table 2.

The results for GDVA are listed in Table 6. Here two effects are pronounced differently within the concentration series of the thiols. The smallest triThiol TMPMP increases Young's modulus and hardness in low concentrations due to improved DBC but with 15% and 30% the reduced network crosslinking density leads to lower values. As already seen in the photorheology measurements the mixture of GDVA with the biggest triThiol ETTMP1300 shows the best values with 15%. Also the formation of S-H bridges should be considered in this interpretation adding another effect on the resulting polymer network.

Table 6: Nanoindenter results for GDVA

mixture	Young's modulus E_r [kPa]	hardness H_{IT} [kPa]
pure	2930 ± 100	470 ± 30
5T	3870 ± 120	530 ± 30
15T	2200 ± 40	320 ± 10
30T	2410 ± 10	360 ± 10
5E7	3370 ± 140	470 ± 50
15E7	3320 ± 70	430 ± 20
30E7	4420 ± 90	650 ± 30
5E13	4960 ± 80	670 ± 30
15E13	5380 ± 80	690 ± 10
30E13	3900 ± 90	530 ± 20

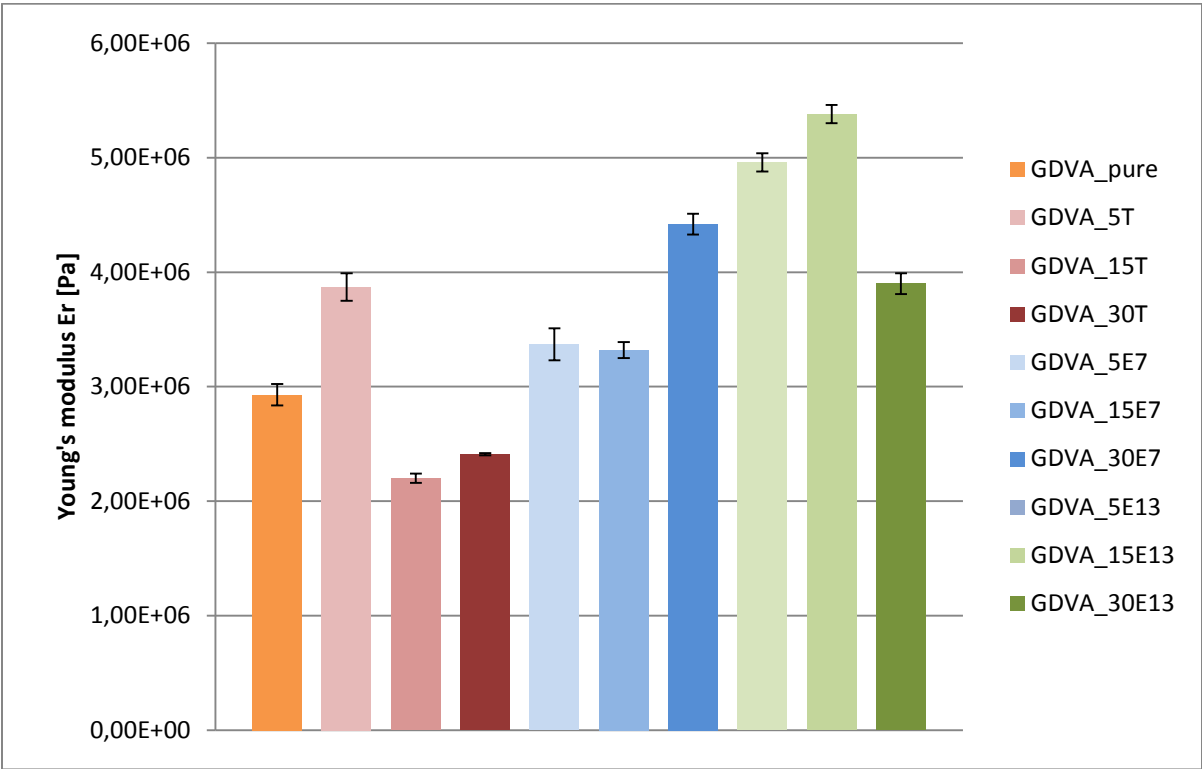


Figure 45: Young's modulus measured via nanoindentation for GDVA

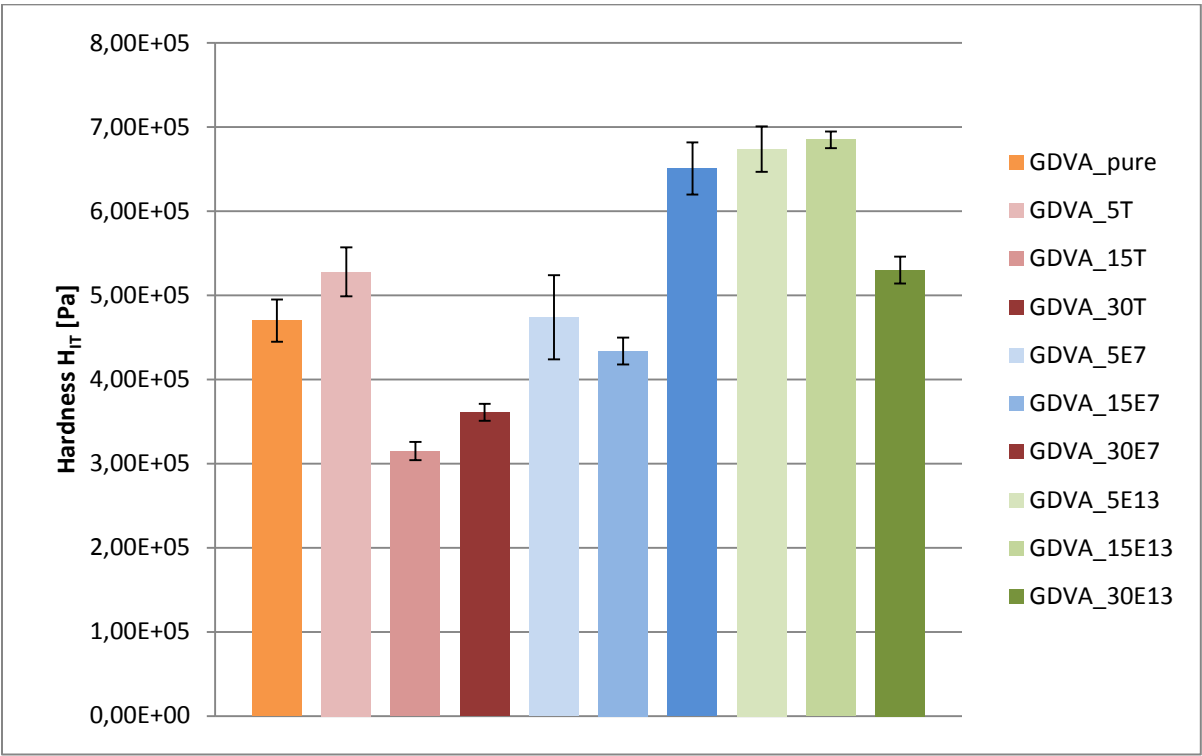


Figure 46: Hardness measured via nanoindentation for GDVA

A problem encountered alongside the curing of the samples for those measurements is oxygen inhibition. The samples for nanoindentation were cured under ambient conditions. It has already been established that chain-growth is the preferred step in the thiol-ene reaction. If peroxy radicals are formed due to reaction with ambient oxygen the homopolymerization of the vinyl monomer gets terminated resulting in lower DBC at the surface of the samples. This effect depends on many factors and is not trivial to predict.

The results for EGDVA are shown in Table 7. For the smallest and the largest triThiol the values are decreasing with increasing amount of thiol in the mixture. Apparently the network-loosening effect seems to be dominant in this case. Within the concentration row of the medium thiol ETTMP700 again the mixture containing 15% shows best results. The combination of higher conversion, uniform network structure and S-H bridges are leading to this outcome.

Table 7: Nanoindenter results for EGDVA

mixture	Young's modulus E_r [kPa]	hardness H_{IT} [kPa]
pure	3500 \pm 720	660 \pm 30
5T	6630 \pm 230	830 \pm 30
15T	5290 \pm 120	750 \pm 30
30T	4110 \pm 100	620 \pm 30
5E7	3060 \pm 120	460 \pm 40
15E7	6500 \pm 190	910 \pm 40
30E7	6120 \pm 160	850 \pm 10
5E13	6150 \pm 170	840 \pm 60
15E13	5080 \pm 60	660 \pm 10
30E13	4260 \pm 330	580 \pm 20

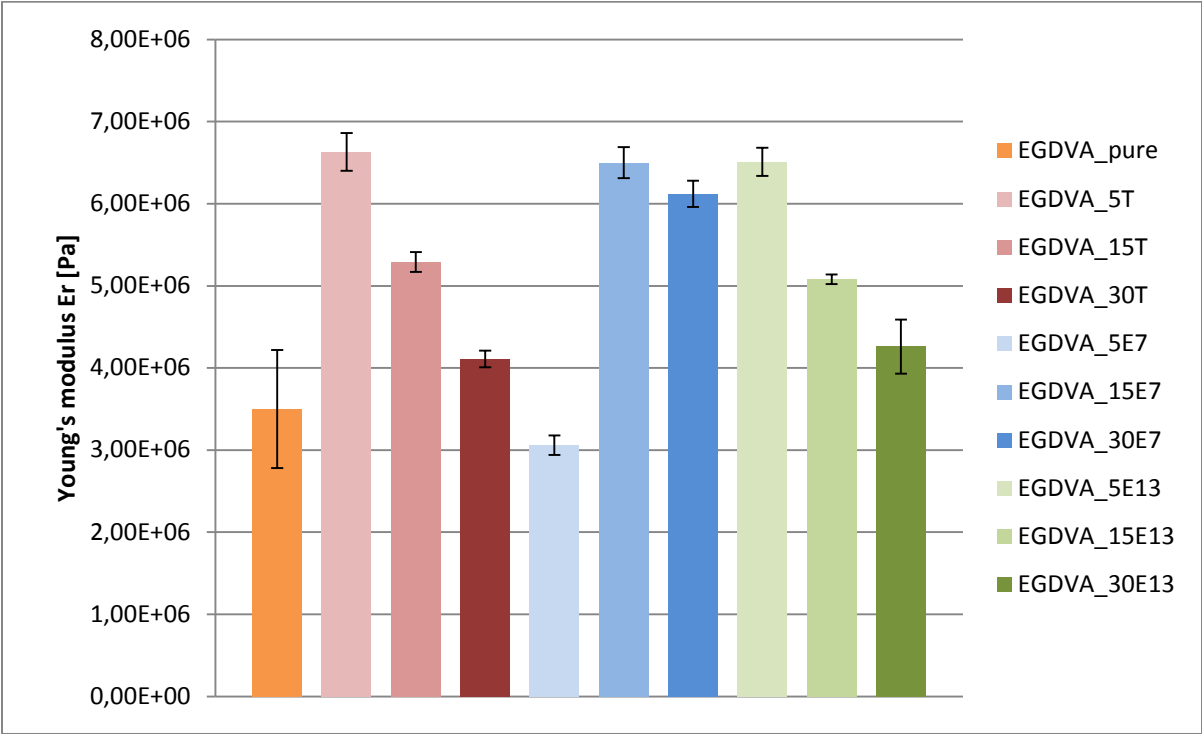


Figure 47: Young's modulus measured via nanoindentation for EGDVA

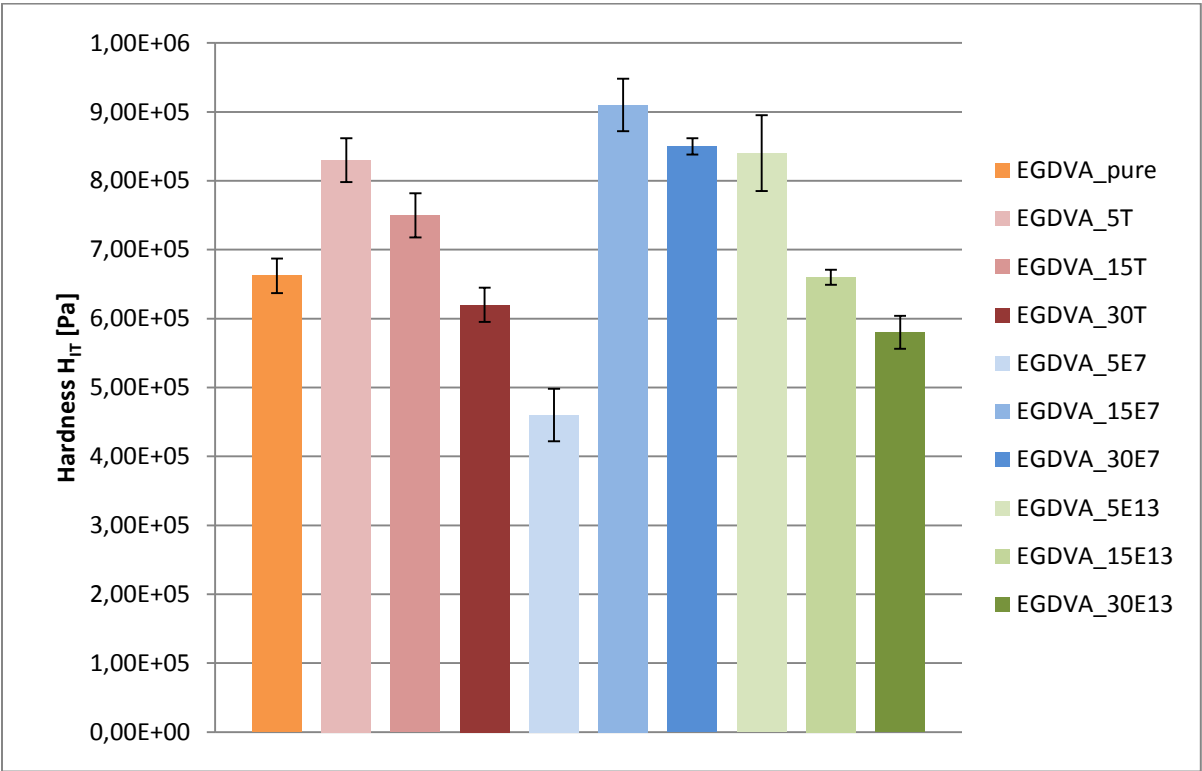


Figure 48: Hardness measured via nanoindentation for EGDVA

6 Degradation Studies

Since degradability of the final implants was one of the important properties in this work, studies on the rate of degradation have been performed.

An often observed problem of biopolymers is so called bulk erosion. Because this can lead to premature failure of the scaffold, surface erosion is the preferred mechanism to achieve homogeneous degradation. This can be assured when the speed of hydrolytically degradation on the surface is significantly faster than the rate of water penetrating the bulk of the matrix.¹²²

Different pathways are possible for degradation of cross-linked polymer networks as shown in the paragraph below.

The first possibility consists of monomers which are first modified with degradable units and afterwards with photoreactive groups. The resulting polymer network is degraded upon cleavage of those degradable units as seen in Figure 49. An example for this type of degradation is PEG-co-PLA diacrylate.

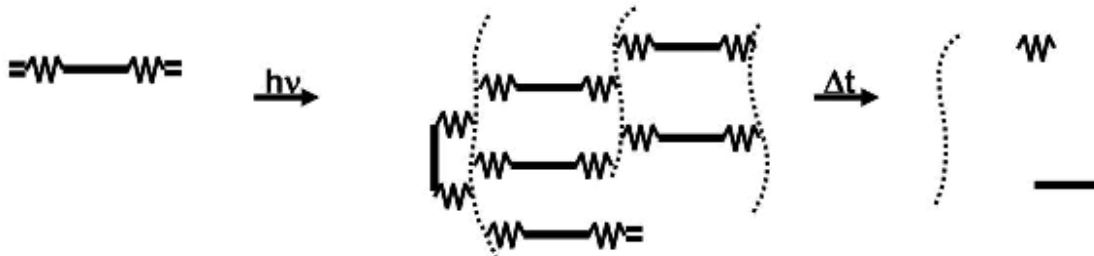


Figure 49: Type 1 degradation of polymer networks

The second mechanism applies for oligomers with photoreactive groups in their backbone that are connected via degradable units. Degradation of this type of photopolymer networks result in starting polymer, degradable units and kinetic chains as for example the degradation of acrylated polyvinyl alcohol (PVA).



Figure 50: Type 2 degradation of polymer networks

The next possible pathway represents monomers with photoreactive moieties along its backbone that are crosslinked under irradiation. The degradation of such polymers leads to kinetic chains and fragments of the starting polymer. This degradation mechanism can be observed for example with polypropylene fumarate (PPF).

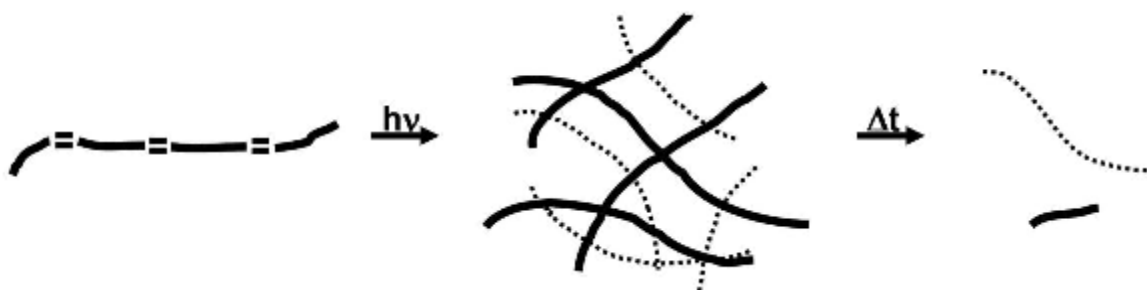


Figure 51: Type 3 degradation of polymer networks

Another mechanism occurs when photoreactive groups are present along a degradable chain. This kind of network degrades into kinetic chains and (sometimes) incorporated parts of the starting materials, as it can be seen in the degradation of acrylated hyaluronic acid.



Figure 52: Type 4 degradation of polymer networks

The ideal degradation behavior of scaffolds for bioimplants matches the time needed to form new tissue and, as previously mentioned, should undergo surface erosion.

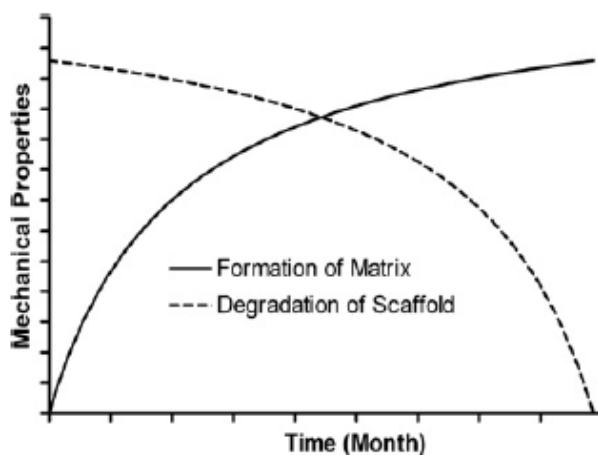


Figure 53: Graph of idealized degradation of scaffolds against formation of new tissue

To get results comparable to the photorheology measurements, the formulations were prepared in the same composition containing 0.5 wt% photoinitiator and 0.5 wt% pyrogallol as storage stabilizer. For two selected mixtures hydrolytical degradation was investigated. This was on one hand done to check if the degradation follows a bulk or surface erosion mechanism and on the other hand to compare the two synthesized vinyl ester monomers towards their degradation behavior. Because the mixtures were expected to degrade rather slowly the experiments were performed at 60°C to accelerate the hydrolysis. Also mixtures with the triThiol ETTMP1300 were selected, expecting the fastest degradation rate because of the highest amount of hydrophilic PEG spacers as well as the least dense network.

Figure 54 shows the degradation behavior of mixtures with 15% of the triThiol ETTMP1300 with GDVA and the triThiol EGDVA. The rather linear slope confirms a surface erosion mechanism which is highly preferred for scaffolds. It is also clearly visible that EGDVA degrades much faster due to additional PEG groups in the vinyl ester. Mixtures with DVA were investigated in our research group by Samusjew and show very slow degradation compared to both GDVA and EGDVA. After 8 weeks under the same conditions, a mixture containing 15% of the triThiol ETTMP1300 and

DVA still has 75% of its initial mass. With this data it should be possible to tune desired degradation behavior by mixing the different vinyl esters.

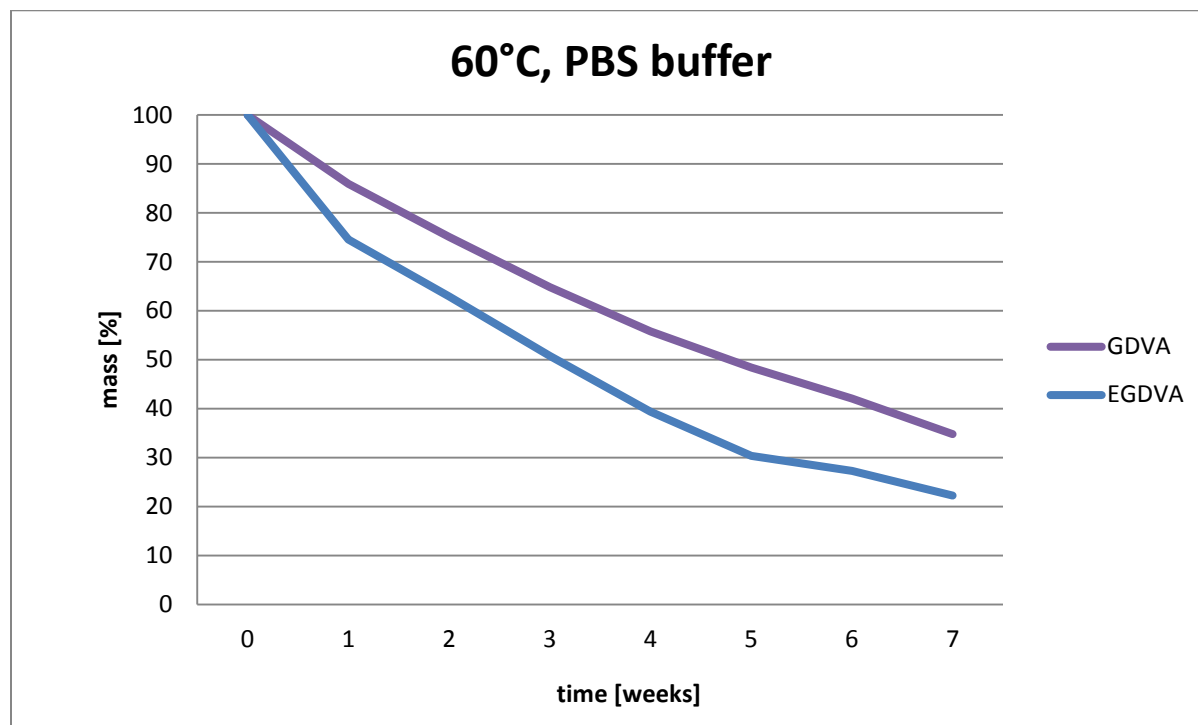


Figure 54: Hydrolytical degradation studies



Figure 55: Samples before (left) and after (right) hydrolytical degradation

7 Lithography-based Ceramic Manufacturing

One of the targets of this work of course was to prove if the newly synthesized vinyl ester monomers can be processed with AMT – especially Lithography-based Ceramic Manufacturing (LCM). Because rather large amounts of monomer mixture (>20 g) are needed for every printing experiment, preliminary tests were done with commercially available DVA. Also the structuring of a cellular geometry to investigate the achievable resolution was done with this system.

Dispersibility test

This test had to be done prior to any further experiments to evaluate the maximum content of inorganic filler that can be incorporated into the organic monomer mixture. Surprisingly a comparable high amount of up to 50% could be added to still obtain a homogeneous, viscous slurry. At higher contents that was no longer possible. Compared to state of the art materials used in LCM the results are very promising and even higher than some of the standard mixtures.

Table 8: Result of dispersibility test

mixture	β-TCP content [g]	β-TCP content [vol%]	dispersible [-]
I	4.20	30	+
II	6.65	40	+
III	10.15	50	+
IV	15.20	60	-

Light penetration test

During the structuring process layers of defined thickness are cured. To find out which light intensity is needed to cure layers with sufficient thickness light penetration tests were done with mixture III containing 50 vol% of β -TCP according to the results of the dispersibility test. The content of photoinitiator was 0.5 wt%. The thickness of the resulting circular shapes was measured with a nanometer screw and the results are listed in Table 9.

Table 9: Results of light penetration test

irradiation time [s]	light intensity [mJ]	layer thickness [μm]
2.9	70	-
4.6	110	-
6.2	150	-
7.9	190	98
10.3	250	119
12.5	300	144

Compared to standard materials used in LCM the intensities needed are slightly higher which can be caused by various factors. One possible explanation is the rather high filler content achievable with this resin. Higher amounts of light energy resulting in elongated building times because each layer takes more time to be cured. For future application it may be necessary to increase the reactivity of the system to speed up the building process.

Structuring experiments

To characterize the printing process for our new monomers and compare the results regarding the achievable double bond conversion a mixture containing the newly synthesized vinyl ester GDVA was used. To get comparable samples the mixture was processed without inorganic particles and cylindrical shapes were manufactured. Those were afterwards analyzed via FTIR-ATR and compared with both the unreacted mixture and the conventionally cured sample.

Based on the results of the previous analysis a mixture GDVA with 15% of the triThiol ETTMP1300 was selected for printing experiments due to its overall performance. Resulting DBC was 15% higher as measured in the samples cured in a silicone mold in the UV oven. This can be easily explained again by oxygen inhibition. During the LCM process the resin is cured from below with little to no ambient oxygen present resulting in higher double bond conversion. Because rather high amount of resin are needed for every printing experiment no further ones were done with GDVA.

To prove that cellular structures can be obtained with LCM a mixture of commercially available DVA with 15% of the triThiol TMPMP was used. According to the previous

experiments 50 vol% β -TCP were added to the resin formulation. It was decided to print a cylindrical structure with a regular pore structure. The results are shown in the Figures 55 and 56 below. This first structuring experiments show that it is possible to create structures with interconnected pores in a range from 270 to 360 μm . For further experiments fine tuning of reactivity and the amount of light absorber should be considered, but this would have gone beyond the scope of this work.

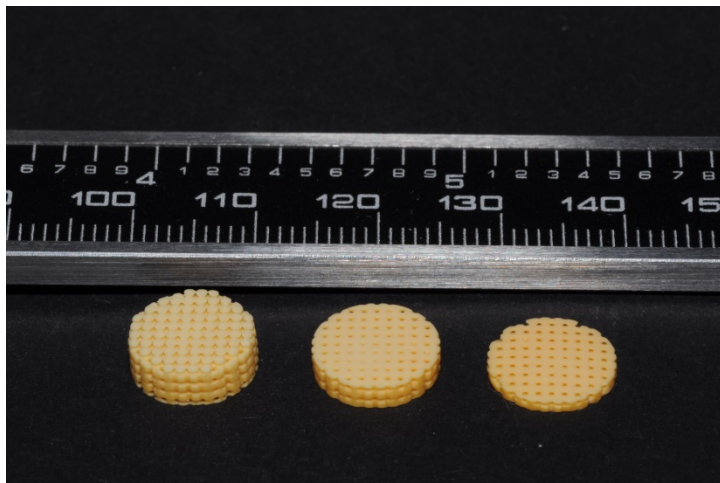


Figure 56: Structures obtained with LCM

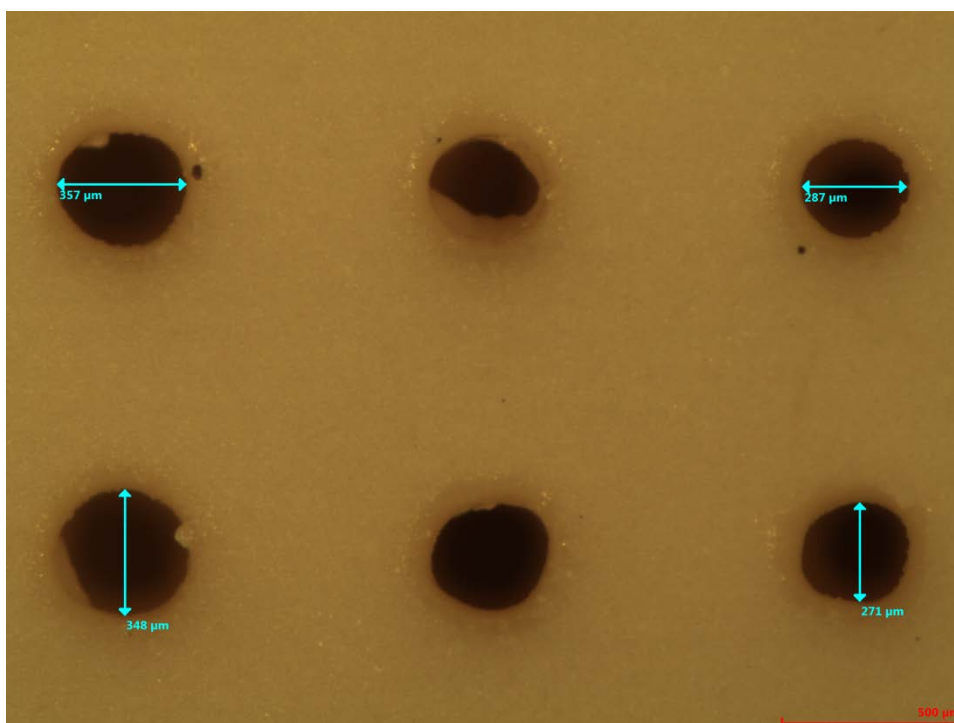
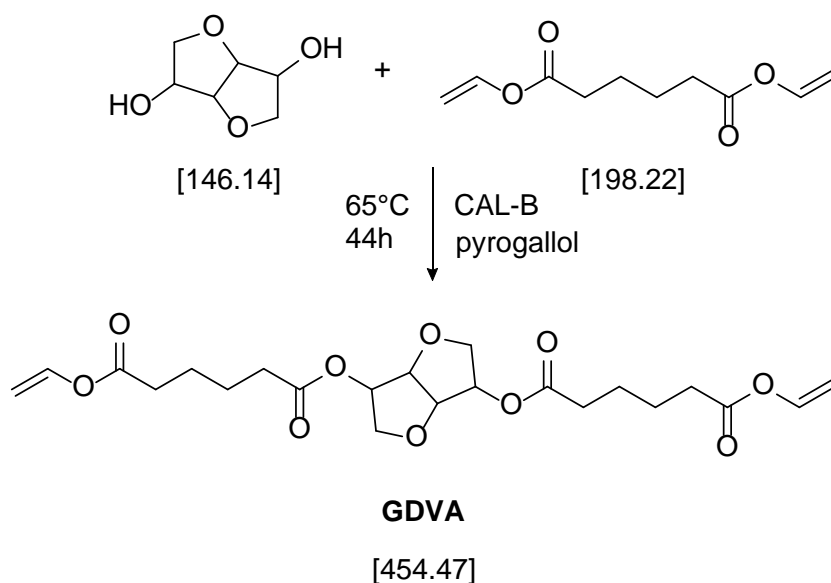


Figure 57: Pore size of the obtained structures

Experimental

3 Synthesis of Monomers

3.1 Synthesis of O,O'-(hexahydrofuro[3,2-b]furan-3,6-diyl) divinyladipate (GDVA)



Materials:

Dianhydro-D-glucitol, recrystallized	1.06 g	(7 mmol, 1 eq)
Divinyl adipate (DVA)	8.63 g	(44 mmol, 6 eq)
Lipase acrylic resin (<i>candida antarctica</i> CAL-B)	100 mg	
Pyrogallol	25 mg	

Preparation:

Prior to the synthesis 25g dianhydro-*D*-glucitol were freshly recrystallized from ~75 mL chloroform. The dianhydro-*D*-glucitol was then grinded and mixed with divinyl adipate in a single-neck flask fitted with a condenser and magnetic stirrer. After most of the dianhydro-*D*-glucitol was dissolved pyrogallol and lipase acrylic resin (*candida antarctica* **CAL-B**) were added and the mixture was heated to 65°C oilbath temperature and stirred for 44 hours. Afterwards the reaction mixture was filtrated

hot to separate the lipase from the reaction solution. The lipase was washed with ~25 mL distilled acetone and the filtrate was combined with the reaction solution. The lipase was dried afterwards and could be reused for similar reactions (reactions done with 1:1 mixtures of fresh and reused lipase). Acetone was removed under vacuum and afterwards excessive DVA (totally 3.15 g) was removed by Kugelrohr distillation (65°C at $7 \cdot 10^{-2}$ mbar). The final purification of the crude product was done by column chromatography (PE:EE+0.5% AcOH = 2:1) to give 1.5 g O,O'-(hexahydrofuro[3,2-b]furan-3,6-diyl) divinyladipate (glucitol divinyl adipate, GDVA) as yellowish oil

Analysis:

Yield: 48 %, $n_D^{20} = 1,4834$, $^1\text{H-NMR}$ (200 MHz, CDCl_3): δ (ppm) = 7.25 (dd, 2H, $J_1 = 14.0$ Hz, $J_2 = 6.4$ Hz, $\text{CH}_2=\text{CH-O-}$), 5.18-5.09 (m, 2H, $-\text{O-OC-CH-}$), 4.89 (m, 1H, $-\text{CH-O-}$) 4.84-4.79 (m, 2H, $\text{CH}_2=\text{CH-O- trans}$), 4.56 (dd, 2H, $J_1 = 6.0$ Hz, $J_2 = 1.6$ Hz, $\text{CH}_2=\text{CH-O- cis}$), 4.47-4.44 (m, 1H, $-\text{CH-O-}$), 3.96-3.74 (m, 4H, $-\text{CH}_2-\text{O-}$), 2.34-2.30 (m, 8H, $\text{VE-CH}_2-\text{CH}_2-\text{CH}_2-$), 1.73-1.63 (m, 8H, $\text{VE-CH}_2-\text{CH}_2-\text{CH}_2-$)

3.1.1 Optimizing GDVA Synthesis

The already established synthesis of GDVA was used to optimize the reaction setup to maximize the yield and simplify the work-up. First prolonged reaction time was investigated. The same mixture as applied in the first synthesis was used but instead of 44h the reaction time was increased to 91h resulting in 1.9 g GDVA (61 % yield). In the next attempt the amount of pyrogallol was reduced to 12 mg (500 ppm) and the lipase was added in 4 equal portions over 4 days, reaction time again >90 hours. Table 10 sums up the optimizing steps and their results.

Table 10: optimizing GDVA synthesis

GDVA synthesis	reaction time [h]	lipase portions [-]	yield [%]
1	44	1	48
2	91	1	61
3	96	4	67

All of the following transesterification reactions were done according to this optimizing experiments which means adding lipase portion wise and an overall reaction time >90 h.

3.1.2 Upscaling GDVA Synthesis

Materials:

Dianhydro-D-glucitol, recrystallized	5.03 g	(35 mmol, 1 eq)
Divinyl adipate (DVA)	43.15 g	(220 mmo, 6 eq)
Lipase acrylic resin (<i>candida antarctica</i> CAL-B)	500 mg	
Pyrogallol	100 mg	

Preparation:

Dianhydro-*D*-glucitol was grinded and mixed with divinyl adipate in a single-neck flask fitted with a condenser and magnetic stirrer. After most of the dianhydro-*D*-glucitol was dissolved pyrogallol and the first quarter of CAL-B were added and the mixture was heated to 65°C oilbath temperature and stirred for 94 hours. The reaction mixture was filtered to separate the lipase which was afterwards washed with ~25 mL distilled acetone. The combined reaction mixture was extracted three times with ~75 mL deionized water. The aqueous phase was then washed twice with dichloromethane and the organic phases were collected, dried with Na₂SO₄ and the solvent was removed under vacuum. After removing a total of 29.30 g excessive DVA by Kugelrohr distillation (65°C at 7*10⁻² mbar) the product was received as 13.31 g of yellowish oil (yield 84 %). The same batch size and reaction procedure

was used in further two experiments to give approximately the same yield (78% and 89%) of GDVA and degree of remaining DVA of 8.3%, which is suitable for further use in LCM.

According to $^1\text{H-NMR}$ analysis DVA can only be completely removed via column chromatography. Since this purification method is not really suitable to work on an industrial scale, and a remaining amount of DVA up to 10% is acceptable for the application in LCM according to Lithoz, it was decided to abstain from column chromatography. To check the residual DVA in every batch in terms of quality control and batch variability a simple analysis method was desired. With the previously obtained clean GDVA from the first synthesis mixtures containing various amounts of DVA were prepared and the refractive index was measured. The results are shown in Figure 58.

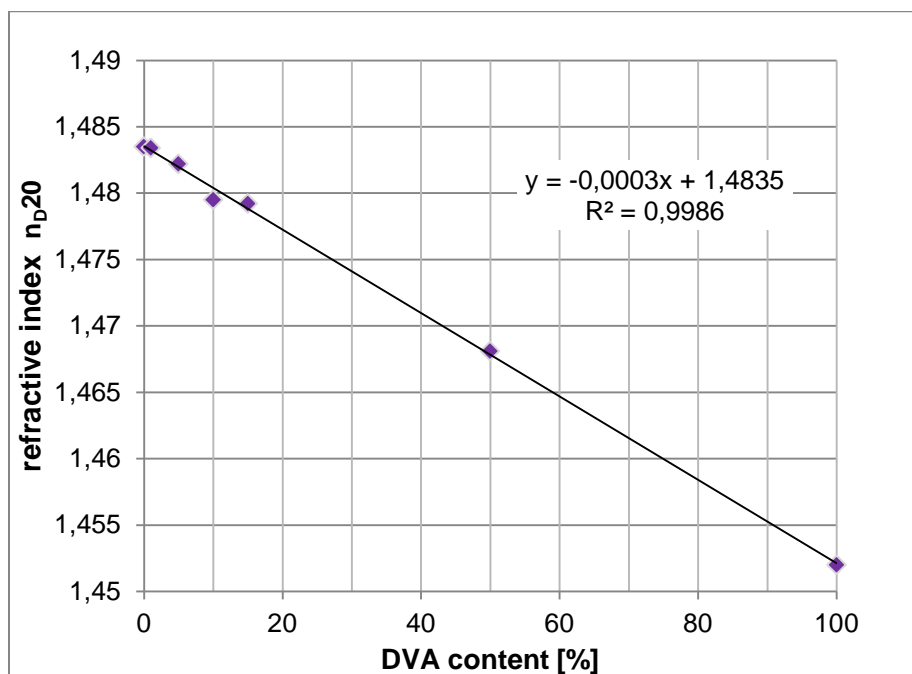
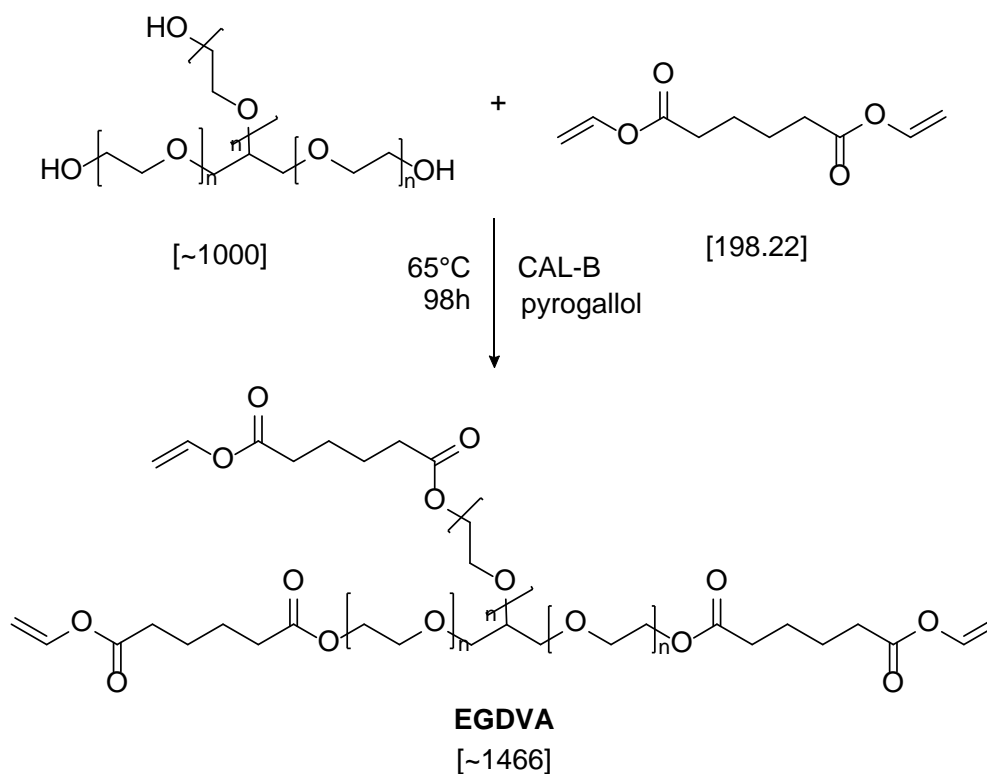


Figure 58: DVA content of GDVA via refractive index

3.2 Synthesis of O,O',O''-((propane-1,2,3-triyltris(oxy))tris(ethane-2,1-diyl))trivinyl triadipate (EGDVA)



Materials:

Ethoxylated glycerol, n=6-7, MW ~1000g/mol	6.15 g	(7 mmol, 1 eq)
Divinyl adipate (DVA)	12.48 g	(63 mmol, 9 eq)
Lipase acrylic resin (<i>candida antarctica</i> CAL-B)	125 mg	
Pyrogallol	11 mg	

Preparation:

Ethoxylated glycerol was used as received and mixed with DVA in a single-neck flask fitted with a condenser and magnetic stirrer. Afterwards pyrogallol and one quarter of the total amount of CAL-B were added. The mixture was heated to 65°C oilbath temperature and stirred for 98 hours. The remaining lipase was added subsequently in portions over 3 days according to the optimization experiments done with the synthesis of GDVA. Afterwards the reaction mixture was filtrated hot to separate the lipase from the reaction solution. The lipase was washed with distilled

acetone which was combined with the reaction solution. Acetone was removed under vacuum and the crude product was extracted three times with deionized water. The aqueous phase was then washed twice with dichloromethane and the organic phases were collected, dried with Na₂SO₄ and the solvent was removed under vacuum. Totally 9.36 g excessive DVA were removed by Kugelrohr distillation (65°C at 7*10⁻² mbar) to receive 6.90 g of O,O',O''-((propane-1,2,3-triyltris(oxy))tris(ethane-2,1-diyl)) trivinyl triadipate (ethoxylated glycerol divinyl adipate, EGDVA) as yellow oil.

Analysis:

Yield: 67 %, ¹H-NMR (200 MHz, CDCl₃): δ (ppm) = 7.18 (dd, 3H, J₁ = 14.0 Hz, J₂ = 6.36 Hz, CH₂=CH-O-), 4.79 (dd, 3H, J₁ = 14.1 Hz, J₂ = 1.6 Hz, CH₂=CH-O- *trans*), 4.48 (dd, 3H, , J₁ = 6.2 Hz, J₂ = 1.6 Hz, CH₂=CH-O- *cis*), 4.16-4.11 (m, 6H, -CO-O-CH₂-CH₂-O-) 3.67-3.44 (m, ~40H, -O-CH₂-), 2.40-2.25 (m, 12H, VE-CH₂-CH₂-CH₂-), 1.63-1.57 (m, 12H, VE-CH₂-CH₂-CH₂-);

¹³C-NMR (400 MHz, CDCl₃): δ (ppm) = 173.29 (CH₂-CH-O-C=O-CH₂), 170.40 (-CH₂-CH₂-C=O-O-CH₂-CH₂-), 141.20 (CH₂-CH-O-C=O-CH₂-), 97.75 (CH₂-CH-O-C=O-CH₂-), 78.48 (-CH₂-CH₂-CH-O-CH₂-), 71.37-69.22 (-O-CH₂-CH₂-O-), 63.60 (-CH₂-CH₂-CH-O-CH₂-), 33.56 (-CH₂-CH₂-C=O-O-CH₂-CH₂-), 24.06 (CH₂-CH₂-CH₂-CH₂-C=O-O-)

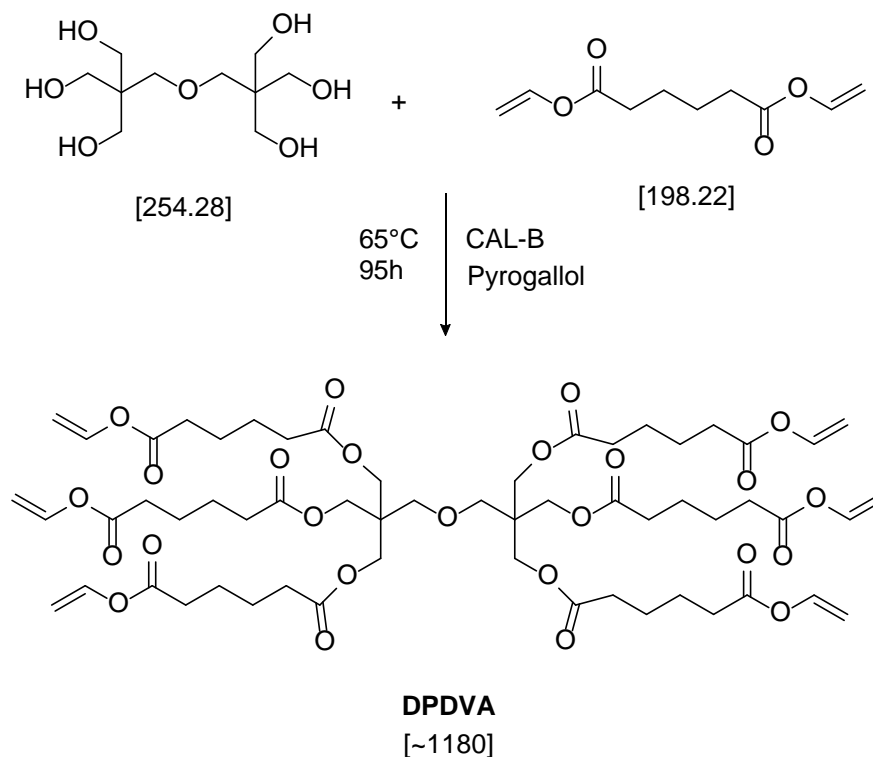
3.2.1 Upscaling EGDVA Synthesis

Materials:

Ethoxylated glycerol	30.75 g	(35 mmol, 1eq)
Divinyl adipate (DVA)	62.40 g	(315 mmol, 9eq)
Lipase acrylic resin (<i>candida antarctica</i> CAL-B)	500 mg	
Pyrogallol	55 mg	

Preparation:

The reaction was carried out twice in the same way as the previous synthesis of EGDVA resulting in 8.28 g (55 %) and 6.61 g (41%) yields.

3.3 Synthesis of Dipentaerythritol divinyl adipate (DPDVA)**Materials (1st attempt):**

Dipentaerythritol	1.78 g	(7 mmol, 1 eq)
Divinyl adipate (DVA)	24.98 g	(126 mmol, 18 eq)
Lipase acrylic resin (<i>candida antarctica</i> CAL-B)	150 mg	
Pyrogallol	11 mg	

Preparation (1st attempt):

Dipentaerythritol was mixed with DVA in a single-neck flask fitted with a condenser and a magnetic stirrer. Afterwards pyrogallol and one quarter of the CAL-B were added. The mixture was heated to 65°C oilbath temperature and stirred for a total of 95 hours. The remaining 90 mg of the lipase were added subsequently in portions over 3 days. Unfortunately dipentaerythritol is not sufficiently soluble in DVA. Therefore as the reaction mixture was filtrated after the reaction, mainly unreacted dipentaerythritol was left in the filter and the remaining lipase could not be separated.

Materials (2nd attempt):

Dipentaerythritol	1.78 g	(7 mmol, 1 eq)
Divinyl adipate (DVA)	24.98 g	(126 mmol, 18 eq)
Lipase acrylic resin (<i>candida antarctica</i> CAL-B)	150 mg	
Pyrogallol	11 mg	
abs. DMSO	25 mL	

Preparation (2nd attempt):

Because of the encountered problems in the first attempt of this reaction the following ones were carried out in solution. Dipentaerythritol was dissolved in 25 mL abs. DMSO and mixed with DVA in a three-neck flask fitted with a condenser, a nitrogen inlet and magnetic stirrer. Afterwards pyrogallol and one quarter of the CAL-B were added. The mixture was heated to 65°C oilbath temperature and stirred for a total of 95 hours under argon. The remaining 90 mg of the lipase were added subsequently in portions over 3 days. After that the reaction mixture was filtrated and the remaining lipase was washed with ~25 mL distilled acetone which was removed again under vacuum. The reaction solution was extracted three times in 250 mL of a mixture of deionized water and PE (1:1). Both the aqueous and the organic phases were collected and the solvents were removed by Kugelrohr distillation. The condensed organic phase contained only DVA according to ¹H-NMR analysis which

was collected for future usage. From the aqueous phase a white solid was obtained after distillation. This still crude product was cooled with liquid N₂, grinded and thoroughly washed with deionized water. The solid was separated via centrifugation to receive 1.01 g of partially substituted dipentaerythritol divinyl adipate (DPDVA) as a white powder.

Analysis:

Yield: 13%; T_m = 190°C; ¹H-NMR (200 MHz, CDCl₃): δ (ppm) = 7.27 (dd, 6H, J₁ = 14.0 Hz, J₂ = 6.36 Hz, CH₂=CH-O-), 4.94 (dd, 6H, J₁ = 14.1 Hz, J₂ = 1.3 Hz, CH₂=CH-O- *trans*), 4.70 (dd, 6H, J₁ = 6.4 Hz, J₂ = 1.4 Hz, CH₂=CH-O- *cis*), 3.40 (s, 12H, -O-CH₂-C-CH₂-), 3.29 (s, 4H, O-CH₂-C-CH₂-), 2.59-2.49 (m, 24H, VE-CH₂-CH₂-CH₂-), 1.60 (m, 24H, VE-CH₂-CH₂-CH₂-); degree of substitution ~2.2 (determined via ¹H-NMR)

1.7 Upscaling DPDVA Synthesis

Materials:

Dipentaerythritol	8.90 g	(35 mmol, 1 eq)
Divinyl adipate (DVA)	124.90 g	(630 mmol, 18 eq)
Lipase acrylic resin (<i>candida antarctica</i> CAL-B)	600 mg	
Pyrogallol	55 mg	
abs. DMSO	125 mL	

Preparation:

The reaction was carried out in the same way as the previous synthesis of DPDVA except for the lipase which was added in one step at the beginning of the reaction to ensure least possible humidity to get into the flask. The up-scaled reaction resulted in 2.50 g (6 %) yield.

4 Photoreactivity

4.1 Photo-Differential Scanning Calorimetry

Procedure:

To measure photo-DSC mixtures were prepared using 0.5 w% photoinitiator (Ivocerin) and 0.05 w% storage stabilizer (pyrogallol). All mixtures were homogenized for 30 minutes using an ultrasonic bath. The formulations were irradiated with a broadband Hg-lamp (320-500 nm filter, 3 W cm^{-2} at the tip of the light guide) and the measurement chamber was purged with dry N_2 . For each ene-component, including DVA, mixtures with three different triThiols in three concentrations were prepared to investigate the influence of concentration and molecular weight of the used thiols. The amount of thiol was always calculates as “% thiol per double bond”. The following tables contain the composition of the used formulations. The abbreviations are explained below.

Table 11: DVA-mixtures for photo-DSC and FTIR-ATR measurements

Mixture	DVA		Thiol			Ivocerin	Pyrogallol
	n [mmol]	m [mg]	n [mmol]	m [mg]	% per DB	m [mg]	m [mg]
DVA_pure	3.90	773.1	-	-	-	3.9	0.4
DVA_5T	3.60	713.6	0.12	47.8	5	3.8	0.4
DVA_15T	3.20	634.3	0.32	127.5	15	3.8	0.4
DVA_30T	2.80	555.0	0.56	223.2	30	3.9	0.4
DVA_5E7	3.50	693.8	0.11	81.7	5	3.9	0.4
DVA_15E7	3.00	594.7	0.30	210.0	15	4.0	0.4
DVA_30E7	2.30	455.9	0.46	322.0	30	3.9	0.4
DVA_5E13	3.50	693.8	0.12	151.7	5	4.2	0.4
DVA_15E13	2.50	495.6	0.25	325.0	15	4.1	0.4
DVA_30E13	1.70	337.0	0.34	442.0	30	3.9	0.4

Table 12: GDVA-mixtures for photo-DSC and FTIR-ATR and measurements

Mixture	GDVA		Thiol			Ivocerin	Pyrogallol
	n [mmol]	m [mg]	n [mmol]	m [mg]	% per DB	m [mg]	m [mg]
GDVA_pure	1.66	755.8	-	-	-	3.8	0.4
GDVA_5T	1.62	736.3	0.05	21.5	5	3.7	0.4
GDVA_15T	1.53	695.4	0.15	61.0	15	3.8	0.4

GDVA_30T	1.42	645.4	0.18	113.2	30	3.9	0.4
GDVA_5E7	1.59	722.6	0.05	37.1	5	3.7	0.4
GDVA_15E7	1.45	659.0	0.15	101.5	15	3.7	0.4
GDVA_30E7	1.28	581.7	0.26	179.2	30	3.9	0.4
GDVA_5E13	1.52	690.8	0.05	65.9	5	3.8	0.4
GDVA_15E13	1.30	590.8	0.13	169.0	15	3.8	0.4
GDVA_30E13	1.06	481.7	0.21	275.6	30	3.9	0.4

Table 13: EGDVA-mixtures for photo-DSC and FTIR-ATR measurements

Mixture	EGDVA		Thiol			Ivocerin	Pyrogallol
	n [mmol]	m [mg]	n [mmol]	m [mg]	% per DB	m [mg]	m [mg]
EGDVA_pure	0.40	586.4	-	-	-	2.9	2.9
EGDVA_5T	0.39	583.4	0.02	7.9	5	3.0	3.0
EGDVA_15T	0.38	570.3	0.06	23.3	15	3.1	3.0
EGDVA_30T	0.37	549.8	0.11	44.8	30	3.0	3.0
EGDVA_5E7	0.39	579.1	0.02	13.8	5	3.2	3.0
EGDVA_15E7	0.37	554.1	0.06	39.7	15	3.0	3.0
EGDVA_30E7	0.35	516.0	0.11	73.9	30	2.9	2.9
EGDVA_5E13	0.38	565.9	0.02	25.1	5	3.0	3.0
EGDVA_15E13	0.35	521.9	0.05	69.4	15	3.1	3.0
EGDVA_30E13	0.32	469.1	0.10	124.8	30	3.0	3.0

The mixture names contain [name of vinyl ester]_[% thiol][symbol of thiol]

eg. *DVA_15E7* is composed of divinyl adipate with 15% ETTMP700

DVA ... divinyl adipate

GDVA ... O,O'-(hexahydrofuro[3,2-b]furan-3,6-diyl) divinyladipat (glucitol divinyl adipate)

EGDVA ... O,O',O''-((propane-1,2,3-triyltris(oxy))tris(ethane-2,1-diyl)) trivinyl triadipate (ethoxylated glycerol divinyl adipate)

T ... TMPMP ... trimethylolpropane tri(3-mercaptopropionate)

E7 ... ETTMP700 ... ethoxylated-trimethylolpropan tri-3-mercaptopropionate MW = 700 g·mol⁻¹

E13 ... ETTMP1300 ... ethoxylated-trimethylolpropan tri-3-mercaptopropionate MW = 1300 g·mol⁻¹

The mixtures were homogenized for 30 minutes using an ultrasonic bath. Afterwards 10 ± 1 mg monomer (-mixture) were weighed accurately into an aluminum pan. The filled pan was placed centrally on the right sensor in the measurement chamber. Two light guides were attached from the top cover of the measurement cell over each pan in 2.5 cm distance. After the crucible was inserted the chamber was closed and purged with N_2 for 4 minutes followed by two irradiation segments of 5 minutes each. The recorded heat flux against the reference was monitored and analyzed. All measurements were done in triplicate.

Results

The different monomers and mixtures were compared regarding their photoreactivity using the calculated t_{95} and t_{max} value.

4.2 FTIR-ATR

Procedure

The samples measured with FTIR-ATR derive from the same mixtures as were used in the photo-DSC measurements containing 0.5 wt% Ivocerin and 0.05wt% pyrogallol. Liquid monomer samples were directly placed onto the crystal layer of the ATR-IR instrument. The corresponding cured polymer samples were photo-cured in an INTELLI-RAY 600 light oven (irradiation power 600W, 80% intensity, 5 minutes of irradiation per side, UV-A: 124 mW cm^{-2} , and VIS: 125 mW cm^{-2}) and were pressed onto the crystal by the “Golden Gate” attachment. Measurements were done at ambient conditions and under light protection for the uncured monomer samples. Spectra were recorded from 2000 cm^{-1} to 1500 cm^{-1} at a resolution of 8 cm^{-1} .

Results

To determine double bond conversion attenuated total reflection (ATR) FT-IR measurements were done. Therefore, IR-spectra of the irradiated samples were compared to those of unreacted monomers. This was done by comparing the peak areas for the vinyl ester C=C bond in both the monomer and the polymer infrared

spectra while using the C=O peak as reference after computer aided baseline correction with the SPECTRUM software. No ATR correction was done. The range of the baseline of the corresponding peak was individually set for each vinyl ester. The double bond conversion was calculated according to formula (4)

4.3 Photorheology

Procedure

All steps for photorheology measurements were done under light protection. 135 µl of all tested formulations were placed in the center of the NaCl plate and measured at 20°C with a gap of 200 µm. The used formulations contained 0.5 wt% Ivocerin and 0.5 wt% pyrogallol and their composition are listed in the tables below. The same abbreviations were used as before.

Table 14: DVA-mixtures for photorheology, nanoindentation and degradation measurements

Mixture	DVA		Thiol			Ivocerin	Pyrogallol
	n [mmol]	m [mg]	n [mmol]	m [mg]	% per DB	m [mg]	m [mg]
DVA_pure	3.50	693.8	-	-	-	3.5	3.5
DVA_5T	3.50	693.8	0.12	46.5	5	3.7	3.7
DVA_15T	3.00	594.7	0.30	119.6	15	3.6	3.6
DVA_30T	2.50	495.6	0.50	199.3	30	3.5	3.5
DVA_5E7	3.50	693.8	0.12	81.7	5	3.9	3.9
DVA_15E7	3.00	594.7	0.30	210.0	15	4.0	4.0
DVA_30E7	2.00	396.4	0.40	280.0	30	3.4	3.4
DVA_5E13	3.50	693.8	0.12	151.7	5	4.2	4.2
DVA_15E13	2.50	495.6	0.25	325.0	15	4.1	4.1
DVA_30E13	1.60	317.2	0.32	416.0	30	3.7	3.7

Table 15: GDVA-mixtures for photorheology, nanoindentation and degradation measurements

Mixture	GDVA		Thiol			Ivocerin	Pyrogallol
	n [mmol]	m [mg]	n [mmol]	m [mg]	% per DB	m [mg]	m [mg]
GDVA_pure	1.30	590.8	-	-	-	3.0	3.0
GDVA_5T	1.24	563.6	0.04	16.5	5	2.9	2.9
GDVA_15T	1.20	545.4	0.12	47.8	15	3.0	3.0
GDVA_30T	1.08	490.8	0.22	86.1	30	2.9	2.9
GDVA_5E7	1.24	563.6	0.04	28.9	5	3.0	3.0

GDVA_15E7	1.13	513.6	0.11	79.1	15	3.2	3.3
GDVA_30E7	1.00	454.5	0.20	140.0	30	3.1	3.1
GDVA_5E13	1.20	545.4	0.04	52.0	5	3.0	2.9
GDVA_15E13	1.02	463.6	0.10	132.6	15	3.1	3.0
GDVA_30E13	0.84	381.8	0.17	218.4	30	3.0	3.0

Table 16: EGDVA-mixtures for photorheology, nanoindentation and degradation measurements

Mixture	EGDVA		Thiol			Ivocerin	Pyrogallol
	n [mmol]	m [mg]	n [mmol]	m [mg]	% per DB	m [mg]	m [mg]
EGDVA_pure	1.30	590.8	-	-	-	3.0	3.0
EGDVA_5T	1.24	563.6	0.04	16.5	5	2.9	2.9
EGDVA_15T	1.20	545.4	0.12	47.8	15	3.0	3.0
EGDVA_30T	1.08	490.8	0.22	86.1	30	2.9	2.9
EGDVA_5E7	1.24	563.6	0.04	28.9	5	3.0	3.0
EGDVA_15E7	1.13	513.6	0.11	79.1	15	3.1	3.1
EGDVA_30E7	1.00	454.5	0.20	140.0	30	3.3	3.0
EGDVA_5E13	1.20	545.4	0.04	52.0	5	3.0	3.2
EGDVA_15E13	1.02	463.6	0.10	132.6	15	3.2	3.3
EGDVA_30E13	0.84	381.8	0.17	218.4	30	3.0	3.0

The formulations were sheered with 1% strain and a frequency of 1Hz. Before the UV light was turned on storage and loss modulus were recorded for 65 seconds with 1 measurement point/s. To start the photopolymerization the UV-light was turned on and projected via waveguides from the downside of the plate and for the following 60 s 1 measurement point/0.2 s was collected. For the remaining 4 minutes of the experiments again 1 measurements point/s was taken. IR measurements started at 60 seconds (5 seconds prior to irradiation) to determine double bond conversion (DBC) and thiol conversion during the reaction. Spectra were recorded from 2000-7000 cm^{-1} and analyzed using OPUS 7.0 software.

Results

At first baseline correction was done with the OPUS software using the rubber-band method. Afterwards the DBC and thiol-conversion was calculated. Therefore the peak areas of the vinyl ester carbonyl peak at $\sim 6120 \text{ cm}^{-1}$ were compared at the

start and the ending of the measurement. Same was done with the SH-peak at $\sim 2580\text{ cm}^{-1}$ of the thiol-containing mixtures.

5 Nanoindentation

Procedure

For nanoindentation measurements pellets with a diameter of 5mm were cured from the same mixtures used in the photo-DSC and FTIR-ATR experiments using a silicone mold and the INTELLI-RAY 600 light oven oven (irradiation power 600W, 80% intensity, 5 minutes of irradiation per side, UV-A: 124 mW cm^{-2} , and VIS: 125 mW cm^{-2}). After transducer and position calibration the samples were glued to the sample holder with fast hardening epoxy resins. The sample holder was placed on the magnetic measuring table. The height of the surface was evaluated via “quick approach”. Two different maximum loads (1 mN and 0.5 mN) were applied with the following profile:

- linear load within 20 s until maximum load
- maximum load constant for 30 s
- unload linear within 10 s

Measurements were repeated 5 times for every sample and maximum load.

Results

Hardness and Young's modulus were calculated from the unload curve according to equation (5) and (6)

6 Degradation studies

Procedure

To investigate the degradation behavior of the new polymers synthesized in this work studies under simulated physiological conditions have been performed. Disk-shaped pellets of 5 mm diameter and approx. 1mm thickness were cured in an INTELLI-RAY 600 light oven oven (irradiation power 600W, 80% intensity, 5 minutes of irradiation per side, UV-A: 124 mW cm^{-2} , and VIS: 125 mW cm^{-2}) from two

selected mixtures from the two newly synthesized liquid monomers were chosen and three samples were prepared per mixture. Those pellets were immersed in Phosphate Buffered Saline (PBS) with a blood-equal pH-value of 7.4 and kept under 60°C for one week. The elevated temperature was chosen to get long-term results in a couple of weeks due to limited time. After each week the buffer was removed and the samples were washed 3 times with distilled methanol and 2 times with deionized water for 15 minutes each. After the washing steps the samples were dried under vacuum for one week and weighted.

PBS composition: NaCl (8.0 g*L⁻¹), KCl (0.2 g*L⁻¹), Na₂HPO₄•2H₂O (1.44 g*L⁻¹), KH₂PO₄ (0.24 g*L⁻¹)

Results

The samples were then dried under vacuum for a week, until their weight was constant, and weighted.

7 Lithography-based Ceramic Manufacturing

Procedure – dispersibility tests

The first step towards LCM was to check how much inorganic filling material can be incorporated into an organic resin. Therefore a mixture of DVA containing 15% of the triThiol TMPMP was chosen, the composition is listed in the table below, noting that no photoinitiator was used in this mixtures.

Table 17: Mixture for dispersibility tests

Component	MW [g*mol ⁻¹]	n [mol]	m [g]
Divinyl adipate	198.21	0.252	50.00
TMPMP*	398.56	0.0252	10.06
Pyrogallol			0.29

*TMPMP ... Trimethylolpropane tri(3-mercaptopropionate)

This master batch was split into 3 g aliquots and loaded with increasing amounts of β -TCP. To ensure dispersibility DisperBYK-111 by Altana was added as standard dispersive agent.

Table 18: Filler content for dispersibility tests

Mixture	DBYK111 [g]	β -TCP [g]	β -TCP [vol%]
I	0.115	4.20	30
II	0.168	6.65	40
III	0.255	10.15	50
IV	0.387	15.20	60

Results – dispersibility tests

The mixtures were mixed using a speed mixer and were afterwards checked towards their homogeneity by pulling a spatula through the slurry and check if the resulting channeling closes itself within 1 minute. This was the case for mixtures up to 50 vol%.

Procedure – light penetration tests

To determine a suitable setup for manufacturing preliminary irradiation tests had to be done. The depth of light penetration at different light intensities had to be measured using a reference mixture containing DVA and 15% of the triThiol TMPMP. The composition of the mixture can be seen in the table below.

Table 19: Mixture for light penetration tests

Component	MW [g* mol^{-1}]	n [mol]	m [g]
Divinyl adipate	198.21	0.076	15.00
TMPMP*	398.56	0.005	2.03
Pyrogallol			0.09
PI Ivocerin			0.09

*TMPMP ... Trimethylolpropane tri(3-mercaptopropionate)

To this organic resin 50 vol% (57.5 g) of β -TCP were added according to the results of the previous dispersibility test and homogenized using a speed mixer to obtain a slurry. This viscous fluid was evenly spread on a microscope slide and placed unto the vat of the printer. Three circular shapes were irradiated using different light intensities. After the polymerization unreacted material was removed using propylene carbonate and a soft cloth.

Results - light penetration tests

The thickness of the cured plates were measured with a nanometer screw

Procedure – manufacturing experiments

According to the previous dispersibility experiments again 50 vol% (a total amount of 95 g) of β -TCP were used in this formulation. The concentration of photoinitiator was 0.5 wt%, and for storage stability 0.05 wt% pyrogallol were added. To prevent overpolymerization and improve the achievable resolution, 0.04 wt% Disperse Orange 3 was used as light absorber. The composition of the resin is shown in Table 20.

Table 20: Mixture for structuring experiments

Component	MW [g*mol⁻¹]	n [mol]	m [g]
Divinyl adipate	198.21	0.118	23.30
TMPMP*	398.56	0.012	4.70
Pyrogallol			0.014
PI Ivocerin			0.14
light absorber			0.011

*TMPMP ... Trimethylolpropane tri(3-mercaptopropionate)

A speedmixer was used to homogenize the resin with the inorganic particles. The slurry was then poured into the glass bottom vat of the printer. The software CeraFab was used to slice the desired geometry into 25 μ m thick layers. Every layer was irradiated for 15 seconds. After the printing process was finished the structure was cleaned with propylene carbonate to remove unreacted material.

Results – manufacturing experiments

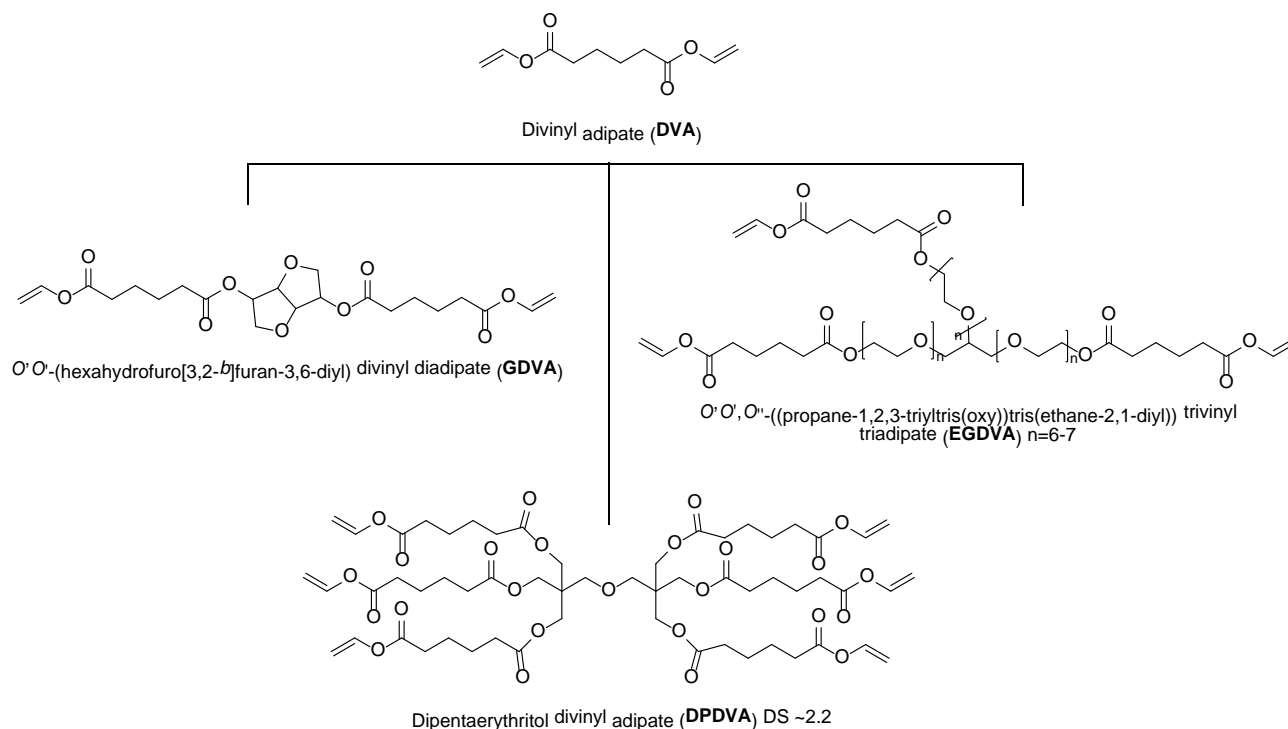
The obtained structures were examined with a light microscope to determine the pore size and pictures were taken.

Conclusion

The future of tissue engineering and regenerative medicine for sure lies in customized scaffolds with tailor-made properties. Great advantages are the possibility to tune mechanical properties as well as degradation behavior alongside with off-the-shelf availability.

The aim of this work was on one hand to synthesize new multifunctional vinyl esters to be used in photopolymerization reactions in combination with thiols to replace state-of-the-art materials like acrylates and methacrylates and on the other hand to prove that Lithography-based Ceramic Manufacturing (LCM) is a suitable manufacturing technique to obtain scaffolds that can be used as potential bone replacements in the future. For these targets the synthesized monomers were examined towards their photoreactivity, mechanical properties and degradation behavior.

The synthesis of novel multifunctional vinyl esters via transesterification with CAL-B was successfully performed and optimized regarding yield and work up. Also up-scaling of the batch sizes was done with good results.



Photoreactivity was investigated via Photo-DSC in order to get values for the time needed to reach the maximum heat of polymerization (t_{\max}) and the time needed to reach 95% of the conversion (t_{95}). Furthermore photo-rheology measurements were done to investigate the real time behavior of the different formulations regarding gel point and conversion. Also FTIR-ATR measurements were performed to calculate the achievable double bond conversion. The novel vinyl ester monomers were compared with the only commercially available difunctional vinyl ester DVA. Regarding photoreactivity the t_{\max} values of the novel vinyl esters outperform those of DVA whereas the t_{95} values are approximately the same. When it comes to double bond conversion (DBC) of the pure vinyl ester formulation DVA is clearly best performing.

Still the reactivity of vinyl esters is too low compared to state-of-the-materials for photopolymerization like acrylates and methacrylates. Therefore another part of the study should cover the influence of thiol-ene chemistry on the reactivity of those vinyl esters. Therefore three different thiols regarding their molecular weight were added in three different concentrations to the vinyl ester monomers. Results show that the addition of thiol improves the photoreactivity of vinyl esters. The maximum heat of polymerization was reached faster and the double bond conversion could be increased. For GDVA the highest DBC of 75% was reached with 30% of the smallest triThiol TMPMP and for EGDVA a DBC of 68% was obtained with the addition of 30% ETTMP700 suggesting that for those monomers the thiols need to fit in terms of size and molecular weight for best outcomes. The results are summarized in the figure below. The numbers in the bars represent the percentage of the thiol-ene ratio. The abbreviations are read as follows:

DVA ...diviny adipate

GDVA...O,O'-(hexahydrofuro[3,2-b]furan-3,6-diyl) divinyladipate (glucitol diviny adipate)

EGDVA...O,O',O''-((propane-1,2,3-triyltris(oxy))tris(ethane-2,1-diyl)) triviny triadipate (ethoxylated glycerol diviny adipate)

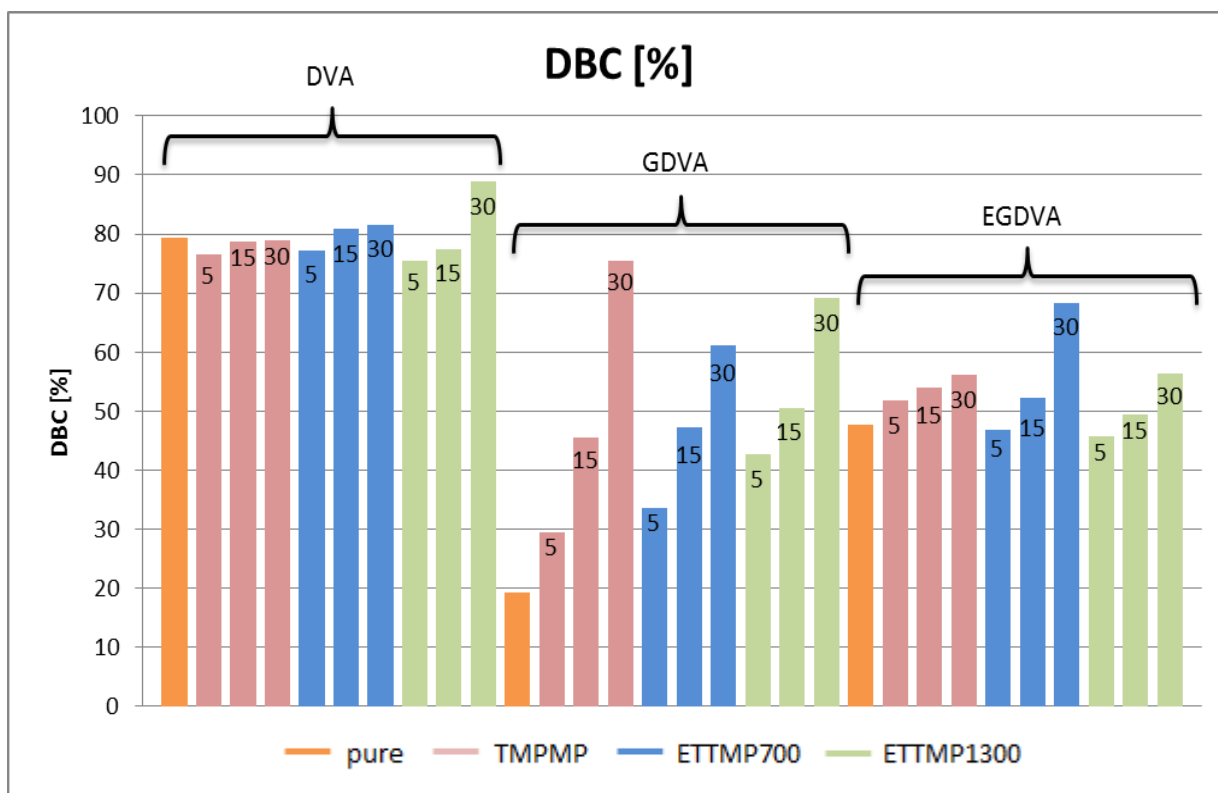
TMPMP...trimethylolpropane tri(3-mercaptopropionate)

ETTMP700...ethoxylated-trimethylolpropan tri-3-mercaptopropionate,

MW = 700 g*mol⁻¹

ETTMP1300...ethoxylated-trimethylolpropan tri-3-mercaptopropionate,

MW = 1300 g*mol⁻¹



To get a first insight in mechanical properties nanoindentation measurements were performed. The results may at first not follow a clear trend but correlate quite well considering the effects of the different thiols on double bond conversion and network density. It is known that addition of thiols results in lower network density and therefore lower mechanical properties. The investigated vinyl esters show different results towards the added thiols both regarding their concentration and size. Also the effect of oxygen inhibition and the resulting impact on surface properties was recorded. An upcoming challenge will be to find balance between enhanced reactivity and increased double bond conversion against a loss of mechanical properties due to loosened networks. For further studies a broad range of

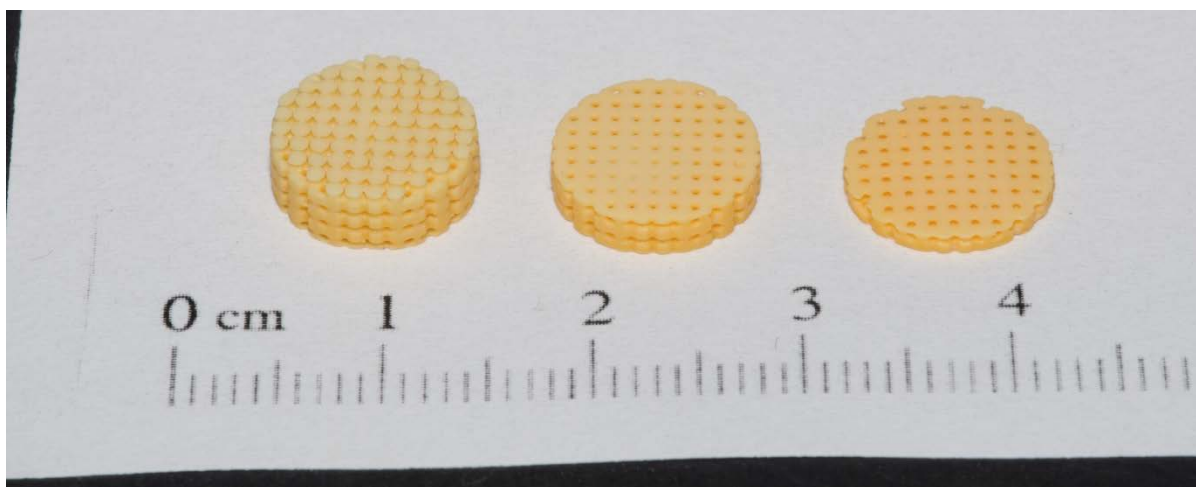
characterization methods such as Dynamic Mechanical Analysis (DMA), Dynstat and 3-point bending seems necessary to fully characterize the obtained materials.

Hydrolytical degradation studies have been performed to monitor degradation behavior and time. For scaffolds dedicated to degrade inside the human body over a certain amount of time is preferred to do so via the mechanism of surface erosion since bulk erosion results in an early loss of mechanical stability whereas samples eroding along the surface mechanism keep their properties quite well over the degradation time. The degradation studies confirmed this kind of surface erosion behavior. The second effect investigated was the influence of the amount of hydrophilic cleavable groups in the final polymer. As expected a mixture of EGDVA with 15% of the triThiol ETTMP1300 with its notable amount of PEG groups degraded significantly faster compared to GDVA with the same amount of the same thiol.

After the characterization of the monomers towards their reactivity preliminary tests with Lithography-based Ceramic Manufacturing were done. The maximum inorganic filler content was explored using ascending amount of β -TCP to obtain homogeneous slurries after speed mixing. It was possible to incorporate up to 50 vol% β -TCP and still receive processable viscosity and homogeneity. This are amounts comparable to currently used systems within LCM and in some cases even better.

The next step was to determine a suitable printer setup to process the previously obtained slurry. Therefore light penetration tests were performed to measure which light intensity is needed to cure layers with sufficient thickness. These measurements indicated that formulations containing vinyl esters tend to be less reactive – as expected – than state-of-the-art acrylate materials. Higher irradiation times, meaning higher light intensities, were needed to cure the desired layers. This finally results in elongated processing times because the longer curing time stacks up with the amount of layers printed. Therefore for future applications it has to be considered to further increase the reactivity of those systems to increase building speed.

Finally structuring experiments using LCM were performed with selected mixtures. GDVA containing 15% of the triThiol ETTMP700 was successfully processed into cylindrical shapes with higher double bond conversion compared to samples cured in the UV oven. Further AMT experiments were also performed with DVA. A composite material of DVA with 15% of the triThiol TMPMP containing 50 vol-% β -TCP was obtained and successfully shaped into a cellular structure with interconnected pores with diameters between 270 and 360 μm .



The examination of the influence of inorganic particles on the mechanical properties and degradation behavior should be part of future studies.

In conclusion it can be stated that the utilization of thiol-ene chemistry significantly improves the reactivity of vinyl esters making them suitable for AMT and possible replacements for acrylates and methacrylates in TERM. Also with the newly synthesized monomers a broad set of mechanical and chemical properties can be accessed by simply combining different vinyl esters and thiols. LCM was successfully performed on selected mixtures both with and without inorganic particles, proving it to be a suitable manufacturing method.

Materials & Characterization Methods

All solvents were applied in a quality common for organic synthesis. All dry solvents were dried following common organic procedures.¹²³

Divinyl adipate was purchased from TCI Europe, the Lipase acrylic resin (candida Antarctica) was purchased from Sigma-Aldrich and the used thiols were thankfully received as a donation from Bruno Bock. Ivocerin was supplied by Ivoclar Vivadent.

All ¹H-NMR were recorded with a BUKER AC-E-200 FT-NMR spectrometer. The chemical shift was reported in ppm (s = singlet, d = doublet, t = triplet, q = quartet, m = multiplet, dd = doublet on doublet, bs = broad singlet). The used solvents were deuterated chloroform (CDCl₃, 99.5 % deuteration) or dimethyl sulfoxide (DMSO-d₆, 99.8 % deuteration)

Column chromatography was performed on Merck silica gel 60 (0.040-0.063 mm). The silica gel chromatography was performed with a Büchi MPLC-system equipped with the control unit C-620, fraction collector C-660 and UV-photometer C-635.

The synthesized monomers were tested towards photoreactivity and cytotoxicity. Mixtures with different multifunctional thiols were examined regarding their photoreactivity as well as their mechanical properties and degradation behavior. Selected mixtures were then filled with β-TCP and processed using LCM to obtain specimens for mechanical testing of the resulting composites.

Photo-differential scanning calorimetry

The measurements of photoreactivity were done on a Netzsch Photo-DSC 204 F1 Phoenix equipped with an autosampler. Figure 60 shows a typical calorigram that is obtained after subtracting the second irradiation segment, where already cured polymer was irradiated, from the first segment, the actual photopolymerization.



Figure 59: left: Netzsch Photo-DSC 204 F1 Phoenix®; right: measurement cell

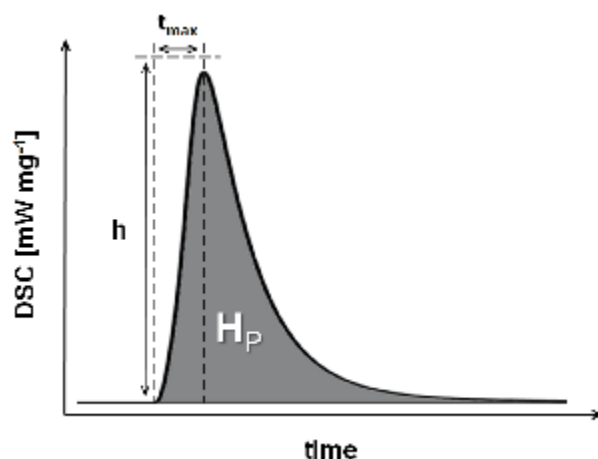


Figure 60: Calorigram from Photo-DSC measurement

This measurement grants access to a couple of useful values describing the reactivity of photopolymers such as double bond conversion (DBC), polymerization rate (R_p) and the time to reach the maximum heat of polymerization (t_{max}).

To calculate the DBC the theoretical heat of 100% conversion is needed ($\Delta H_{0,p}$) as well as the heat enthalpy resulting from the polymerization experiment in the measurement chamber (ΔH_p).

$$DBC = \frac{\Delta H_p}{\Delta H_{0,p}} \quad (1)$$

This simple calculation can only be made for pure monomers. When it comes to monomer mixtures additional data is required such as molar masses (M_w), mole fractions (M_f) and polymerization heats of every monomer contained in the mixture.

$$DBC = \frac{\Delta H_p}{\Delta H_{0,p}} = \Delta H_p \cdot \sum \frac{M_w \cdot M_f}{\Delta H_0} \quad (2)$$

The rate of polymerization (R_p) monitors the rate at which the monomer is converted. It can be calculated from the value of the maximum of the Photo-DSC peak (h), the mixtures density (ρ), the number of photoreactive groups per molecule (f) and the polymerization heat of the single constituent parts of the monomer mixture (ΔH_0)

$$R_p = \frac{h \cdot \rho}{\Delta H_0} = h \cdot \sum \frac{\rho \cdot M_f \cdot f}{\Delta H_0} \quad (3)$$

To measure reactivity towards photopolymerization monomers and thiol-ene mixtures were tested using photo-differential scanning calorimetry.

Photorheology

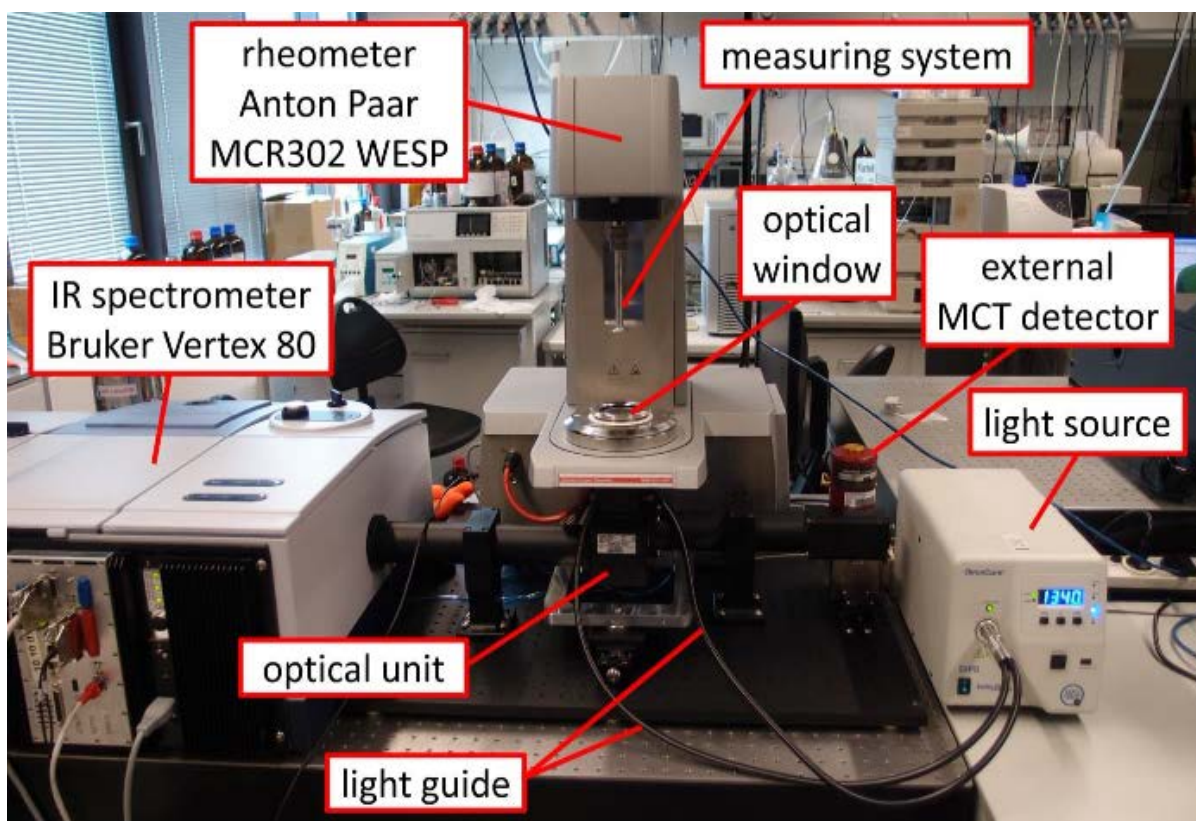


Figure 61: Experimental set up for RT-NIR/MIR-photoreology experiments

RT-NIR/MIR-photoreology measurements were performed on an Anton Paar MCR 302 WESP with a P-PTD 200/GL Peltier NaCl plate and a disposable PP25 measuring system. Additionally the rheometer was coupled with a Bruker Vertex 80 FTIR spectrometer with external mirrors to guide the IR beam through the sample during the rheology measurement. The IR beam passes through the NaCl plate and is reflected by the flat plate rheology head before returning to the external MCT-detector. For UV curing an Exfo OmnuCure™ 2000 with a broadband Hg-lamp (320-500 nm, 3 W cm^{-2} at the tip of the light guide) was used. The IR chamber was continuously purged with dry air.

FTIR-ATR Measurements

The measurements were performed on a Spectrum 65 FTIR-ATR spectroscope from Perkin-Ellmer in UATR mode using the Golden Gate device for solid samples. The solid samples were prepared by irradiation in an INTELLI-RAY 600 light oven from Uvitron. The monomer samples were measured under light protection. Spectra were recorded from 2000 cm^{-1} to 1500 cm^{-1} at a resolution of 8 cm^{-1} .

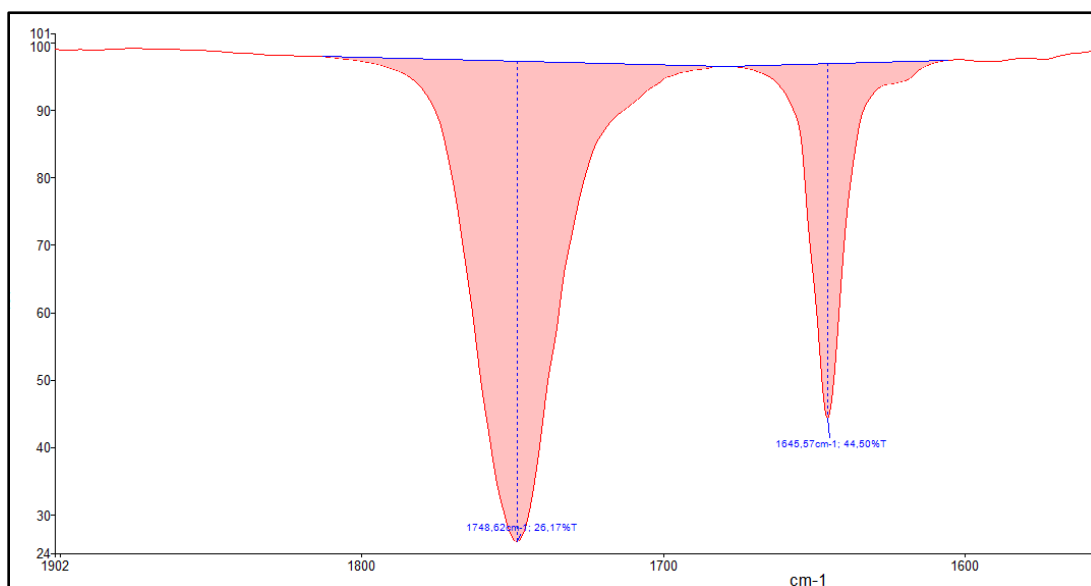


Figure 62: Example spectrum of a liquid resin formulation

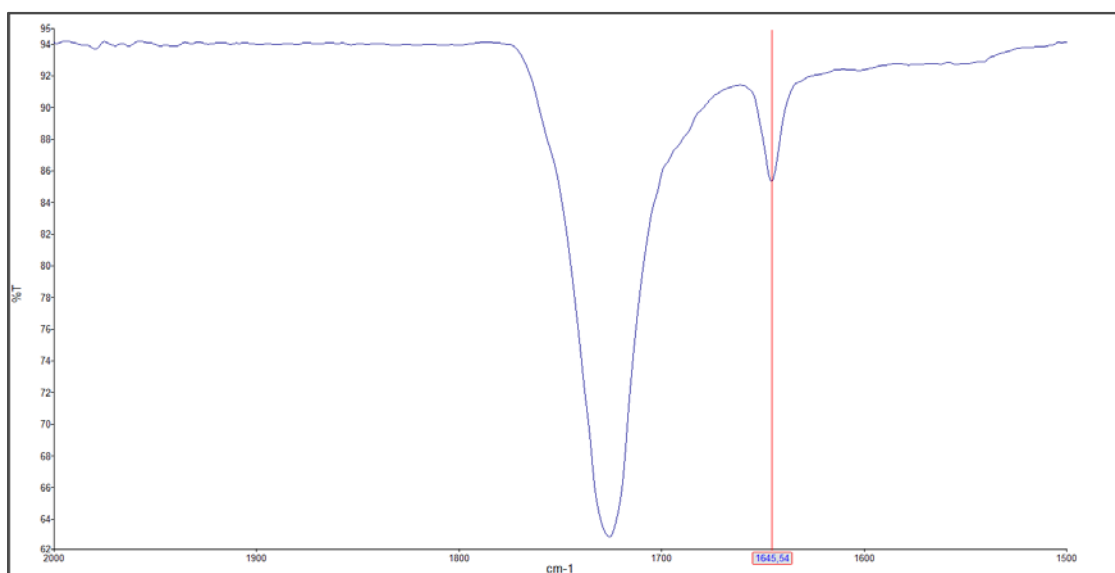


Figure 63: Example spectrum of a cured polymer sample

To calculate the double bond conversion peak areas of the vinyl ester peak were used and the carbonyl peak was used as reference. With the aid of the SPECTRUM software baseline correction was applied and the peak-areas were calculated. The DBC was calculated according to the following equation:

$$DBC [\%] = \left[1 - \frac{\left(\frac{C=C_{peak\ start}}{C=O_{peak\ start}} \right)}{\left(\frac{C=C_{peak\ end}}{C=O_{peak\ end}} \right)} \right] \cdot 100\% \quad (4)$$

For all spectra automatic baseline correction was done by the Spectrum software and afterwards the peaks were integrated. For each set of monomers the same ranges of wavenumbers were chosen to assure comparability.

Nanoindentation

For nanoindentation experiments a Hysitron Ubi 750 with extended z-stage and Berkovich indenter tip was used

This is a very convenient measurement because only small sample volumes are needed. Also a number of values can be measured namely Young's modulus, hardness and strain-rate sensitivity.

During the measurement a diamond-tipped probe indents the specimen with defined force and indenting rate. The displacement of the tip is measured and with the known shape of the indenter the contact area at full load is calculated from the cavity of penetration.¹²⁴

A typical nanoindentation curve is shown in Figure 64.

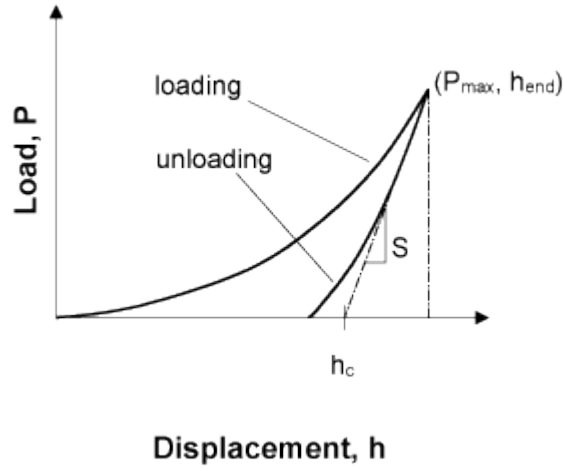


Figure 64: Idealized nanoindentation curve

This recorded load-displacement curve can be used to calculate various mechanical properties of the material.

Young's modulus (E_r) is calculated via the stiffness (S) of the contact which again can be calculated from the slope of the curve dP/dh upon unloading.

$$E_r = \frac{1}{\beta} \frac{\sqrt{\pi}}{2} \frac{S}{\sqrt{A_p(h_c)}} \quad (5)$$

$A_p(h_c)$ is the projected area of the indentation at the contact depth h_c and β is a geometrical constant.

The hardness (H) relates the maximum load (P_{max}) to the indentation area (A_r) and is given by the following equation:

$$H = \frac{P_{max}}{A_r} \quad (6)$$

Finally the strain-rate sensitivity of the flow stress (m) is defined as:

$$m = \frac{\partial \ln \sigma}{\partial \ln \dot{\epsilon}} \quad (7)$$

In this equation $\sigma = \sigma(\dot{\epsilon})$ is the flow stress and $\dot{\epsilon}$ is the strain rate produced under the indenter.

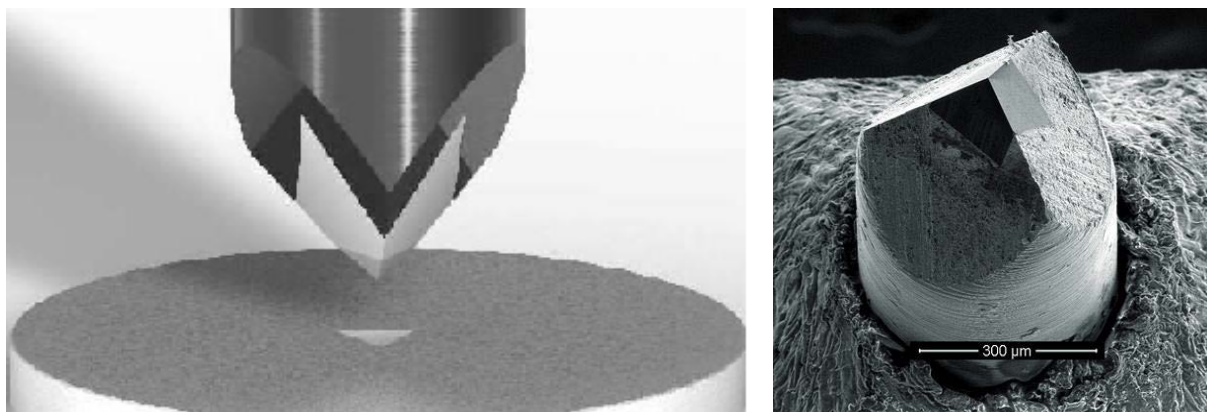


Figure 65: left: Cubecorner nanoindenter-tip¹²⁵; right: SEM picture of nanoindenter tip¹²⁶

Polymer specimens for degradations studies, nanoindentation and FTIR-ATR measurements were photo-cured in a INTELLI-RAY 600 **light oven** from Uvitron (irradiation power 600W, UV-A: 124 mW cm⁻², and VIS: 125 mW cm⁻²).

Preparations of photoreactive formulations and substances were carried out in a **yellow light laboratory**. The laboratory has adhesive foils from IFOHA company attached to all windows and the fluorescent lamps were type Osram lumilux with chip controlled light colour 62 (wavelength below 480 nm are filtered)

Lithography-based Ceramic Manufacturing

One of the goals of this work was to obtain composite photopolymers using AMT. The most suitable technique to do so is lithography-based Ceramic Manufacturing (LCM), a method developed by members of the Vienna University of Technology. Usually LCM is used to print ceramic green parts that are afterwards sintered to obtain dense ceramic parts with very low porosity. To produce degradable scaffolds

suitable for TERM this post-processing step is canceled and the parts can be used as printed. The main parts of the printing setup are shown in the scheme below.

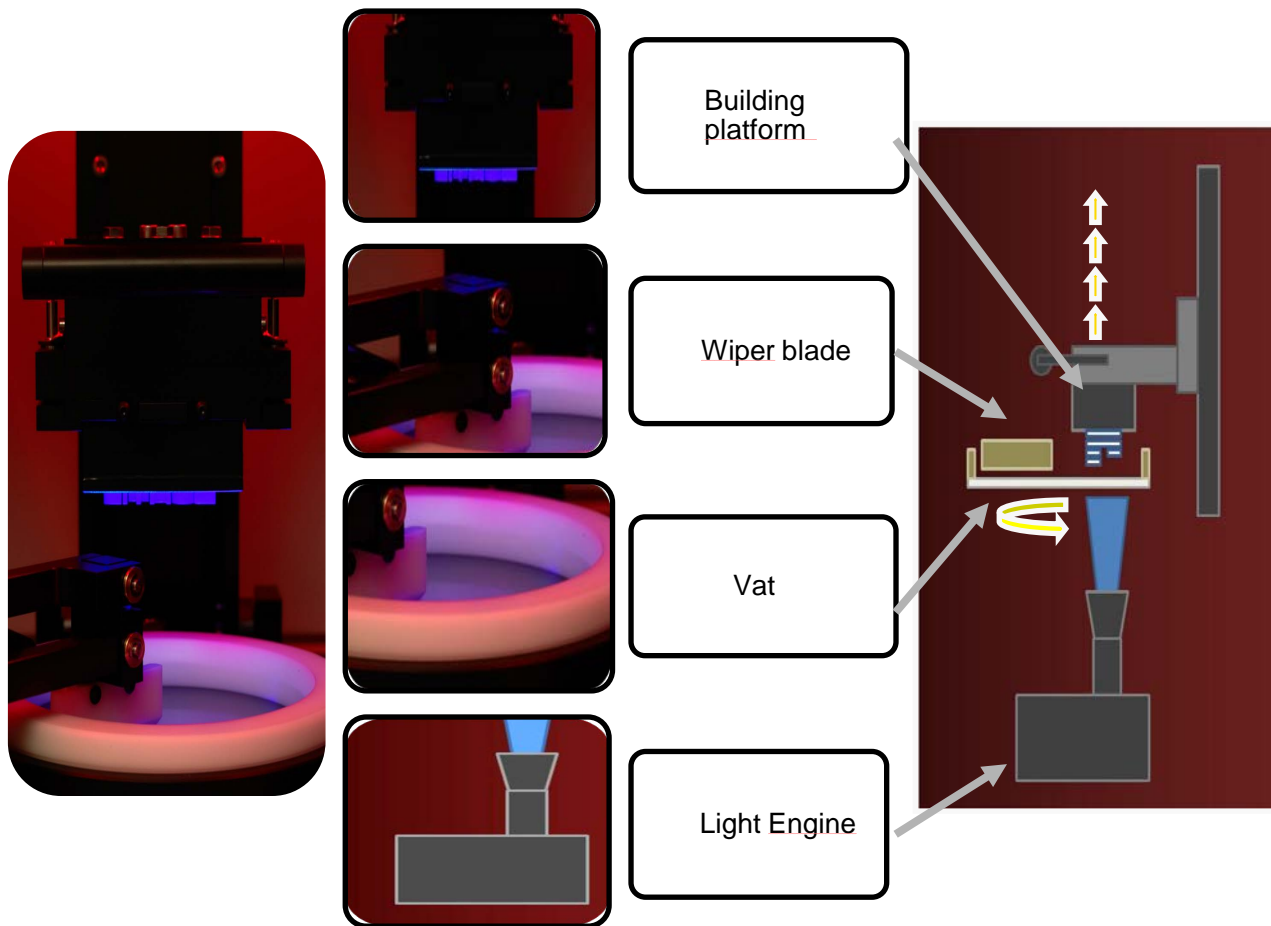


Figure 66: LCM printer © Lithoz 2014

Each layer is built in the same manner:

1. The building platform is lowered into the vat that contains the resin.
2. The light engine irradiates the photosensitive resin through the glass bottom of the vat curing layer of desired shape at a time.
3. After irradiation the platform is moved up again and the vat rotates 360° to spread fresh slurry over the glass plate.

Abbreviations

A

AcOH	acetic acid
AEMA	2-aminoethyl methacrylate
AMT	Additive Manufacturing Technologies
abs.	absolute

B

β -TCP	
BPM	Ballistic Particle Manufacturing

C

CAD	Computer Aided Design
CAL-B	Candida Antarctica Lipase B
CDCl ₃	deuterated chloroform
CT	Computer Tomography
CQ	camphor quinone

D

δ	chemical shift
ΔH_p	heat of polymerization
$\Delta H_{p,0}$	theoretical heat of polymerization
DBC	double bond conversion
DEF	diethyl fumarate
DLP	Digital Light Processing
DMA	Dynamic Mechanical Analysis
DMAB	dimethylamine benzoate
DMSO	dimethyl sulfoxide
DS	degree of substitution
DSC	differential scanning calorimetry
DPDVA	dipentaerythritol divinyl adipate
DVA	divinyl adipate

E

ε	tensile strain
E	Young's modulus
EA	ethyl acetate
EGDVA	ethoxylated glycerol divinyl adipate
ETTMP	ethoxilated-trimethylolpropan tri-3-mercaptopropionate
eq	equivalents

F

F	tensile force
FDA	Food & Drug Administration
FDM	Fused Deposition Modeling
FTIR-ATR	Fourier transformd infrared spectroscopy – Attenuated total reflectance

G

GDVA	glucitol divinyl adipate
GMA	glycidyl methacrylate

H

h	height
HA	hydroxyl apatite

I

ICEMA	2-isocyanatoethyl methacrylate
-------	--------------------------------

L

l	length
λ	wavelength
LCM	lithography-based ceramic manufacturing
LED	light emitting diode
LENS	Laser Engineered Net Shaping
LOM	Laminated Object Manufacturing
LTP	Liquid Thermal Polymerization

M

MAA	methacrylic acid
MCPH	1,3-bis(4-carboxyphenoxy)hexane
MIR	mid-infrared
mN	Millinewton
MPMA-ala	pyromellityl imido alanine
MPLC	medium pressure liquid chromatography
MRI	Magnetic Resonance Imaging
poly MSA	polymerized methacrylated sebacic acid
MTCA	tricarballic acid
MW	molecular weight

N

n_D20	refractive index, sodium-D-line, at 20°C
NIR	near-infrared
NVP	N-vinylpyrrolidone

P

PBAE	poly(β -aminoester)
PBS	phosphate buffered saline
PCL	poly(ϵ -caprolacton)
PCLF	poly(ϵ -caprolacton fumarate)
PE	petroleum ether
PEG	poly(ethylene glycol)
PEGDA	poly(ethylene glycol diacrylate)
PEGDMA	poly(ethylene glycol dimethacrylate)
PI	photoinitiator
PLA	poly(lactic acid)
PNB	poly(norbornene)
PPF	poly(propylene fumarate)
PPGDMA	poly(propylene glycol dimethacrylate)
PTMC	poly(trimethylene carbonate)
PVA	poly(vinyl alcohol)

R

ρ	density
RP	rapid prototyping
R_p	rate of polymerization
RT	room temperature

S

σ	tensile stress
SEM	scanning electron microscope
SF	Spatial Forming
SFF	solid free-forming fabrication
SFP	Solid Foil Polymerization
SGC	Solid Ground Curing
SLA	Stereolithography
SLS	Selective Laser Sintering
SMD	Shape Deposition Manufacturing

T

2PP	Two-photon induced Polymerization
3DP	tree-dimensional printing
3PB	three-point bending
TE	tissue engineering
TEA	tetraethyl ammonia
TERM	tissue engineering and regenerative medicine
TMPMP	trimethylolpropane tri(3-mercaptopropionate)

U

UATR	universal attenuated total reflection
UV	ultraviolet

V

VIS	visible
-----	---------

Literature

- (1) Chiara, G.; Letizia, F.; Lorenzo, F.; Edoardo, S.; Diego, S.; Stefano, S.; Eriberto, B.; Barbara, Z. "*Nanostructured biomaterials for tissue engineered bone tissue reconstruction*"; Int. J. Mol. Sci. 2012, **13**, 737-757.
- (2) Currey, J. In *The structure and mechanical properties of bone*, Woodhead Publishing Ltd.: 2008; pp 3-27.
- (3) Olszta, M. J.; Cheng, X.; Jee, S. S.; Kumar, R.; Kim, Y.-Y.; Kaufman, M. J.; Douglas, E. P.; Gower, L. B. "*Bone structure and formation: A new perspective*"; Mater. Sci. Eng., R 2007, **R58** (3-5), 77-116.
- (4) Bose, S.; Roy, M.; Bandyopadhyay, A. "*Recent advances in bone tissue engineering scaffolds*"; Trends Biotechnol 2012, **30** (10), 546-54.
- (5) Feng, B.; Jinkang, Z.; Zhen, W.; Jianxi, L.; Jiang, C.; Jian, L.; Guolin, M.; Xin, D. "*The effect of pore size on tissue ingrowth and neovascularization in porous bioceramics of controlled architecture in vivo*"; Biomed Mater 2011, **6** (1), 015007.
- (6) Murphy, C. M.; Haugh, M. G.; O'Brien, F. J. "*The effect of mean pore size on cell attachment, proliferation and migration in collagen-glycosaminoglycan scaffolds for bone tissue engineering*"; Biomaterials 2010, **31** (3), 461-6.
- (7) Kawamura, N.; Kugimiya, F.; Oshima, Y.; Ohba, S.; Ikeda, T.; Saito, T.; Shinoda, Y.; Kawasaki, Y.; Ogata, N.; Hoshi, K.; Akiyama, T.; Chen, W. S.; Hay, N.; Tobe, K.; Kadowaki, T.; Azuma, Y.; Tanaka, S.; Nakamura, K.; Chung, U.-i.; Kawaguchi, H. "*Akt1 in Osteoblasts and Osteoclasts Controls Bone Remodeling*"; PLoS ONE 2007, **2** (10), e1058.
- (8) Fan, Y.; Fan, Y.; Li, Z.; Loan, M.; Lv, C.; Bo, Z. "*Optimal Principle of Bone Structure*"; PLoS ONE 2011, **6** (12), e28868.
- (9) Heinemann, S.; Gelinsky, M.; Worch, H.; Hanke, T. "*Resorbable bone substitution materials: An overview of commercially available materials and new approaches in the field of composites*"; Orthopade 2011, **40** (9), 761-73.
- (10) Salgado, A. J.; Coutinho, O. P.; Reis, R. L. "*Bone tissue engineering: state of the art and future trends*"; Macromol Biosci 2004, **4** (8), 743-65.
- (11) Raposo-Amaral, C. E.; Almeida, A. B.; Alonso, N.; Bueno, D. F.; Costa, C. C.; Gouveia, C. H.; Fanganiello, R. D.; Passos-Bueno, M. R.; Jorgetti, V.; Vulcano, L. C. "*Is bone transplantation the gold standard for repair of alveolar bone defects?*"; J Tissue Eng 2014, **5**, 2041731413519352.
- (12) Vallet-Regi, M.; Colilla, M.; Gonzalez, B. "*Medical applications of organic-inorganic hybrid materials within the field of silica-based bioceramics*"; Chem Soc Rev 2011, **40** (2), 596-607.
- (13) Pina, S.; Oliveira, J. M.; Reis, R. L. "*Natural-Based Nanocomposites for Bone Tissue Engineering and Regenerative Medicine: A Review*"; Advanced Materials 2015, n/a-n/a.
- (14) S.M.Schnürer, U. G., K.-D. Kühn, S.j. Breusch "*Knochenersatzwerkstoffe*"; Orthopäde 2003, **32**:2-10.
- (15) Balla, V. K.; Bodhak, S.; Bose, S.; Bandyopadhyay, A. "*Porous tantalum structures for bone implants: fabrication, mechanical and in vitro biological properties*"; Acta Biomater 2010, **6** (8), 3349-59.

- (16) Balla, V. K.; Banerjee, S.; Bose, S.; Bandyopadhyay, A. "Direct laser processing of a tantalum coating on titanium for bone replacement structures"; *Acta Biomater* 2010, **6** (6), 2329-34.
- (17) Lee, S.-H.; Shin, H. "Matrices and scaffolds for delivery of bioactive molecules in bone and cartilage tissue engineering"; *Advanced Drug Delivery Reviews* 2007, **59** (4-5), 339-359.
- (18) Jones, J. R.; Ehrenfried, L. M.; Hench, L. L. "Optimising bioactive glass scaffolds for bone tissue engineering"; *Biomaterials* 2006, **27** (7), 964-973.
- (19) Pereira, M. M.; Jones, J. R.; Hench, L. L. "Bioactive glass and hybrid scaffolds prepared by sol-gel method for bone tissue engineering"; *Adv. Appl. Ceram.* 2005, **104** (1), 35-42.
- (20) Hsu, H.; Lacey, D. L.; Dunstan, C. R.; Solovyev, I.; Colombero, A.; Timms, E.; Tan, H.-L.; Elliott, G.; Kelley, M. J.; Sarosi, I.; Wang, L.; Xia, X.-Z.; Elliott, R.; Chiu, L.; Black, T.; Scully, S.; Capparelli, C.; Morony, S.; Shimamoto, G.; Bass, M. B.; Boyle, W. J. "Tumor necrosis factor receptor family member RANK mediates osteoclast differentiation and activation induced by osteoprotegerin ligand"; *Proceedings of the National Academy of Sciences* 1999, **96** (7), 3540-3545.
- (21) Santavirta, S.; Konttinen, Y.; Saito, T.; Gronblad, M.; Partio, E.; Kempainen, P.; Rokkanen, P. "Immune response to polyglycolic acid implants"; *Journal of Bone & Joint Surgery, British Volume* 1990, **72-B** (4), 597-600.
- (22) Jandt, K. D. "Evolutions, Revolutions and Trends in Biomaterials Science – A Perspective"; *Advanced Engineering Materials* 2007, **9** (12), 1035-1050.
- (23) Stańczyk, M. "Study on modelling of PMMA bone cement polymerisation"; *Journal of Biomechanics* 2005, **38** (7), 1397-1403.
- (24) Dorozhkin, S. "Calcium orthophosphate-based biocomposites and hybrid biomaterials"; *J Mater Sci* 2009, **44** (9), 2343-2387.
- (25) Rezwan, K.; Chen, Q. Z.; Blaker, J. J.; Boccaccini, A. R. "Biodegradable and bioactive porous polymer/inorganic composite scaffolds for bone tissue engineering"; *Biomaterials* 2006, **27** (18), 3413-3431.
- (26) Murugan, R.; Ramakrishna, S. "Development of nanocomposites for bone grafting"; *Composites Science and Technology* 2005, **65** (15-16), 2385-2406.
- (27) R. Z. LeGeros, J. P. L., G. Daculsi, R. Kijkowska "Encyclopedia handbook of biomaterials and bioengineering"; Marcel Dekker, New York 1995, **2**.
- (28) Oliveira, J. M.; Silva, S. S.; Malafaya, P. B.; Rodrigues, M. T.; Kotobuki, N.; Hirose, M.; Gomes, M. E.; Mano, J. F.; Ohgushi, H.; Reis, R. L. "Macroporous hydroxyapatite scaffolds for bone tissue engineering applications: Physicochemical characterization and assessment of rat bone marrow stromal cell viability"; *Journal of Biomedical Materials Research Part A* 2009, **91A** (1), 175-186.
- (29) De Nardo, L.; Bertoldi, S.; Tanzi, M. C.; Haugen, H. J.; Fare, S. "Shape memory polymer cellular solid design for medical applications"; *Smart Mater. Struct.* 2011, **20** (3), 035004/1-035004/12.
- (30) Janik, H.; Marzec, M. "A review: Fabrication of porous polyurethane scaffolds"; *Materials Science and Engineering: C* 2015, **48** (0), 586-591.
- (31) Silva, T. H.; Alves, A.; Ferreira, B. M.; Oliveira, J. M.; Reis, L. L.; Ferreira, R. J. F.; Sousa, R. A.; Silva, S. S.; Mano, J. F.; Reis, R. L. "Materials of marine origin: a

review on polymers and ceramics of biomedical interest"; International Materials Reviews 2012, **57** (5), 276-306.

(32) Nam, Y. S.; Yoon, J. J.; Park, T. G. "A novel fabrication method of macroporous biodegradable polymer scaffolds using gas foaming salt as a porogen additive"; Journal of Biomedical Materials Research 2000, **53** (1), 1-7.

(33) Liu, X.; Ma, P. X. "Phase separation, pore structure, and properties of nanofibrous gelatin scaffolds"; Biomaterials 2009, **30** (25), 4094-4103.

(34) Paletta, J. R. J.; Mack, F.; Schenderlein, H.; Theisen, C.; Schmitt, J.; Wendorff, J. H.; Agarwal, S.; Fuchs-Winkelmann, S.; Schofer, M. D. "Incorporation of osteoblasts (MG63) into 3D nanofiber matrices by simultaneous electrospinning and spraying in bone tissue engineering"; Eur. Cells Mater. 2011, **21**, 384-395.

(35) Gatford, J., A diagram of the electrospinning process showing the onset of instability.

http://en.wikipedia.org/wiki/Electrospinning#mediaviewer/File:Electrospinning_Diagram.jpg, 2008.

(36) Darwish, O. A. A. a. S. M. "Fabrication of Tissue Engineering Scaffolds Using Rapid Prototyping Techniques"; World Academy of Science, Engineering and Technology 2011, **59**.

(37) Technology, V. U. o., AMT - Research and Projects. 2013.

(38) Gebhardt, A. "Rapid Prototyping - Werkzeuge für die schnelle Produktentstehung". 2 ed.; Hanser Fachbuch: 2000.

(39) Hutmacher, D. W.; Sittinger, M.; Risbud, M. V. "Scaffold-based tissue engineering: rationale for computer-aided design and solid free-form fabrication systems"; Trends in Biotechnology 2004, **22** (7), 354-362.

(40) Leong, K. F.; Cheah, C. M.; Chua, C. K. "Solid freeform fabrication of three-dimensional scaffolds for engineering replacement tissues and organs"; Biomaterials 2003, **24** (13), 2363-2378.

(41) Ian Gibson, D. W. R., Brent Strucker "Additive Manufacturing Technologies". Springer: US, 2010.

(42) C. S. Taylor, P. C., H. Hampton, J. F. Frantzen, B. O. Shah, W. B. Tiffany, L. Nanis, P. Booker, A. Salahieh, R. Hansen "Patial Foming" A Tree Dimensional Printing Process"; Proc. IEEE MEMS (Amsterdam) 1995, 203.

(43) Technology, V. U. o., St. Stephan's cathedral, Vienna. 2010.

(44) M. Schwentenwein, P. S., J. Homa "Lithography-based Ceramic Manufacturing: A Novel Technique for Additive Manufacturing of High-Performance Ceramics"; Advances in Science and Technology 2014, **88**, 60-64.

(45) Ciba, S. C. I. "Photoinitiators for UV Curing"; Inc., C. S. C. 2013.

(46) MADSEN, N. J.; Sehnal, P.; Anderson, D. G.; Nielsen, B. R., Novel polymeric photoinitiators and photoinitiator monomers. Google Patents: 2014.

(47) Bryant, S. J.; Nuttelman, C. R.; Anseth, K. S. "Cytocompatibility of UV and visible light photoinitiating systems on cultured NIH/3T3 fibroblasts in vitro"; J Biomater Sci Polym Ed 2000, **11** (5), 439-57.

(48) Davis, K. A. B., J. A., Anseth, K. S. Biomaterials 2003, **24**, 2485.

(49) Hoyle, C. E.; Bowman, C. N. "Thiol-Ene Click Chemistry"; Angew. Chem., Int. Ed. 2010, **49** (9), 1540-1573.

- (50) Zonca, M. R., Jr.; Falk, B.; Crivello, J. V. "LED-Induced Thiol-ene Photopolymerizations"; J. Macromol. Sci., Pure Appl. Chem. 2004, **A41** (7), 741-756.
- (51) Gush, D. P.; Ketley, A. D. "Thiol/acrylate hybrid systems"; Mod. Paint Coat. 1978, **68** (11), 58, 61-2, 64, 66.
- (52) Marketsandmarkets "Bio-Implants Market - by Type (Cardiovascular, Spine, Orthopedics, Trauma, Dental), by ROA (Surgical/Injectable), by Origin (Allo/Auto/Xenograft, Synthetic) & Material (Cermics, Biomaterial, Alloys, Polymers) - Global Trends & Forecasts till 2017"; Marketsandmarkets2012 2012.
- (53) Mautner, A.; Qin, X.; Wutzel, H.; Ligon, S. C.; Kapeller, B.; Moser, D.; Russmueller, G.; Stampfl, J.; Liska, R. "Thiol-ene photopolymerization for efficient curing of vinyl esters"; J. Polym. Sci., Part A: Polym. Chem. 2013, **51** (1), 203-212, S203/1-S203/6.
- (54) Chen, Y.-C.; Lin, R.-Z.; Qi, H.; Yang, Y.; Bae, H.; Melero-Martin, J. M.; Khademhosseini, A. "Functional Human Vascular Network Generated in Photocrosslinkable Gelatin Methacrylate Hydrogels"; Adv. Funct. Mater. 2012, **22** (10), 2027-2039.
- (55) Schuster, M.; Turecek, C.; Weigel, G.; Saf, R.; Stampfl, J.; Varga, F.; Liska, R. "Gelatin-based photopolymers for bone replacement materials"; J. Polym. Sci., Part A: Polym. Chem. 2009, **47** (24), 7078-7089.
- (56) Schuster, M.; Turecek, C.; Kaiser, B.; Stampfl, J.; Liska, R.; Varga, F. "Evaluation of biocompatible photopolymers I: photoreactivity and mechanical properties of reactive diluents"; J. Macromol. Sci., Part A: Pure Appl. Chem. 2007, **44** (5), 547-557.
- (57) Ovsianikov, A.; Deiwick, A.; Van Vlierberghe, S.; Dubruel, P.; Moeller, L.; Draeger, G.; Chichkov, B. "Laser Fabrication of Three-Dimensional CAD Scaffolds from Photosensitive Gelatin for Applications in Tissue Engineering"; Biomacromolecules 2011, **12** (4), 851-858.
- (58) Ovsianikov, A.; Deiwick, A.; Van Vlierberghe, S.; Pflaum, M.; Wilhelmi, M.; Dubruel, P.; Chichkov, B. "Laser fabrication of 3D gelatin scaffolds for the generation of bioartificial tissues"; Materials 2011, **4**, 288-299.
- (59) Marklein, R. A.; Soranno, D. E.; Burdick, J. A. "Magnitude and presentation of mechanical signals influence adult stem cell behavior in 3-dimensional macroporous hydrogels"; Soft Matter 2012, **8** (31), 8113-8120.
- (60) Bae, M. S.; Kim, S. E.; Na, J. S.; Kwon, I. K. In *The effect of simvastatin acid loaded photocurable hyaluronic acid hydrogel for bone regeneration in vitro and in vivo*, CRC Press: 2010; pp 354-357.
- (61) Bencherif, S. A.; Srinivasan, A.; Horkay, F.; Hollinger, J. O.; Matyjaszewski, K.; Washburn, N. R. "Influence of the degree of methacrylation on hyaluronic acid hydrogels properties"; Biomaterials 2008, **29** (12), 1739-1749.
- (62) Rossi, C. A.; Flaibani, M.; Blaauw, B.; Pozzobon, M.; Figallo, E.; Reggiani, C.; Vitiello, L.; Elvassore, N.; De Coppi, P. "In vivo tissue engineering of functional skeletal muscle by freshly isolated satellite cells embedded in a photopolymerizable hydrogel"; FASEB J. 2011, **25** (7), 2296-2304, 10.1096/fj.10-174755.
- (63) Hu, J.; Hou, Y.; Park, H.; Choi, B.; Hou, S.; Chung, A.; Lee, M. "Visible light crosslinkable chitosan hydrogels for tissue engineering"; Acta Biomater. 2012, **8** (5), 1730-1738.

- (64) Li, Q.; Yang, D.; Ma, G.; Xu, Q.; Chen, X.; Lu, F.; Nie, J. "Synthesis and characterization of chitosan-based hydrogels"; *Int. J. Biol. Macromol.* 2009, **44** (2), 121-127.
- (65) Tsuda, Y.; Hattori, H.; Tanaka, Y.; Ishihara, M.; Kishimoto, S.; Amako, M.; Arino, H.; Nemoto, K. "Ultraviolet light-irradiated photocrosslinkable chitosan hydrogel to prevent bone formation in both rat skull and fibula bone defects"; *J. Tissue Eng. Regener. Med.* 2013, **7** (9), 720-728.
- (66) Qiu, Y.; Zhang, N.; Kang, Q.; An, Y.; Wen, X. "Chemically modified light-curable chitosans with enhanced potential for bone tissue repair"; *J. Biomed. Mater. Res., Part A* 2009, **89A** (3), 772-779.
- (67) Burdick, J. A.; Frankel, D.; Dernell, W. S.; Anseth, K. S. "An initial investigation of photocurable three-dimensional lactic acid based scaffolds in a critical-sized cranial defect"; *Biomaterials* 2003, **24** (9), 1613-20.
- (68) Burdick, J. A.; Padera, R. F.; Huang, J. V.; Anseth, K. S. "An investigation of the cytotoxicity and histocompatibility of in situ forming lactic acid based orthopedic biomaterials"; *J Biomed Mater Res* 2002, **63** (5), 484-91.
- (69) Burdick, J. A.; Mason, M. N.; Anseth, K. S. "In situ forming lactic acid based orthopaedic biomaterials: influence of oligomer chemistry on osteoblast attachment and function"; *J Biomater Sci Polym Ed* 2001, **12** (11), 1253-65.
- (70) Davis, K. A.; Burdick, J. A.; Anseth, K. S. "Photoinitiated crosslinked degradable copolymer networks for tissue engineering applications"; *Biomaterials* 2003, **24** (14), 2485-95.
- (71) Burdick, J. A.; Philpott, L. M.; Anseth, K. S. "Synthesis and characterization of tetrafunctional lactic acid oligomers: a potential in situ forming degradable orthopaedic biomaterial"; *J. Polym. Sci., Part A: Polym. Chem.* 2001, **39** (5), 683-692.
- (72) Wang, Y.; Noga, D. E.; Yoon, K.; Wojtowicz, A. M.; Lin, A. S. P.; Garcia, A. J.; Collard, D. M.; Weck, M. "Highly porous crosslinkable PLA-PNB block copolymer scaffolds"; *Adv. Funct. Mater.* 2008, **18** (22), 3638-3644.
- (73) Castro, N.; Goldstein, P.; Cooke, M. N. "Synthesis and manufacture of photocrosslinkable poly(caprolactone)-based three-dimensional scaffolds for tissue engineering applications"; *Adv. Biosci. Biotechnol.* 2011, **2** (3), 167-173.
- (74) Sharifi, S.; Mirzadeh, H.; Imani, M.; Atai, M.; Ziaee, F. "Photopolymerization and shrinkage kinetics of in situ crosslinkable N-vinyl-pyrrolidone/poly(epsilon-caprolactone fumarate) networks"; *J Biomed Mater Res A* 2008, **84** (2), 545-56.
- (75) Schueller-Ravoo, S.; Feijen, J.; Grijpma, D. W. "Flexible, elastic and tear-resistant networks prepared by photo-crosslinking poly(trimethylene carbonate) macromers"; *Acta Biomater.* 2012, **8** (10), 3576-3585.
- (76) Matsuda, T.; Mizutani, M. "Liquid acrylate-endcapped biodegradable poly(epsilon-caprolactone-co-trimethylene carbonate). II. Computer-aided stereolithographic microarchitectural surface photoconstructs"; *J Biomed Mater Res* 2002, **62** (3), 395-403.
- (77) Mizutani, M.; Arnold, S. C.; Matsuda, T. "Liquid, phenylazide-end-capped copolymers of epsilon-caprolactone and trimethylene carbonate: preparation, photocuring characteristics, and surface layering"; *Biomacromolecules* 2002, **3** (4), 668-75.

- (78) Timbart, L.; Tse, M. Y.; Pang, S. C.; Amsden, B. G. "Tissue response to, and degradation rate of, photocrosslinked trimethylene carbonate-based elastomers following intramuscular implantation"; *Materials* 2010, **3**, 1156-1171.
- (79) Zhang, C.; Subramanian, H.; Grailer, J. J.; Tiwari, A.; Pilla, S.; Steeber, D. A.; Gong, S. "Fabrication of biodegradable poly(trimethylene carbonate) networks for potential tissue engineering scaffold applications"; *Polym. Adv. Technol.* 2009, **20** (9), 742-747.
- (80) Lynn, D. M.; Langer, R. "Degradable Poly(β -amino esters): Synthesis, Characterization, and Self-Assembly with Plasmid DNA"; *J. Am. Chem. Soc.* 2000, **122** (44), 10761-10768.
- (81) Anderson, D. G.; Tweedie, C. A.; Hossain, N.; Navarro, S. M.; Brey, D. M.; Van Vliet, K. J.; Langer, R.; Burdick, J. A. "A combinatorial library of photocrosslinkable and degradable materials"; *Adv. Mater. (Weinheim, Ger.)* 2006, **18** (19), 2614-2618.
- (82) Brey, D. M.; Chung, C.; Hankenson, K. D.; Garino, J. P.; Burdick, J. A. "Identification of osteoconductive and biodegradable polymers from a combinatorial polymer library"; *J. Biomed. Mater. Res., Part A* 2010, **93A** (2), 807-816.
- (83) Tessmar, J. K.; Gopferich, A. M. "Customized PEG-derived copolymers for tissue-engineering applications"; *Macromol Biosci* 2007, **7** (1), 23-39.
- (84) Killion, J. A.; Geever, L. M.; Devine, D. M.; Grehan, L.; Kennedy, J. E.; Higginbotham, C. L. "Modulating the mechanical properties of photopolymerised polyethylene glycol-polypropylene glycol hydrogels for bone regeneration"; *J. Mater. Sci.* 2012, **47** (18), 6577-6585.
- (85) Li, H.; Fu, Y.; Niu, R.; Zhou, Z.; Nie, J.; Yang, D. "Study on the biocomposites with poly(ethylene glycol) dimethacrylate and surfaced-grafted hydroxyapatite nanoparticles"; *J. Appl. Polym. Sci.* 2013, **127** (3), 1737-1743.
- (86) Arcaute, K.; Mann, B. K.; Wicker, R. B. "Stereolithography of three-dimensional bioactive poly(ethylene glycol) constructs with encapsulated cells"; *Ann Biomed Eng* 2006, **34** (9), 1429-41.
- (87) Ovsianikov, A.; Malinauskas, M.; Schlie, S.; Chichkov, B.; Gittard, S.; Narayan, R.; Lobler, M.; Sternberg, K.; Schmitz, K. P.; Haverich, A. "Three-dimensional laser micro- and nano-structuring of acrylated poly(ethylene glycol) materials and evaluation of their cytotoxicity for tissue engineering applications"; *Acta Biomater* 2011, **7** (3), 967-74.
- (88) Domb, A. J.; Amselem, S.; Shah, J.; Maniar, M. "Polyanhydrides: synthesis and characterization"; *Adv. Polym. Sci.* 1993, **107** (Biopolymers I), 93-141.
- (89) Brem, H.; Piantadosi, S.; Burger, P. C.; Walker, M.; Selker, R.; Vick, N. A.; Black, K.; Sisti, M.; Brem, S.; Mohr, G. "Placebo-controlled trial of safety and efficacy of intraoperative controlled delivery by biodegradable polymers of chemotherapy for recurrent gliomas. The Polymer-brain Tumor Treatment Group"; *Lancet* 1995, **345** (8956), 1008-12.
- (90) Muggli, D. S.; Burkoth, A. K.; Keyser, S. A.; Lee, H. R.; Anseth, K. S. "Reaction Behavior of Biodegradable, Photo-Cross-Linkable Polyanhydrides"; *Macromolecules* 1998, **31** (13), 4120-4125.
- (91) Anseth, K. S.; Shastri, V. R.; Langer, R. "Photopolymerizable degradable polyanhydrides with osteocompatibility"; *Nat Biotechnol* 1999, **17** (2), 156-9.

- (92) Young, J. S.; Gonzales, K. D.; Anseth, K. S. "*Photopolymers in orthopedics: characterization of novel crosslinked polyanhydrides*"; *Biomaterials* 2000, **21** (11), 1181-8.
- (93) Weiner, A. A.; Shuck, D. M.; Bush, J. R.; Prasad, S. V. "*In vitro degradation characteristics of photocrosslinked anhydride systems for bone augmentation applications*"; *Biomaterials* 2007, **28** (35), 5259-70.
- (94) Muggli, D. S.; Burkoth, A. K.; Anseth, K. S. "*Crosslinked polyanhydrides for use in orthopedic applications: degradation behavior and mechanics*"; *J Biomed Mater Res* 1999, **46** (2), 271-8.
- (95) Li, H.-Y.; Chen, Y.-F.; Xie, Y.-S. "*Nanocomposites of cross-linking polyanhydrides and hydroxyapatite needles: mechanical and degradable properties*"; *Mater. Lett.* 2004, **58** (22-23), 2819-2823.
- (96) Cooke, M. N.; Fisher, J. P.; Dean, D.; Rimnac, C.; Mikos, A. G. "*Use of stereolithography to manufacture critical-sized 3D biodegradable scaffolds for bone ingrowth*"; *J Biomed Mater Res B Appl Biomater* 2003, **64** (2), 65-9.
- (97) Lee, K.-W.; Wang, S.; Fox, B. C.; Ritman, E. L.; Yaszemski, M. J.; Lu, L. "*Poly(propylene fumarate) bone tissue engineering scaffold fabrication using stereolithography: Effects of resin formulations and laser parameters*"; *Biomacromolecules* 2007, **8** (4), 1077-1084.
- (98) Fisher, J. P.; Dean, D.; Mikos, A. G. "*Photocrosslinking characteristics and mechanical properties of diethyl fumarate/poly(propylene fumarate) biomaterials*"; *Biomaterials* 2002, **23** (22), 4333-4343.
- (99) Andrews, L. S.; Clary, J. J. "*Review of the toxicity of multifunctional acrylates*"; *J Toxicol Environ Health* 1986, **19** (2), 149-64.
- (100) Calnan, C. D. "*Acrylates in industry*"; *Contact Dermatitis* 1980, **6** (1), 53-54.
- (101) Dworak, C.; Koch, T.; Varga, F.; Liska, R. "*Photopolymerization of biocompatible phosphorus-containing vinyl esters and vinyl carbamates*"; *J. Polym. Sci., Part A: Polym. Chem.* 2010, **48** (13), 2916-2924.
- (102) Heller, C.; Schwentenwein, M.; Russmueller, G.; Koch, T.; Moser, D.; Schopper, C.; Varga, F.; Stampfl, J.; Liska, R. "*Vinylcarbonates and vinylcarbamates: Biocompatible monomers for radical photopolymerization*"; *J. Polym. Sci., Part A: Polym. Chem.* 2011, **49** (3), 650-661.
- (103) Heller, C.; Schwentenwein, M.; Russmueller, G.; Varga, F.; Stampfl, J.; Liska, R. "*Vinyl esters: Low cytotoxicity monomers for the fabrication of biocompatible 3D scaffolds by lithography based additive manufacturing*"; *J. Polym. Sci., Part A: Polym. Chem.* 2009, **47** (24), 6941-6954.
- (104) Husar, B.; Heller, C.; Schwentenwein, M.; Mautner, A.; Varga, F.; Koch, T.; Stampfl, J.; Liska, R. "*Biomaterials based on low cytotoxic vinyl esters for bone replacement application*"; *J. Polym. Sci., Part A: Polym. Chem.* 2011, **49** (23), 4927-4934.
- (105) Husar, B.; Liska, R. "*Vinyl carbonates, vinyl carbamates, and related monomers: synthesis, polymerization, and application*"; *Chem. Soc. Rev.* 2012, **41** (6), 2395-2405.
- (106) Mautner, A.; Qin, X.; Kapeller, B.; Russmueller, G.; Koch, T.; Stampfl, J.; Liska, R. "*Efficient Curing of Vinyl Carbonates by Thiol-Ene Polymerization*"; *Macromol. Rapid Commun.* 2012, **33** (23), 2046-2052, S2046/1-S2046/7.

- (107) Esfandiari, P.; Ligon, S. C.; Lagref, J. J.; Frantz, R.; Cherkaoui, Z.; Liska, R. "Efficient stabilization of thiol-ene formulations in radical photopolymerization"; J. Polym. Sci., Part A: Polym. Chem. 2013, **51** (20), 4261-4266.
- (108) Ballyns, J. J.; Bonassar, L. J. "Image-guided tissue engineering"; Journal of Cellular and Molecular Medicine 2009, **13** (8a), 1428-1436.
- (109) Reichert, J. C.; Saifzadeh, S.; Wullschlegel, M. E.; Epari, D. R.; Schütz, M. A.; Duda, G. N.; Schell, H.; van Griensven, M.; Redl, H.; Hutmacher, D. W. "The challenge of establishing preclinical models for segmental bone defect research"; Biomaterials 2009, **30** (12), 2149-2163.
- (110) Melchels, F. P. W.; Domingos, M. A. N.; Klein, T. J.; Malda, J.; Bartolo, P. J.; Hutmacher, D. W. "Additive manufacturing of tissues and organs"; Progress in Polymer Science 2012, **37** (8), 1079-1104.
- (111) Cima, L. G.; Vacanti, J. P.; Vacanti, C.; Ingber, D.; Mooney, D.; Langer, R. "Tissue engineering by cell transplantation using degradable polymer substrates"; J Biomech Eng 1991, **113** (2), 143-51.
- (112) Hutmacher, D. W. "Scaffolds in tissue engineering bone and cartilage"; Biomaterials 2000, **21** (24), 2529-2543.
- (113) Hutmacher, D. W.; Schantz, T.; Zein, I.; Ng, K. W.; Teoh, S. H.; Tan, K. C. "Mechanical properties and cell cultural response of polycaprolactone scaffolds designed and fabricated via fused deposition modeling"; J Biomed Mater Res 2001, **55** (2), 203-16.
- (114) Schantz, J.-T.; Hutmacher, D. W.; Ng, K. W.; Khor, H. L.; Lim, M. T. C.; Teoh, S. H. "Evaluation of a tissue-engineered membrane-cell construct for guided bone regeneration"; Int J Oral Maxillofac Implants 2002, **17** (2), 161-74.
- (115) Sudarmadji, N.; Tan, J. Y.; Leong, K. F.; Chua, C. K.; Loh, Y. T. "Investigation of the mechanical properties and porosity relationships in selective laser-sintered polyhedral for functionally graded scaffolds"; Acta Biomaterialia 2011, **7** (2), 530-537.
- (116) Duan, B.; Wang, M.; Zhou, W. Y.; Cheung, W. L. "Synthesis of Ca-P nanoparticles and fabrication of Ca-P/PHBV nanocomposite microspheres for bone tissue engineering applications"; Appl. Surf. Sci. 2008, **255** (2), 529-533.
- (117) Arcaute, K.; Mann, B.; Wicker, R. "Stereolithography of spatially controlled multi-material bioactive poly(ethylene glycol) scaffolds"; Acta Biomater. 2010, **6** (3), 1047-1054.
- (118) Mautner, A. *Development of low cytotoxic Photopolymers*. Vienna University of Technology, 2012.
- (119) Vivadent, I. *State of the Art: Photopolymerization in dentistry*; 2013.
- (120) Anderson, E. M.; Larsson, K. M.; Kirk, O. "One biocatalyst - many applications: the use of *Candida antarctica* B-lipase in organic synthesis"; Biocatal. Biotransform. 1998, **16** (3), 181-204.
- (121) Miyazawa, T.; Hamada, M.; Morimoto, R.; Murashima, T.; Yamada, T. "Highly regioselective propanoylation of dihydroxybenzenes mediated by *Candida antarctica* lipase B in organic solvents"; Tetrahedron Lett. 2008, **49** (1), 175-178.
- (122) Chandorkar, Y.; Bhaskar, N.; Madras, G.; Basu, B. "Long-Term Sustained Release of Salicylic Acid from Cross-Linked Biodegradable Polyester Induces a

Reduced Foreign Body Response in Mice"; Biomacromolecules 2015, **16** (2), 636-649.

(123) D. D. Perrin, W. L. F. A. "*Purification of Laboratory Chemicals*". 3rd Ed. ed.; Pergamon Press: 1988.

(124) Fischer-Cripps, A. C. "*Nanoindentation*". Springer New York: 2011.

(125) AG, S.-M. Cubecorner Nanoindenterspitze. <http://www.synton-mdp.ch/de/produkte/nanoindenterspitzen.40.html>.

(126) Nebraska-Lincoln, U. o. Hysitron Nanoindenter. <http://bm3.unl.edu/hysitron-nanoindenter>.